Impacts of clogging minerals and groundwater extraction on mobility of arsenic in aquifers

---

Zur Erlangung des akademischen Grades eines

DOKTORS DER NATURWISSENSCHAFTEN (Dr. rer. nat.)

von der KIT-Fakultät für

Bauingenieur-, Geo- und Umweltwissenschaften

des KARLSRUHER INSTITUTS FÜR TECHNOLOGIE (KIT)

genehmigte

DISSERTATION

von

M.Sc. Yefim Shtirkin

aus Baku

Tag der mündlichen Prüfung:

16.02.22

Referent:	Prof. Dr. Stefan Norra
Korreferent:	PD Dr. Ulf Mohrlok
Korreferent:	Prof. Dr. Jochen Kolb

Karlsruhe 2022

Erklärung

Hiermit erkläre ich, dass ich die vorliegende Dissertation selbständig verfasst und keine anderen als die angegebenen Hilfsmittel benutzt habe. Die Stellen der Arbeit, welche anderen Quellen im Wortlaut oder dem Sinn nach entnommen wurden, sind durch Zitation kenntlich gemacht. Dies gilt auch für bildliche Darstellungen, Tabellen sowie für Quellen aus dem Internet.

Nürnberg, den 07.11.2021 Yefim Shtirkin

Acknowledgements

Undertaking this PhD has been a truly life-changing experience for me, and it would not have been possible to do without the support and guidance that I received from many people. Although it is just my name on the cover, many people have contributed to the research in their own particular way and for that I want to give these very inspiring, competent, and nice people special thanks. I would like to thank…

… my supervisor Prof. Dr. Stefan Norra for giving me the chance to do a PhD at the Institute. I greatly appreciate the freedom you have given me to find my own path and the guidance and support you offered when needed. Your mix of straightforward criticism combined with heart-warming support have given me great confidence as a researcher. Without your guidance and constant feedback this PhD would not have been achievable.

… Dr. Michael Reinhard who always had more than one open ear for my problems. You have created the invaluable space for me to do this research and develop myself not only as a researcher in the best possible way. Thanks for the many scientific discussions, giving the encouragement and sharing insightful suggestions. They have played a major role in polishing this work.

Dr. Ulf Mohrlok and Prof. Dr. Jochen Kolb, for their encouragement and supervisory role. I greatly appreciate your support and valuable input. I would like to extend my sincere thanks to Dr. Ulf Mohrlok for providing guidance and comments on this thesis.

… Dr. Annette Oberle who convinced me during our discussions that I should pursue my doctoral degree. Thanks for the useful advices you had for me.

… Dr. Elisabeth Eiche and Dr. Harald Neidhardt. For this research, data were essential. Your works have formed the basis for my research. Without your generosity there would be nothing to work with.

… the members of my PhD committee, Prof. Dr. Philipp Blum, Prof. Dr. Nico Goldscheider, Prof. Dr. Kolb, PD Dr. Mohrlok, Prof. Dr. Norra, Prof. Dr. Neumann und Prof. Dr. Jörg-Detlef Eckhardt

Thank you for investing time and providing interesting and valuable feedback. I feel proud and honored that you have accepted to be on my committee.

… the students who worked on the practical projects: Liselle Hauck, Julia Rotscholl, Jonas Bauer and Alisa Memmesheimer. Thank you so much for thinking with me and your time. You often brought new unconsidered ideas to the table.

… my current and former colleagues at Arcadis who gave me interesting feedback and valuable suggestions: Sandra Rettermeier, Christian Schreiber, Joachim Gfrörer, Christopf Schöpfer, Dietmar Reiersloh, Volker Ackermann and Hans-Peter Klein.

… all colleagues at the Karlsruhe Institute of Technology for the collaborative work and support: Dr. Johannes Lützenkirchen, Ilse Engelmann, Andreas Shenk, Ralf Wachter, Volker Zibat, Gesine Preuss and Kristian Nikoloski.

… my parents Marina and Vitaliy to whom I want to dedicate this thesis. You have always been there for me, supported me, and believed in me.

Abstract

In many countries around the world, arsenic (As) is one of the most important chemical contaminants in drinking water. The problem is most severe in Asia. Here, millions of people are at risk of chronic As poisoning through the consumption of As-enriched groundwater.

The release and mobility of As in groundwater is significantly controlled by hydrogeochemical and microbiological processes occurring at solid-water interfaces. It is widely accepted that Fe minerals, especially Fe oxides or sulfides, play an important role with respect to As mobility in groundwater. Besides Fe minerals, As incorporation into calcite is potentially an important process controlling the distribution of As in aquifers. In this thesis, Fe minerals, mainly Fe oxides, and calcite are referred to as clogging material. Iron oxides and calcite generally represent clogging material in pumping wells. Based on numerous literatures, both minerals can act as sorption surface and control the partitioning of As between solid and aqueous phases in an aquifer. In agreement with CORNELL & SCHWERTMANN (2003) in this thesis, goethite (α-FeOOH), ferrihydrite ($Fe_3HO_8*4H_2O$), lepidocrocite (γ FeOOH), hematite (α-Fe_2O_3), green rust ($Fe(OH)_3$) are collectively referred to as Fe oxides.

The present thesis aims at assessing the relative roles of clogging material and groundwater extraction that underlie As enrichment and mobility at three study sites with the heterogenous spatial distributions of As. Based on comprehensive sampling campaigns as a part of the PhD thesis by EICHE (2009) in the Red River Delta (Vietnam), the master thesis by SHTIRKIN (2013) in South-West Germany and the PhD thesis by NEIDHARDT (2012) in the Bengal Delta Plain (India), statistical and reactive transport modelling approaches are conducted. All study cases are based on real-world data. For the first two studies, reactive transport modelling is conducted. For the last one, a multivariate statistical analysis is used. The developed concept is transferable to groundwater extraction activities in systems such as drinking water supply, pump-and-treat or aquifer thermal energy storage.

In the first part, the impact of calcite on As retention in a fluvial aquifer in Vietnam is quantified. In South and South East Asia, Pleistocene aquifers are known to be low in dissolved As. However, active groundwater extraction for drinking water purposes in this region induces migration of As contaminated groundwater from an aquifer containing high levels of As (high-As) into an aquifer with low As concentrations (low-As) aquifer. This study examines extensive As retention in the Pleistocene aquifer, considers possible explanations for observed lateral changes of hydrogeochemical

parameters induced by intensive groundwater extraction in Hanoi and identifies the effect of clogging minerals on the groundwater As distribution.

Reactive transport simulations in 2D are used to assess the retention capabilities of calcite and Fe minerals. The models give a good impression on the extent and location of hydrogeochemical processes along the groundwater flow direction. The surface complexation model developed for ferrihydrite and sorption data for calcite are used to explore the retarded As transport. A cooperative effect of calcite and ferrihydrite on the As distribution in groundwater is observed. Arsenic is found to be retarded through the adsorption onto ferrihydrite and calcite surfaces. The results demonstrate retarded intrusion of As contamination into the previously uncontaminated Pleistocene aquifer for more than 150 m. In the model, a significant amount of As is adsorbed by Fe oxide. Ferrihydrite adsorbs over 80 % of As^{3+}. The spatial distribution of adsorption processes is strongly influenced by the extent of calcite precipitation and Fe oxides reduction. The reduction of Fe oxides plays a key role in the secondary release of newly adsorbed As. Likewise, the precipitated calcite at the boundary of redox zones plays an important role in As retention. While increasing the amount of calcite over time due to a constant inflow of Ca^{2+} and HCO_3^-, the impact of calcite on the As retention process grew up to 20%. In contrast, the presence of HCO_3^- and PO_4^{3-} reduced the adsorption capabilities of the sediments.

In the second part of the study, the As enrichment processes on the clogging material in the vicinity of pumping wells are assessed by using reactive transport modeling at a pump-and-treat system in South-West Germany. Well clogging is a widespread problem in aquifers with varying hydrogeochemical conditions. However, the interactions between physical and hydrogeochemical processes during groundwater extraction are not well understood. A reactive transport modeling approach is used to elucidate the effect of alternating extraction rates near the redox boundary on the precipitation of Fe minerals. Subsequent reactive transport simulations describe the spatial and temporal evolution of the redox zonation. Due to the variation of extraction rates, the model shows a growth in the amount of clogging material, especially Fe minerals, which act as adsorption surfaces for dissolved As. According to these investigations As mobilization results from the combined effect of clogging material dissolution and desorption of As due to competition processes, especially with HCO_3^- and PO_4^{3-}.

In the third part of the study, multivariate statistical analyses are used to assess hydrochemical data from the Bengal Delta Plain (India) to define relations between chemical and physical parameters and to deduce processes controlling the As distribution in groundwater. A review of 174 wells that extract groundwater from depths of up to 270 m shows that 130 of them contain more than 0.13 µmol/L of As. Using a multivariate statistical approach, sixteen physicochemical parameters are

analysed. The results show a strong correlation between the age of wells and dissolved As concentrations. In agreement with both previous studies, the association suggests that clogging material has been formed consisting mainly of Fe oxide and calcite and act as enrichment surface for As. Another important factor making As contamination a regional issue is groundwater temperature. Temperature plays an important role in the solubility of minerals, reactions kinetics, redox and sorption processes. In contrast to Europe, where mean temperatures in an aquifer lie between 10 °C and 15 °C, the average temperature in the study site is found to be 26.4 °C. Due to a large difference, groundwater temperature should be observed as a factor making As contamination a regional issue. However, the usage of geothermal plants, which are receiving a growing interest in Europe, can make As contamination also an issue for European counties.

This PhD makes the essential contribution to the understanding of the heterogeneous As distribution in an aquifer through the As accumulation on clogging material. The adsorption of As on calcite, whose retention capabilities were substantially underestimated for a long time, is observed as a process controlling As mobility in groundwater. Many theories have been published to explain the patchy As distribution in groundwater. However, all these theories observed only hydrogeochemical processes as key factors controlling As mobility. Besides the effects of hydrogeochemical reactions, microbiological processes, mixing of different water qualities also have an influence on As mobility in groundwater. The PhD presents an approach considering lateral groundwater movements induced though extraction and infiltration activities and assesses the effect on the As enrichment process in the vicinity of extraction wells. The work discusses for the first time also temperature as an important factor regionalising the As issue.

Kurzfassung

Weltweit stellen mit Arsen (As) belastete Grundwässer eine große Gefahr für die Menschen dar. Am stärksten ist Asien von diesem Problem betroffen. Hier ist die Gesundheit von Millionen Menschen betroffen.

Die Freisetzung und die Mobilität von As im Grundwasser werden maßgeblich durch hydrogeochemische und mikrobiologische Prozesse gesteuert. Es ist allgemein anerkannt, dass Fe-Mineralien, insbesondere Fe-Oxide oder -Sulfide, eine wichtige Rolle in Bezug auf die As-Mobilität im Grundwasser spielen. Neben Fe-Mineralien ist der Einbau von As in Calcit potenziell ein wichtiger Prozess, der die Verteilung von As in Grundwasserleitern steuert. In dieser Arbeit wird der Einfluss von Fe-Mineralien, hauptsächlich Fe-Oxide, und Calcit als Verblockungsmaterial im Umfeld von Brunnen auf die Arsenmobilität untersucht. Diese Minerale können als Sorptionsoberfläche wirken und die Verteilung von As zwischen der festen und der wässrigen Phase in einem Grundwasserleiter steuern. In Übereinstimmung mit CORNELL & SCHWERTMANN (2003) sind in dieser Arbeit sind Goethit (α-FeOOH), Ferrihydrit (Fe_3HO_8*$4H_2O$), Lepidocrocit (γ- FeOOH), Hämatit (α-Fe_2O_3), Grünrost ($Fe(OH)_3$) zusammenfassend als Fe-Oxide bezeichnet.

Die vorliegende Dissertation zielt darauf ab, die relativen Rollen von Verblockungsmaterial und Grundwasserentnahme zu untersuchen, die der As-Anreicherung und -Mobilität an drei Untersuchungsstandorten mit der heterogenen räumlichen Verteilung von As zugrunde liegen. Basierend auf umfangreichen Probenahmekampagnen im Rahmen der Dissertation von EICHE (2009) im Red River Delta (Vietnam), der Masterarbeit von SHTIRKIN (2013) in Südwestdeutschland und der Dissertation von NEIDHARDT (2012) im Bengal Delta Plain (Indien) werden statistische und reaktive Transportmodellierungen durchgeführt. Alle Untersuchungsfälle basieren auf realen Daten. Für die ersten beiden Studien wird eine reaktive Transportmodellierung angewendet. Für die letztere Studie wird eine multivariate statistische Analyse verwendet. Das entwickelte Konzept ist auf Grundwasserentnahmeaktivitäten in Systemen wie Trinkwasserversorgung, Pump-and-Treat oder Aquifer Thermal Energy Storage übertragbar.

Im ersten Teil wird der Einfluss von Calcit auf die As-Retention in einem fluvialen Grundwasserleiter in Vietnam quantifiziert. In Süd- und Südostasien ist bekannt, dass pleistozäne Grundwasserleiter wenig gelöstes As aufweisen. Die aktive Grundwasserentnahme zu Trinkwasserzwecken in dieser Region führt jedoch zu einer Migration von As-kontaminiertem Grundwasser aus einem Grundwasserleiter mit hohem As-Gehalt (High-As) in einen Grundwasserleiter mit niedrigen As-

Konzentrationen (Low-As). Diese Studie untersucht As-Retentionen am Übergang vom holozänen in den pleistozänen Grundwasserleiter, erarbeitet Erklärungen für die beobachteten lateralen Veränderungen hydrogeochemischer Parameter, die durch intensive Grundwasserentnahme in Hanoi induziert werden, und identifiziert die Auswirkungen von Verblockungsmineralien auf die As-Verteilung im Grundwasserleiter.

Im zweiten Teil der Studie werden die As-Anreicherungsprozesse am Verblockungsmaterial in der Nähe von Pumpbrunnen mittels reaktiver Transportmodellierung an einer Pump-and-Treat-Anlage in Südwestdeutschland untersucht. Die Verblockung von Brunnen ist ein weit verbreitetes Problem in Grundwasserleitern mit heterogenen hydrogeochemischen Bedingungen. Allerdings sind die Wechselwirkungen zwischen physikalischen und hydrogeochemischen Prozessen bei der Grundwasserentnahme noch nicht umfassend erforscht. Ein reaktiver Transportmodellierungsansatz wird verwendet, um den Einfluss alternierender Extraktionsraten nahe der Redoxgrenze auf die Ausfällung von Fe-Mineralien aufzuklären. Die Ergebnisse der reaktiven Transportsimulationen beschreiben die räumliche und zeitliche Entwicklung der Redoxzonierung. Aufgrund der Variation der Extraktionsraten zeigt das Modell eine Zunahme der Menge an Verblockungsmaterial, insbesondere von Fe-Mineralien, die als Adsorptionsflächen für gelöstes As dienen. Nach diesen Untersuchungen resultiert die As-Mobilisierung aus der kombinierten Wirkung von Auflösung des Verblockungsmaterials und Desorption von As aufgrund von Konkurrenzprozessen um Sorptionsplätze, insbesondere mit HCO_3^- und PO_4^{3-}.

Im dritten Teil der Studie werden multivariate statistische Analysen verwendet, um hydrochemische Daten aus dem Bengal Delta Plain (Indien) auszuwerten. So werden Zusammenhänge zwischen chemischen und physikalischen Parametern identifiziert und Prozesse abgeleitet, die die As-Verteilung im Grundwasser steuern. Eine Untersuchung von 174 Brunnen, die von NEIDHARDT (2012) durchgeführt wurde, zeigt, dass 130 davon mehr als 0,13 µmol/L As enthalten. Unter Verwendung der multivariaten statistischen Methoden werden in der vorliegenden Arbeit sechzehn physikalisch-chemische Parameter analysiert. Die Ergebnisse zeigen eine starke Korrelation zwischen dem Alter der Brunnen und den gelösten As-Konzentrationen. In Übereinstimmung mit den beiden ersten Studien zeigt die Korrelation, dass die Minerale, die zu Brunnenverblockungen führen, als Anreicherungsoberfläche für As in Frage kommen. Ein weiterer wichtiger Faktor, der die Kontamination zu einem regionalen Problem macht, ist die Grundwassertemperatur. Die Temperatur spielt eine wichtige Rolle bei der Löslichkeit von Mineralien, Reaktionskinetik, Redox- und Sorptionsprozessen. Im Gegensatz zu Europa, wo die mittleren Temperaturen in einem Aquifer zwischen 10 °C und 15 °C variieren, liegt die Durchschnittstemperatur im Untersuchungsgebiet bei 26,4 °C. Aufgrund des großen Unterschieds sollte die Grundwassertemperatur als

Faktor betrachtet werden, der die As-Kontamination zu einem regionalen Problem macht. Hier kann die Nutzung von Geothermieanlagen, die in Europa ein wachsendes Interesse erfährt, die As-Kontamination auch für Europa zum Problem machen.

Diese Dissertation leistet den wesentlichen Beitrag zum Verständnis der heterogene As-Verteilung in einem Grundwasserleiter durch die As-Anreicherung auf Verblockungsmaterial. Die Rückhaltevermögen von Calcit wurden lange Zeit stark unterschätzt. Viele Theorien wurden veröffentlicht, um die As-Verteilung im Grundwasser zu erklären. Alle diese Theorien beobachteten primär jedoch nur hydrogeochemische Prozesse als Schlüsselfaktoren, die die As-Mobilität steuern. Neben den Auswirkungen hydrogeochemischer Reaktionen haben auch mikrobiologische und die Vermischungsprozesse einen Einfluss auf die As-Mobilität im Grundwasser. Diese Doktorarbeit stellt einen Ansatz vor, der laterale durch Extraktions- und Infiltrationsaktivitäten induzierte Grundwasserbewegungen berücksichtigt und die Auswirkungen auf die As-Anreicherungsprozesse in der Nähe von Extraktionsbrunnen untersucht. Die Arbeit thematisiert erstmals auch die Temperatur als einen wichtigen Faktor, der die As-Thematik regionalisiert.

Table of content

List of Figures

List of Tables

Abbreviations

As	Arsenic
As^{3+}	AsO_3^{3-}
As^{5+}	AsO_4^{3-}
ATES	Aquifer Thermal Energy Storage
ASR	Aquifer Storage and Recovery
BDP	Bengal Delta Plain
BTEX	mixtures of benzene, toluene, and the three xylene isomers, all of which are aromatic hydrocarbons
DFG	German Research Foundation
DOC	dissolved organic carbon
EPSG	geodetic parameter dataset developed by European Petroleum Survey Group Geodesy
Hfo	hydrous ferric oxides
Hfo_w	binding site in the surface complexation model
NAPL	non-aqueous phase liquid
NSO-HET	heterocyclic aromatic hydrocarbons
PAH	organic compounds, which are composed of multiple aromatic rings
PZC	point of zero charge
SI	saturation index
WHO	World Health Organization

Chapter 1. Introduction and objective of the study

1.1 BACKGROUND

Millions of people worldwide are exposed to arsenic (As) contaminated groundwater above the WHO drinking water limit of 0.13 µmol/L (SMEDLEY & KINNIBURG, 2002; BERG ET AL., 2006; VAN GEEN ET AL., 2013). Asia is the region that is most affected by As contamination in groundwater (NICKSON ET AL., 1998; BERG ET AL., 2001; VAN GEEN ET AL., 2003; WAGNER, 2005; HARVEY ET AL., 2006; BUSCHMANN ET AL., 2007; BERG ET AL., 2007; AZAM ET AL., 2008; MCARTHUR ET AL., 2010; HOQUE ET AL., 2012; NORRA ET AL., 2012; MAI ET AL., 2014; HOQUE ET AL., 2014). Estimated 35 million people have been drinking As contaminated water for the past 30 years (BERG ET AL., 2007). There are also areas in Europe contaminated with As (DI BENEDETTO ET AL., 2006; COSTAGLIOLA ET AL., 2007; BARDELLI ET AL., 2011; ROWLAND ET AL., 2011; WINKEL ET AL., 2013; ROTIROTI ET AL., 2014). The spatial variability of As in groundwater makes the management of groundwater resources very difficult (NICKSON ET AL., 1998; VAN GEEN ET AL., 2003; BERG ET AL., 2007; JAKOBSEN ET AL., 2018). To develop suitable water supply systems, a consideration of vertical (HARVEY ET AL., 2002; SWARTZ ET AL., 2004) as well as lateral occurring hydrogeochemical processes is required (VAN GEEN ET AL., 2006; RATHI ET AL., 2017 JAKOBSEN ET AL., 2018).

In order, to assess the processes controlling As mobility in groundwater a literature overview is carried out (APPELO & POSTMA, 2005; BONTE ET AL., 2013; POSSEMIERS, 2014). From this review, three groups of processes can be distinguished: (1) hydrogeological, (2) chemical and microbiological, and (3) thermal. Table 1 presents main processes in each group.

Table 1. Overview of processes controlling arsenic distribution in an aquifer.

Group	Processes
Hydrogeological	Changing local and regional groundwater flow direction
	Mixing
	Changing water level
	Changing of well capture zone
Chemical and microbiological	Dissolution/precipitation of Fe minerals and calcite
	Redox processes
	Sorption of As onto mineral surface
	Organic matter degradation
Thermal	Changing temperature of groundwater

Chemical and microbiological processes

Most published research suggests that the As mobility in aquifers is controlled by redox processes (HARVEY ET AL., 2006; BERG ET AL., 2007) and interactions with the surfaces of Fe minerals (NICKSON ET AL., 1998; APPELO ET AL., 2002; BUSCHMANN ET AL., 2007; STOLLENWERK ET AL., 2007; EICHE, 2009; RATHI ET AL., 2017) and carbonates (ZHENG ET AL., 2004; ROMAN-ROSS ET AL., 2006; SØ, 2007; YOKOYAMA ET AL., 2009; BARDELLI ET AL., 2011). Generally, these minerals are corresponding to clogging material (HOUBEN, 2003; ROMERO ET AL., 2004; VAN BEEK, 2011; MEDINA ET AL., 2013). Thus, the solubility and amount of these minerals in the vicinity of pumping wells can influence the As concentration in extracted groundwater. Identification of physical and chemical processes controlling the growth and distribution of clogging material will provide insight into the heterogeneous As distribution in groundwater.

Clogging of extraction wells by Fe oxide incrustations due to the mixing of anoxic and oxic groundwater is a common well-aging problem (HOUBEN, 2003; HOUBEN & TRESKATIS, 2003; STUYFZAND 2007; MEDINA ET AL., 2013; POSSEMIERS, 2014). HARVEY ET AL. (2006) determined average extraction rates from irrigation rates in Bangladesh as 24.1 L/s. Such high pumping rates will induce vertical as well as lateral mixing processes and intensify the precipitation of clogging material in the vicinity of extraction wells. Iron oxides clog the screen slots of wells as well as a surrounding aquifer and filter material (HOUBEN, 2006; HOUBEN & WEIHE, 2010). These incrustations are mainly composed of poorly ordered ferrihydrite and to less extent of more crystalline Fe oxides such as goethite and lepidocrocite (HOUBEN & TRESKATIS, 2003). Iron oxides that coat aquifer particles appear to be the enrichment surface for As (NICKSON ET LA., 1998; HARVEY ET AL., 2002). Rice root coatings consist of a similar assemblage of As bearing minerals (KRAMAR ET AL., 2017). The authors have found that As was mainly associated with Fe oxides.

Groundwater often shows saturation with respect to calcite. The kinetics of calcite precipitation in simple systems is well understood (APPELO & POSTMA, 2005). But there is little information available on the calcite dissolution/precipitation processes at redox boundaries, which can exist within groundwater extraction areas and aquifer parts with different mineralogical compositions (EICHE, 2009; VAN GEEN ET AL., 2013). Calcite precipitation plays an important role in well clogging (STUMM & MORGAN, 1981; GRIFFIOEN & APPELO, 1993; SHTIRKIN, 2013). This mineral has received little attention as a mineralogical trap although As is preferentially incorporated into calcite over a wide range of pH values (ROMAN-ROSS ET AL., 2006; COSTAGLIOLA ET AL., 2007; YOKOYAMA ET AL., 2009; YOKOYAMA ET AL., 2012). Sorption of As onto calcite can occur under either reducing or under oxic conditions (ROMAN-ROSS ET AL., 2006). Exclusion of calcite as the sorption surface of As can lead to an overestimation of the sorption capabilities of other minerals, for example Fe oxides. Therefore, the consideration of calcite in the

conceptual model of As mobility in groundwater advances the understanding of the heterogeneous As distribution.

In contaminated or organic rich aquifers, the high availability of organic carbon combined with a higher microbial activity causes the redox zoning to shift towards more reducing conditions that induces the reduction of Fe oxide. The reductive dissolution of Fe oxides is widely accepted to be one of the main processes controlling As mobilization (NICKSON ET AL., 2000; MCARTHUR ET AL., 2001; APPELO ET AL., 2002). In addition to that, the CO_2 partial pressure increase results in much higher HCO_3^- concentration in groundwater, which acts as a competitor for the sorption sites (APPELO ET AL., 2002). Mixing of groundwater with different CO_2 partial pressure, which is often observed in aquifers with organic contaminants, can lead to calcite precipitation (PALMER ET AL., 1992).

Hydrogeological processes

Extraction and infiltration wells, which are used in different systems (i.e. pump-and-treat, aquifer thermal energy storage system, aquifer storage and recovery, and drinking water wells), induce noticeable perturbation in the groundwater flow pattern up to several kilometers (FERGUSON, 2006; BERG ET AL., 2008; BRIELMANN ET AL., 2011; VAN GEEN ET AL., 2013; BONTE ET AL., 2013B). Groundwater is often characterized by concentration gradients in a spatial context. Depending on hydrogeochemical conditions in an aquifer, these systems can induce changes in hydrochemistry mainly by mixing of different water types. The expected impact of mixing depends on the type (redox, pH or concentration) and the size of gradient over which mixing occurs. For example, mixing of waters with contrasting redox conditions or CO_2 partial pressure can result in the precipitation of Fe oxides or calcite, respectively (POSSEMIERS, 2014).

The effects of extraction wells in aquifer thermal storage (ATES) and pump-and-treat systems on hydrogeochemical composition in an aquifer are comparable to the effects observed in drinking water wells (POSSEMIERS, 2014). Hydrogeochemical processes related to the infiltration of water are also observed in aquifer storage and recovery (ASR) (PROMMER & STUYFZAND, 2005; DESCOURVIÈRES ET AL., 2010) and pump-and-treat (SHTIRKIN, 2013) systems. In these systems, oxic/treated water that is infiltrated into an anoxic aquifer induces large hydrogeochemical changes.

During the subsurface planning stages of systems extracting groundwater, capture zones are often considered at steady-state conditions. However, in reality the distribution of hydrogeochemical conditions varies due to the transient nature of groundwater extraction and infiltration (BONTE, 2013). The alternating groundwater extraction rates generally can lead to physical and chemical well clogging (DE ZWART, 2007; HOUBEN & WEIHE, 2010; VAN BEEK, 2011; MEDINA ET AL., 2013).

Precipitation of Fe oxide and calcite is known to reduce well performance (HOUBEN & WEIHE, 2010; VAN BEEK, 2011). Installed wells near the redox boundary induce the mixing of waters and are characterized by different redox conditions. This can lead to the precipitation of Fe minerals and calcite (PROMMER & STUYFZAND, 2005; WALLIS ET AL., 2011; BONTE ET AL., 2014; POSSEMIERS, 2014). However, previous studies observed mixing processes only in vertical and transversal orientation. Groundwater extraction also causes groundwater flow in longitudinal orientation. In aquifers with redox zoning, these groundwater movements can induce or intensify hydrogeochemical processes at the redox boundary. The assessment of mixing processes in lateral orientation allows to identify and quantify more precisely hydrogeochemical processes.

Thermal processes

Both, chemical and physical processes influence the As speciation and mobility in groundwater. Temperature plays a key role in the solubility of minerals, reaction kinetics, redox processes and sorption-desorption of anions and cations (BRONS ET AL., 1991; GRIFFIOEN & APPELO, 1993; SOWERS ET AL., 2006).

GRIFFIOEN & APPELO (1993) and HOLM ET AL. (1987) observed mineral precipitation at high temperatures (>60 °C). However, the effects of temperatures below 30 °C on mineral equilibrium are expected to be limited (BRIELMANN ET AL., 2009; HARTOG ET AL., 2013).

Redox reactions are determined by kinetic constants (APPELO & POSTMA, 2005). PROMMER & STUYFZAN (2005) showed that even small temperature variations affect redox reactions. Redox reactions proceed significantly faster at higher temperatures (PROMMER & STUYFZAND, 2005; HARTOG, 2011; VAN HALEM ET AL., 2012).

Increasing temperature may enhance the dissolution of contaminants from NAPL bodies (ZUURBIER ET AL., 2013). BRONS ET AL. (1991) and JESUßEK ET AL. (2013) reported an increase of the solubility of dissolved organic carbon (DOC) with increasing temperature in laboratory experiments. The increased availability of organic carbon combined with a higher microbial activity shifts groundwater towards more reducing conditions (JESUßEK ET AL., 2013).

Previous studies observed temperature effects on the hydrogeochemical composition in an aquifer with respect to the operation of geothermal plants. However, there is still a gap in understanding how relatively high groundwater temperatures in the Asia region in comparison to Europe influence the distribution of As in aquifers.

In addition, energy storage techniques are receiving a growing interest in Europe. The increasing number of such systems leads to local warming of groundwater up to 25°C. Therefore, the usage of geothermal plants can bring As groundwater contamination in the foreground in Europe. Besides energy storage systems, the temperature effects of

climate change and urbanization on the aquifer system cause this parameter to be more pronounced for the As distribution in Europe. MUEHE & FENDORF (2016) showed within the DFG project the relevance of climate change for the As mobility in groundwater. Arsenic becomes more mobile in the pore water with increasing temperature. BONTE ET AL. (2013B) revealed that sorption of anions decreases with raising temperature.

1.2 ARSENIC IN AN AQUIFER – AN OVERVIEW

Arsenic in groundwater

Arsenic mobility varies with its chemical form and state of valence. In water, As shows anionic behaviour. The dominant inorganic forms of As in groundwater are arsenite AsO_3^{3-} (As^{3+}) and arsenate AsO_4^{3-} (As^{5+}). The speciation is mainly determined by the redox state and the pH-value (Figure 1). Under oxidizing conditions As^{5+} is the dominant form. $HAsO_4^{2-}$ dominates at neutral pH conditions. The prevailing form under reducing conditions is As^{3+} (SMEDLEY & KINNIBURG, 2002).

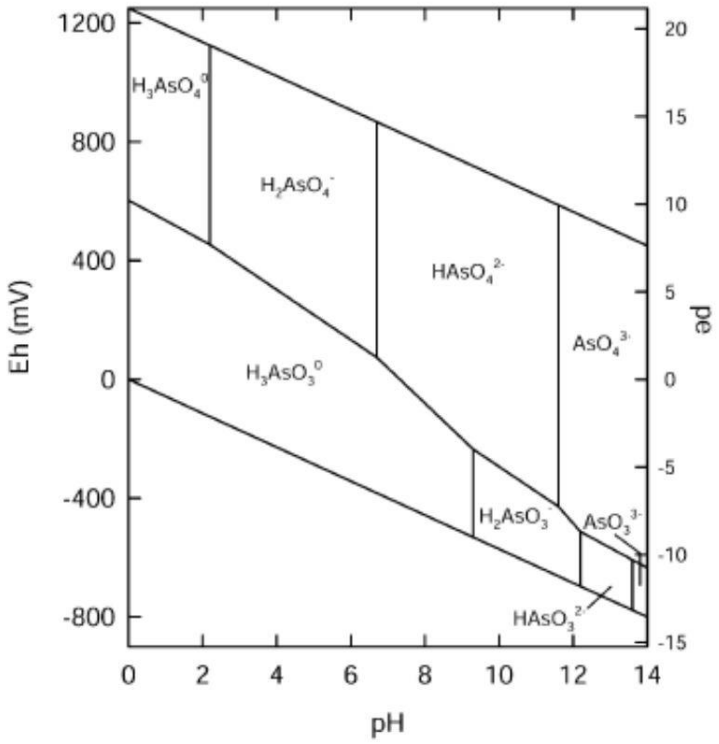

Figure 1. Eh-pH stability diagram of As species (Smedley & Kinniburg, 2002).

Under acidic and neutral pH values, H_3AsO_3 prevails. Inorganic As species can be transformed due to redox processes as well as microbiological activity.

Arsenic in sediments

Arsenic minerals are rare in aquifer environments. In aquifers, As is primarily incorporated into different minerals or is adsorbed onto surfaces (APPELO & POSTMA, 2005). Depending on the hydrogeochemical conditions in an aquifer, sediments can act as source as well as sink of As. The concentrations in sediments vary according to the hydrogeochemical situation that has established during the deposition of the aquifer material (SMEDLEY & KINNIBURG, 2002). In an As contaminated aquifer, As concentrations in this solid phase ranges between 0.3 mg/kg and 44 mg/kg (HARVEY ET AL., 2002; ANAWAR ET AL., 2003; STOLLENWERK ET AL., 2007; EICHE, 2009; SHARIF ET AL., 2011; POSTMA ET AL., 2016; STAHL ET AL., 2016; JAKOBSEN ET AL., 2018).

Adsorption/desorption processes affect the mobility of As in groundwater. Sorption behaviour of As is primarily influenced by hydrogeochemical conditions, the presence of available sorption sites and concentrations of competing ions in groundwater (APPELO & POSTMA, 2005). Total concentrations of As in the sediments is not the main factor giving the information about its potential mobility. More important is the bonding form of As to the sediment (FENDORF ET AL., 2010).

On the mineral surface, As can be weakly or strongly bound. Surface adsorbed As interacts easily with dissolved compounds. Arsenic adsorption densities vary with pH. The greatest adsorption was observed for As^{3+} at pH 7 and for As^{5+} at pH 4 (APPELO & POSTMA, 2005). In contrast to As^{5+}, adsorption of As^{3+} over the pH range 4-9 is not strongly dependent on pH (WILKIE & HERING, 1996). For As^{5+}, a stronger effect of pH was observed.

Both, As^{3+} and As^{5+} have binding affinities for Fe oxides, especially ferrihydrite. Fe oxides having a high As adsorption capacity enhances the average concentrations up to 30 mg As/kg sediment or more (HORNEMAN ET AL., 2004). Fe oxides are one of the primary sources for dissolved As under reducing conditions (NICKSON ET AL., 2000; SWARTZ ET AL., 2004).

The mobility of As can be influenced by its interaction with green rust (PEREZ ET AL., 2019). Green rust showed high As adsorption capacities at circum-neutral pH and in anoxic conditions (WANG ET AL., 2010). However, the main adsorption parameters (e.g., effects of pH, competing ions), as well as adsorption kinetics, necessary for understanding interactions between green rust and As species in groundwaters have still not been quantified.

A wide range of data on the adsorption of both anions and cations onto ferrihydrite has been surveyed by DZOMBAK & MOREL (1990). The developed surface complexation model by the authors is commonly used to simulate the sorption of trace elements on ferrihydrite. APPELO ET AL. (2002), POSTMA ET AL. (2007) and RAWSON ET AL. (2017) have used

this model for ferrihydrite, which incorporate mass balance equations for the adsorbate and for the surface adsorption sites, to assess the distribution of As between water and sediment.

Siderite is also known to host As (5-20 mg/kg) (GUO ET AL., 2007). Under reducing conditions As is mainly found in considerable concentrations in pyrite (PLANT ET AL., 2005). Arsenic is also associated with Mn oxides, clay minerals and calcium carbonates (ROMAN-ROSS ET AL., 2006; JONES ET AL., 2013).

1.3 MODELLING AND STATISTICS

1.3.1 MODELLING

There have been many different codes developed in recent years that solve the reactive transport equations. Among them, PHT3D (PROMMER & POST, 2010) and PHAST (PARKHURST ET AL., 2010) have the advantage that they are widely used, tested and open source. Both codes use the code PHREEQC (PARKHURST & APPELO, 2013) for hydrogeochemical simulations (STEEFEL ET AL., 2015; DATTA ET AL., 2017). PHAST (JAKOBSEN ET AL., 2018), PHT3D (WALLIS ET AL., 2010; WALLIS ET AL., 2011; RAWSON ET AL., 2016) and PHREEQC (POSTMA ET AL., 2016) are frequently used to simulate As mobility in groundwater.

PHREEQC is a computer code designed to perform a variety of hydrogeochemical calculations. The PHREEQC databases include a range of equilibrium reactions. PHREEQC allows to formulate kinetical expressions, for example Michaelis-Menten or Monod equation. The PHREEQC database can be extended with reacting species.

PHT3D is a three-dimensional multicomponent reactive transport code that couples groundwater flow and reactive transport processes in saturated porous media. PHT3D couples the multispecies transport code MT3DMS with PHREEQC.

The PHAST code incorporates the groundwater flow model HST3D (KIPP, 1997) and PHREEQC. Through the flexible, generic nature of PHREEQC, PHAST can handle a broad range of equilibrium and kinetic reactive processes, including aqueous complexation, mineral precipitation/dissolution, cation exchange, and surface complexation reactions. The PHAST code also has the capability to simulate kinetically reacting immobile components. Typical reactive processes such as microbial activity, NAPL dissolution, and isotopic fractionation can also be simulated.

In contrast to PHT3D, PHAST is better suited for the simulation of spatial hydrogeochemical problems because of a well-structured definition of input files (APPELO & ROLLE, 2010). For this reason, PHAST is selected in the current PhD thesis.

The geochemical model PHREEQC is used to reconstruct the initial water, sediment, surface concentrations and compositions. The code includes also a two-layer surface complexation model of DZOMBAK & MOREL (1990) simulating the sorption of ions on ferrihydrite and calculating competitive sorption of species for the sorption site on ferrihydrite is implemented in the model. WATEQ4F thermodynamic database extended with compilation of STOLLENWERK ET AL. (2007), APPELO ET AL. (2002) and RAWSON ET AL. (2017) for As speciation is used in the calculations performed under equilibrium conditions.

The two-step partial equilibrium approach (BRUN & ENGESGAARD, 2002; JAKOBSEN & COLD, 2007) is considered in the simulation of redox processes. Kinetic degradation is simulated by transforming conservative BTEX and PAH compounds into „reactive" CH_2O, which is oxidized in the PHREEQC code according to the thermodynamic equilibrium (PROMMER ET AL., 1999; PROMMER ET AL., 2006; D'AFFONSECA ET AL., 2008).

1.3.2 STATISTICS

Multivariate statistical analyses including factor analysis and cluster analysis are applied to the hydrogeochemical data. Statistical methods are used to generate groups of correlated elements and support the interpretation of the governing processes. These methods were frequently used to investigate hydrogeochemical compositions of aquifers (NARANY ET AL., 2013; LEDESMA-RUIZ ET AL., 2015; LIU ET AL., 2003; GHOSH & MONDAL, 2018). The analysis is performed using STATISTICA version 8 (WEIß, 2007) to simplify the complex relationships that exist among the observed variables.

The factor analyses technique involves two steps. For the beginning, all variables are standardized to ensure that each variable is weighted equally. After that, a correlation matrix is created for each pair of constituents, which can be used to point out interactions between variables. In the second step, the factor loadings are calculated. Factor analysis is based on the diagonalization of the correlation matrix.

Principal component and Varimax factor rotation are applied in the factor analysis. Principal component analysis uses a linear combination of variables to get the highest variance from the variables. A Varimax rotation is a change of coordinate system to maximize the variance of the squared loadings. Kaiser's varimax rotation scheme is applied (KAISER, 1958).

The number of factors is obtained using a scree plot, which helps to visualize the relative importance of the factors. A flattening in the graph informs that subsequent factors can be ignored.

Loadings on each of the factors are interpreted such that loadings greater than ± 0.75 are considered strong correlation, loadings between ± 0.5 and ± 0.75 are considered

significant loadings, and loadings less than ± 0.5 are considered insignificant (OSBORNE & COSTELLO, 2009). The negative values show inverse relations between parameters. Factor analysis is used to expose the processes responsible for observed variations in parameter values. The strong correlation is an indication of common source.

Cluster analysis is a method for gathering objects into homogeneous groups exhibiting similar hydrochemistry. The similarity between objects is obtained using squared Euclidean distances. In the approach Wards linkage rule is used. This rule indicates that the shorter the distance between classes, the higher the similarity between them.

1.4 RESEACH OBJECTIVE AND QUESTIONS

The main objective of this PhD thesis is to improve the qualitative and quantitative understanding of the impacts of Fe minerals and calcite on the mobilization and enrichment of As in groundwater by means of modelling approaches. To reach this objective, the following research questions should be answered:

(1) What is the impact of calcite in contrast to Fe minerals on the As distribution in groundwater?

- Can As adsorption onto calcite explain inconsistences in the relation between dissolved As and Fe^{2+} concentrations in groundwater?
- Can calcite act as an important As trap where Fe and Mn oxides have low concentrations or lost their adsorbing effectiveness?

(2) What are the driving physical and hydrogeochemical processes determining the enrichment of As in the vicinity of pumping and infiltration wells?

- What is the extent and location of clogging minerals precipitation acting as the enrichment surface of As?
- What is the effect of alternating groundwater extraction near the redox boundary on the precipitation of Fe minerals and calcite which are corresponding to clogging material?

(3) What is the impact of extracting activities in the long term on chemical composition and As enrichment?

- Which parameters control the As enrichment onto the clogging material in the vicinity of extraction wells?

(4) What is the impact of temperature on As mobility?

- Why is As contamination widely distributed mainly in Asia?
- What is reported in literature on the effects of temperature on As mobility?

The questions will be answered in the following chapters and discussed in last chapter.

1.5 STATEMENT OF NOVELTY

New aspects and approaches covered by the study are:

- Calcite as mineral controlling partial As adsorption. For a long time, the retention capabilities of calcite are largely ignored. The results of this study show that calcite can act as As trap in the aquifers oversaturated in respect to calcite and with active redox zoning.
- Clogging material as enrichment surface of As. This work presents a first approach explaining the heterogeneous As distribution in an aquifer through the As enrichment process onto clogging material.
- Time aspect. The operation time of wells can give an information about the amount of clogging material in the vicinity of wells. The process of As enrichment onto clogging material becomes more pronounced and quantitatively remarkable over time.
- Temperature differences between Europe and Asia aquifers. Temperature has not been intensively investigated as a factor controlling the behaviour of As in an aquifer and responsible for the regionalisation of the As issue. This finding can partially explain the regional character of As contamination.

1.6 METHODOLOGY AND OUTLINE OF THIS THESIS

Data from three different study sites are used to assess the effects of each process on the As distribution in aquifers.

In the first part of the study, based on the field data gathered by EICHE (2009) in the Van Phuc village, in Vietnam, a reactive transport modelling approach is used to investigate the impacts of clogging minerals on the mobility of As. The numerical approach with a long simulation period up to 50 years focuses on the occurrence and rates of adsorption and redox processes.

In the second part of the study, a reactive transport model is used to assess the effect of altering groundwater extraction near the redox boundary by a pump-and-treat system on the precipitation of Fe minerals and calcite, and the enrichment process of As on clogging material for the case in South-West Germany. The model describes interactions between physical and chemical processes around extraction and infiltration wells, and predicts their effect on the clogging material distribution.

In the third part of the study, the distribution of As within aquifers in the western part of the Bengal Delta Plain is assessed by means of a literature review and a multivariate statistical analyses of groundwater chemistry data from 174 extracting wells. The data were gathered as part of PhD thesis by NEIDHARDT (2012) in the frame of a DFG ("Deutsche Forschungsgemeinschaft") project.

In the last part, a summary is provided followed by a synthesis and discussion of the main results. The postulated processes are integrated into a conceptual model. Finally, an overview of new research questions and recommendation resulting from this PhD thesis is given.

Chapter 2. Retardation of arsenic controlled by adsorption processes onto ferrihydrite and calcite in the Red River flood plain aquifer, Vietnam. Conceptual analysis using 2D reactive transport modeling

2.1 INTRODUCTION

In the Red River Delta, about 11 million people do not have access to public water supply and therefore extract water from private wells (BERG ET AL., 2006; BERG ET AL., 2007). Untreated groundwater from these wells is the principal source of drinking water in the region. Groundwater contamination by As is a big threat to the health of these people in Vietnam. Many studies already focused on As contamination in the Red River Delta region (e.g. EICHE ET AL., 2008; EICHE, 2009; JESSEN ET AL., 2012; POSTMA ET AL., 2016; STAHL ET AL., 2016; RATHI ET AL., 2017; JAKOBSEN ET AL., 2018). The spatial variability of As hosting deposits suggests that the understanding of As mobilization processes requires the consideration of processes in lateral (VAN GEEN ET AL., 2006; VAN GEEN ET AL., 2013; RATHI ET AL., 2017) and vertical (with depth) alignment (HARVEY ET AL., 2002; SWARTZ ET AL., 2004). Several researchers (BGS, 2001; HARVEY ET AL., 2002; VAN GEEN ET AL., 2013) describe two types of aquifer sediments in Vietnam: orange sediments (Pleistocene), and grey sediments (Holocene). The Pleistocene aquifers are typically reported to be free or low in dissolved As. The majority of wells in Holocene aquifers are frequently associated with high dissolved As concentrations (>> 0.013 µmol/L). The distribution of both deposits generally reflects the distribution of the dissolved As contamination (VAN GEEN ET AL., 2006; STOLLENWERK ET AL., 2007; MCARTHUR ET AL., 2010; VAN GEEN ET AL., 2013). However, changes in groundwater flow direction in aquifers can cause an increase of dissolved As concentration in the Pleistocene aquifers, which were previously known as uncontaminated (BERG ET AL., 2006; VAN GEEN ET AL., 2013). In the Red River Delta, the large-scale extraction of groundwater in the city of Hanoi, which began more than 110 years ago, influences groundwater flow direction on a relatively extended area (NGUYEN, 1995; BERG ET AL., 2001; PHI & STROKOVA, 2015). A study conducted by VAN GEEN ET AL. (2013) has shown that the groundwater exploitation in the Hanoi region enhances the risk of As contaminated groundwater migration into the uncontaminated Pleistocene aquifer. They examined to what extent the boundary between the low-As and high-As sites in Van Phuc has shifted in response to groundwater extraction in Hanoi. According to the authors, the induced groundwater movement caused a lateral intrusion of As contamination for more than 120 m into the Pleistocene aquifer. The intrusion of dissolved As is largely retarded (by a factor of 16 to 20) through adsorption.

The mobility of As in groundwater has received increasing attention over last years. There is no simple relationship between the concentrations of As in groundwater and other hydrogeochemical properties of the aquifer. Adsorption on mineral surfaces is one of the key processes controlling the partitioning of As between groundwater and sediments (APPELO & POSTMA, 2005; POSTMA ET AL., 2010; JESSEN ET AL., 2012). Arsenic adsorption onto sediments varies depending on pH, Eh, mineralogical composition and ion competition processes. Most studies consider As sorption onto Fe oxides, Al oxides,

and Mn oxides as most prominent (APPELO ET AL., 2002; ANAWAR ET AL., 2003; AMIRBAHMAN ET AL., 2006; HARVEY ET AL., 2006; BERG ET AL., 2007; MAI ET AL., 2014; LAZAREVA ET AL., 2015). Other researchers have focused on As interaction with carbonate minerals (ROMAN-ROSS ET AL., 2006; ALEXANDRATOS ET AL., 2007; BARDELLI ET AL., 2011; JONES ET AL., 2013; CATELANI ET AL., 2018). Currently, the microbiological induced reductive dissolution of Fe oxides coupled to organic matter decomposition has been widely accepted to explain As mobilization into groundwater (POSTMA ET AL., 2007, BERG ET AL., 2008; POSTMA ET AL., 2010; RAWSON ET AL., 2016; RAWSON ET AL., 2017; SØ ET AL., 2017). However, the generally poor correlation between Fe^{2+} and dissolved As (APPELO ET AL., 2002; WINKEL ET AL., 2011) shows that the mobility of As in groundwater is controlled through a group of processes. In contrast to Fe oxides, calcite has received less attention as a possible trap for As. The adsorbing behavior of As onto calcite is not well established in the literature, yet. Only some studies (DI BENEDETTO ET AL., 2006; ROMAN-ROSS ET AL., 2006; COSTAGLIOLA ET AL., 2007; JONES ET AL., 2013) suggest that As can also be strongly adsorbed onto calcite, which is more stable under changing redox conditions.

Reactive transport modeling enables the assessment of integrated effects of variations in hydrogeochemical conditions on the groundwater As distribution. However, despite a large amount of experimental research (WILKIE & HERING, 1996; BOTHE & BROWN, 1999; ROMAN-ROSS ET AL., 2006; GOLDBERG, 2002; HUDSON-EDWARDS ET AL., 2004; AZAM ET AL.,2008; BARDELLI ET AL., 2011; YOKOYAMA ET AL., 2012; JONES & LOEPPERT, 2013; WINKEL ET AL., 2013; CATELANI ET AL., 2018), only a small number of reactive transport models that include all main geochemical processes have been performed to simulate As mobility (POSTMA ET AL., 2007; WALLIS ET AL., 2011; JESSEN ET AL., 2012; POSTMA ET AL., 2016; RAWSON ET AL., 2017; RATHI ET AL., 2017; JAKOBSEN ET AL., 2018, WALLIS ET AL., 2020). Besides, all these models do not observe calcite in their systems. Therefore, there is still a gap to provide a process-based quantification of the As mobility controlling processes.

Previous numerical and conceptual modelling approaches in Van Phuc (VAN GEEN ET AL., 2013; RATHI ET AL., 2017) seek to understand the mechanisms of As retention in the Pleistocene aquifer. The closest analog to the work presented here is a modelling approach reported by RATHI ET AL. (2017). However, the limited number of processes in that study did not clearly demonstrate hydrogeochemical changes in the Pleistocene deposits. Iron oxides are likely to play an important role in controlling As distribution in the aquifer. The As adsorption onto Fe oxides seemed to explain the observed data (RATHI ET AL., 2017). But the absence of the sorption processes onto calcite might lead to an overestimation of the adsorption rates onto Fe minerals und an underestimation of the residence time. This work extends the previous studies of As adsorption by investigating the effects of calcite on the As fate.

The study aims to investigate and quantify the impact of typical clogging minerals, especially calcite, on As mobility and elucidates the mechanisms of As retention in Van Phuc village. The issue of spatial variability at the village scale is revisited by conducting numerical modelling. A two-dimensional modeling approach is used to identify and assess factors controlling the spatial distribution of As in groundwater. The initial model development is guided by field data and hypothesized processes. Subsequently, a number of alternative conceptual models are observed. The objectives of this study are the following: (1) to determine the hydrogeochemical conditions in the aquifer, (2) to reconstruct hydrogeochemical processes at the boundary between the Holocene and Pleistocene aquifers, (3) to assess the As adsorption processes onto calcite and Fe oxides, and (4) to determine the contribution of calcite on As^{3+} retention.

2.2 MATERIALS AND METHODS

2.2.1 STUDY SITE. DATA SET DESCRIPTION

A requirement for performing reactive transport modeling is the availability of data sets that contain both, a detailed hydrogeological and a hydrogeochemical description. The model development is mainly based on a comprehensive data set collected by EICHE (2009). The research area is Van Phuc village, which is located approximately 10 km southeast of Hanoi on the banks of the Red River. The groundwater flow in the region is induced by large groundwater withdrawal for the municipal water supply of Hanoi (BERG ET AL., 2008).

Within the sedimentological context, two sedimentological settings are recognized here, which have a general meaning for As pollution. The aquifer consists of Holocene and Pleistocene sediments up to a depth of more than 40 m (EICHE, 2009). The unique factor of the study site is a juxtaposition of the sediments. The Pleistocene and Holocene aquifers are mainly composed of sand and gravel with a hydraulic conductivity equal to 1.1×10^{-3} m/s (WALLIS ET AL., 2020) (Figure 2).

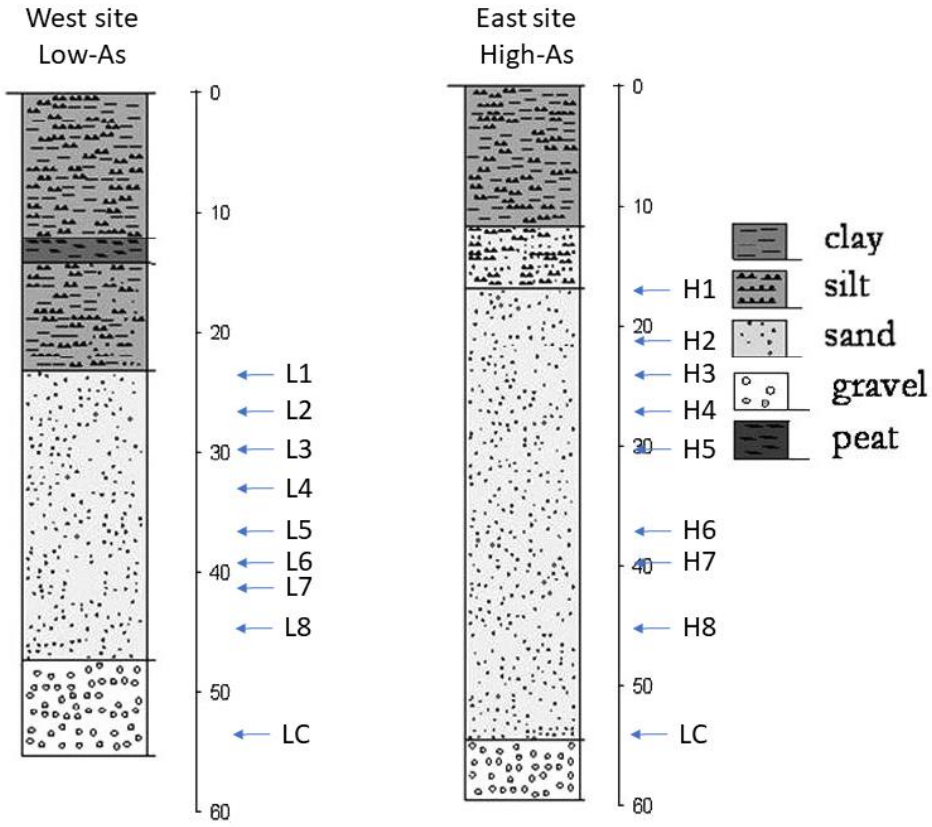

Figure 2. Hydrogeological profiles with the sampling locations from the west part and the east part of the aquifer (figure is provided by courtesy of E. Eiche).

The overlaying clayey silt layer with variable thickness is characterized by a low hydraulic conductivity (K_f: 7 x 10^{-8} m/s) and can be considered as aquitard (EICHE, 2009). Average flow velocity in the Van Phuc aquifer is between 1.2 x 10^{-6} m/s and 1.5 x 10^{-6} m/s (VAN GEEN ET AL., 2013). Information on hydraulic gradient, which is equal to 2.7 x 10^{-4} m/m, along the transect is taken from WALLIS ET AL. (2020). Based on the high groundwater ages of more than 15 years, EICHE (2009) suggested low recharge rates either by river or through surface water infiltration. STAHL ET AL. (2016) confirmed a low groundwater recharge rate at Van Phuc. The authors found that a massive clay layer on top of a sandy aquifer allows only very low recharge. Therefore, recharge is neglected in the model.

Dissolved As concentrations in Van Phuc vary greatly over short distances. Some of these variations are caused by differences in bulk sediment composition. High dissolved As concentrations are mainly related to young alluvial deposits (Holocene), whereas the older sediments (Pleistocene) host low dissolved As concentrations (BGS, 2001; EICHE, 2009; HOQUE ET AL., 2012; VAN GEEN ET AL., 2013; EICHE ET AL., 2017). The Holocene deposits cover mainly the southeast part of the study area, whereas the northwest part of the aquifer system is dominated by the Pleistocene deposits (Figure 3). The older

Pleistocene sediments are typically yellow-brown-orange in color with Fe oxides as minerals. The content of Fe in the sediment ranges between 2 wt-% and 5 wt-%. In contrast, the Holocene sediments are greyish to greenish in color with lower solid Fe concentration (EICHE, 2009).

The hydrochemistry is noticeably different at the two sites. In the western part of the village (low-As), the extracted groundwater contains less than 0.13 µmol/L of As. In the eastern portion (high-As), As concentration exceeds 2 µmol/L in most wells. The boundary between the low-As and high-As sites is assumed to have been shifted in response to groundwater extraction in Hanoi (Figure 3).

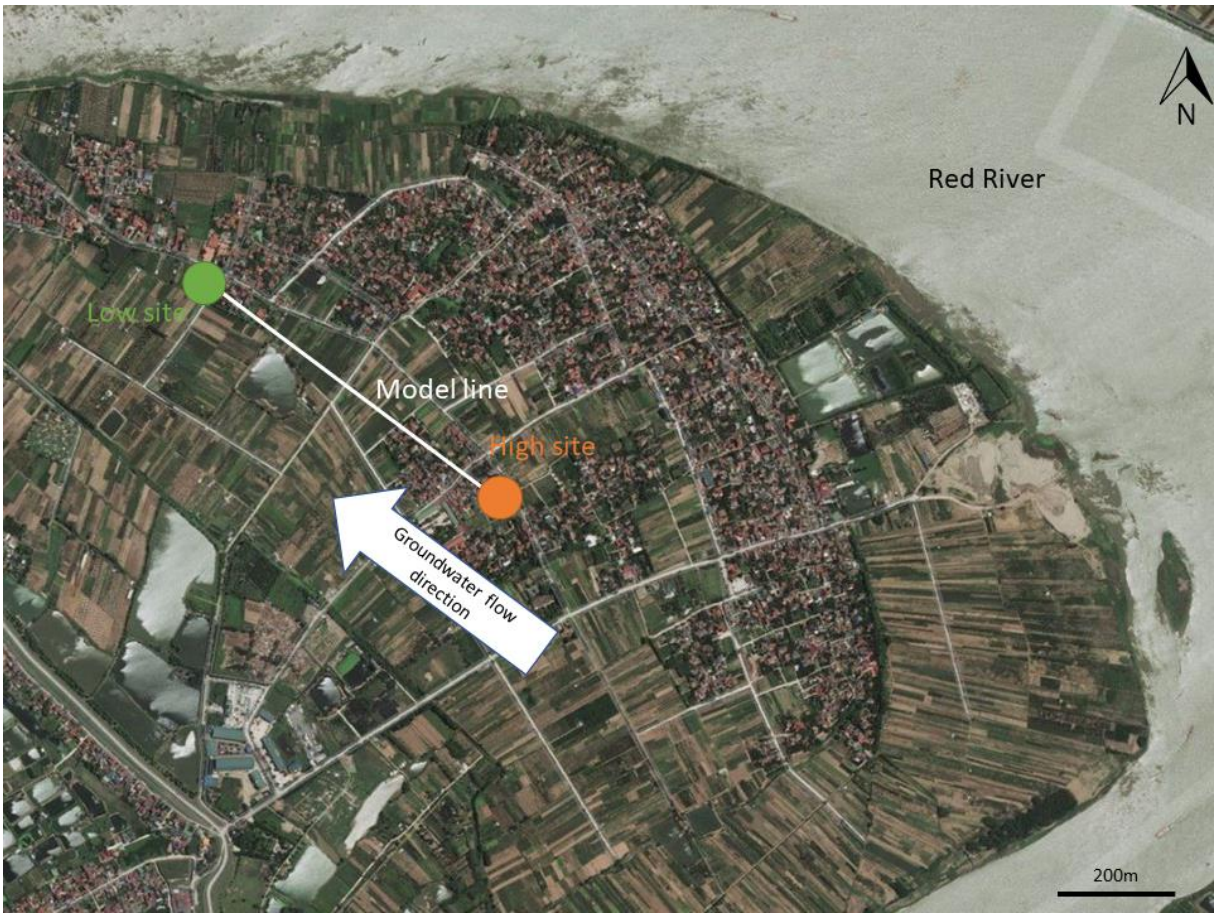

Figure 3. Map of Van Phuc village showing arsenic concentrations in groundwater (background image from: google.com/maps).

Two distinct hydrogeochemical zones are identified with sharp measured concentration gradients for Ca^{2+}, NH_4^+, Fe^{2+} and As correspond to low-As and high-As sites. Mean values of physical and chemical parameters of the groundwater samples are provided in Table 2.

Table 2. The hydrochemical composition of groundwater from the low-As and high-As sites. Mean measured concentrations of aqueous compounds (calculation is based on data from Eiche (2009), measured Apr 2006 (initial values are in Table A-1 and Table A-2)).

Parameter	Unit	High-As site	Low-As site
pH	[-]	7.0	6.6
pe	[-]	-2.2	1.1
DOC	[mmol/L]	0.16	0.06
Ca^{2+}	[mmol/L]	2.9	0.5
HCO_3^-	[mmol/L]	8.6	3.7
Fe^{2+}	[mmol/L]	0.22	0.02
Mn^{2+}	[mmol/L]	0.01	0.02
NO_3^-	[mmol/L]	<0.001	<0.001
NH_4^+	[mmol/L]	0.5	0.01
SO_4^{2-}	[mmol/L]	<0.001	0.06
As_{tot}	[µmol/L]	4.1	0.02
As^{3+}	[µmol/L]	3.9	0.02
PO_4^{3-}	[µmol/L]	4.2	0.6

Table 2 shows that the pH values of groundwater at both sites range from 6.6 to 7.1. The pH (7.0 ± 0.1) at the high-As site is slightly higher than at the low-As site (6.6 ± 0.2). The redox state has a major impact on the composition of groundwater in the study site. Based on NO_3^-, $Fe^{2+}$and SO_4^{2-} concentrations, the redox state at the high-As site can be considered as sulfate reducing. Under sulfate reducing conditions at the high-As site, As^{3+} is the main As species. The measurements conducted in the field indicate that >90% of the dissolved As is present as As^{3+}.

The redox species concentration profiles indicate a shift to more oxidizing conditions along the transect. Dissolved Fe^{2+} and As^{3+} concentrations decrease rapidly in the transect zone. The sharp reduction in DOC across the geological boundary from 0.16 mmol/L to about 0.06 mmol/L indicates rapid organic carbon mineralization.

At the high-As site, the HCO_3^- concentration is higher than at the low-As site, indicating CO_2 production coupled to microbial degradation of organic matter. The measured drop of Ca^{2+} concentration could correspond to calcite precipitation at the redox boundary.

In contrast to the low-As site, the groundwater at the high-As site is supersaturated with respect to calcite (Figure 4).

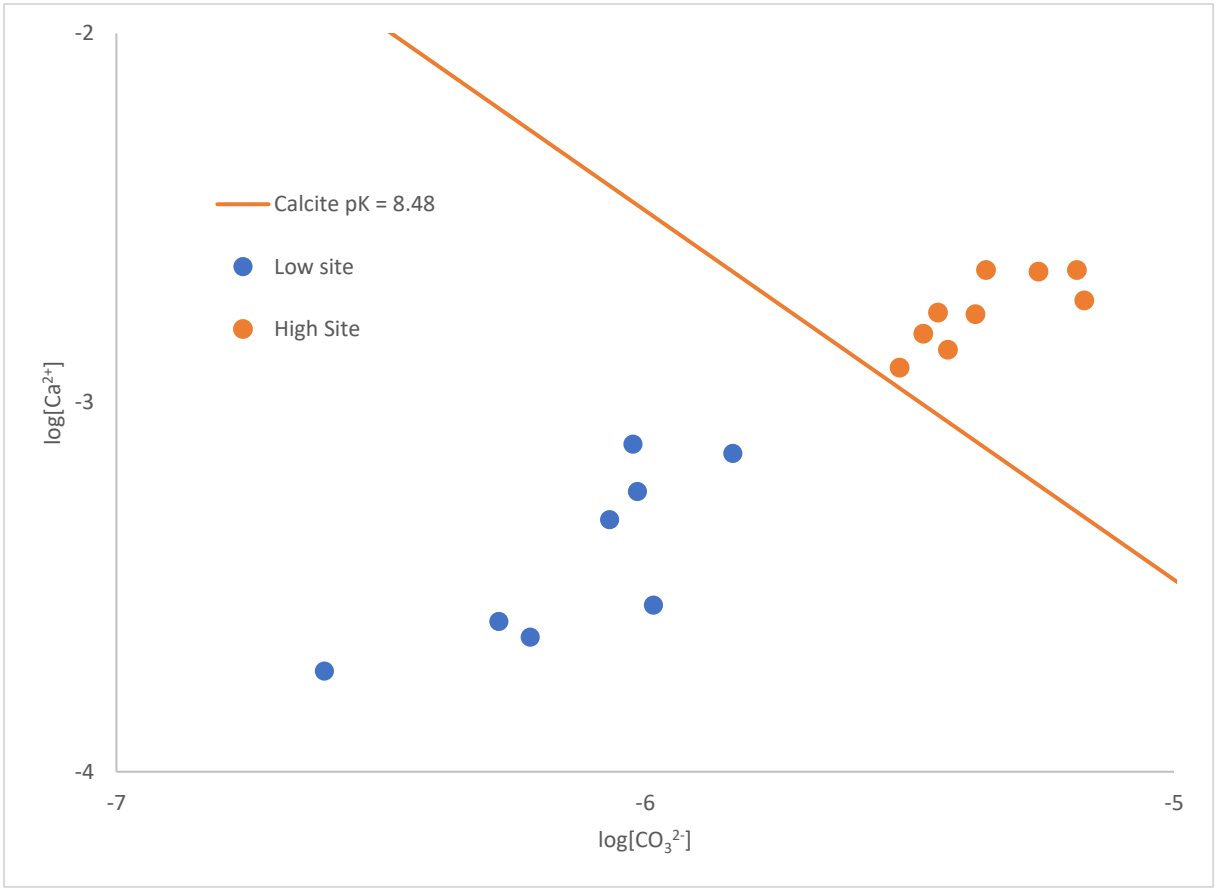

Figure 4. The activities of Ca^{2+}, CO_3^{2-} in groundwater as compared to the solubility products of siderite and calcite. The line indicates the stability for calcite, pK = 8.48 (based on data from Eiche (2009)).

Within the high-As site VAN GEEN ET AL. (2013) measured solid-phase Ca concentrations over 2.0 g/kg, while the Ca content at the low-As site was less than 0.1 g/kg.

The mobility and speciation of As in the aquifer are closely associated with hydrogeochemical processes. The delineation of redox boundary helps to estimate As intrusion into the Pleistocene aquifer.

2.2.2 CONCEPTUAL MODEL AND REACTION NETWORK IMPLEMENTATION

Based on the field data, a conceptual model is constructed in order to depict the fate of As. The spatial movement of As is accompanied by many hydrogeochemical reactions, among them, microbiological, sorption/desorption, precipitation/dissolution and redox processes.

Changes in groundwater and sediment composition linked to redox gradients and the behavior of As in response to changing redox conditions have been documented for numerous contaminated aquifers (ANAWAR ET AL., 2003; VAN GEEN ET AL., 2013; WALLIS ET AL., 2011; POSTMA ET AL., 2016). A redox boundary represents an important hydrogeochemical interface controlling the speciation and mobility of many compounds (APPELO & POSTMA, 2005; POSSEMIERS, 2014). The delineation of a redox boundary helps estimating the distribution of compounds and identifying hydrogeochemical processes (LEE ET AL., 2008). The speciation of As^{3+} and As^{5+} is assumed to be redox equilibrium controlled (SMEDLEY & KINNIBURG, 2002). At the study site, the microbiological degradation of organic matter coupled e.g. to the reduction of Fe oxides leads to the formation of various redox zones along the groundwater flow direction. Arsenic is preferentially mobile under reducing conditions, which have been developed the high-As site. Iron oxide reduction generally prevails in reduced environments, and it is widely accepted as an explanation for high dissolved As concentrations in anoxic groundwater (NICKSON ET AL., 2000; WANG ET AL., 2012). Based on the high measured Fe^{2+} concentration, As is believed to be mobilized into groundwater in the Holocene aquifer through the reductive dissolution of Fe oxides (EICHE, 2009). The As mobilization processes in the Holocene aquifer are not implemented into the modelling approach. The contamination at the high-As site is reflected in the models through groundwater inflow with the measured hydrochemical composition.

Adsorption of As on the sediment has been intensively investigated by field (HARVEY ET AL., 2002; VAN GEEN ET AL., 2013; RATHI ET AL., 2017) and laboratory (STOLLENWERK ET AL., 2007; BONTE ET AL., 2014) approaches. Most of the recent studies investigating As sorption focus on As^{5+} due to a higher sorption affinity in contrast to As^{3+}. Arsenic retention is more convoluted and controlled through specific hydrogeochemical conditions. However, at the current study site, As is primarily present as As^{3+}. Therefore, sorption of As^{3+} on various minerals is investigated in detail. The adsorption of As on Fe oxides is considered among the most important and widespread factors controlling the mobility and transport of As in groundwater (APPELO ET AL., 2002; STOLLENWERK ET AL., 2007; GUO ET AL., 2008; GUO ET AL., 2011; MAI ET AL., 2014). The distribution of As in groundwater is not solely controlled by a single solid phase. Besides, carbonate minerals, especially calcite, are ubiquitous in an aquifer and can trap ions and ion complexes (DAVIS ET AL., 2000; ALEXANDRATOS ET AL., 2007; YOLCUBAL & AKYOL, 2008; WINKEL ET AL., 2013; RENARD ET AL., 2015; XIAO ET AL., 2017). Adsorption processes play an important role in As retention in the Pleistocene aquifer (EICHE ET AL., 2010; VAN GEEN ET AL., 2013; RATHI ET AL., 2017). The observed As distribution is the effect of the As adsorption onto Fe oxides and calcite.

The hydrogeological and hydrogeochemical data form the basis of the conceptual site model. In the next step, the conceptual model is translated into a numerical reactive transport model. The numerical model is constructed using the PHAST code. WATEQ4F thermodynamic database is used in the calculations performed under equilibrium conditions.

The code includes also a two-layer surface complexation model of DZOMBAK & MOREL (1990) simulating the sorption of ions on ferrihydrite and calculating competitive sorption of species for the sorption site on ferrihydrite is implemented in the model.

2.2.2.1 Reaction network

A model is set up to schematically reflect the groundwater flow conditions described by VAN GEEN ET AL. (2013) and WALLIS ET AL. (2020). These investigations showed a relatively constant flow direction. The model is aligned with the main groundwater flow direction (from the southeast to northwest (Figure 3)). A 2D PHAST model is set up with 300 m in length and 40 m in depth. The model is discretized into 2 layers (Figure 5).

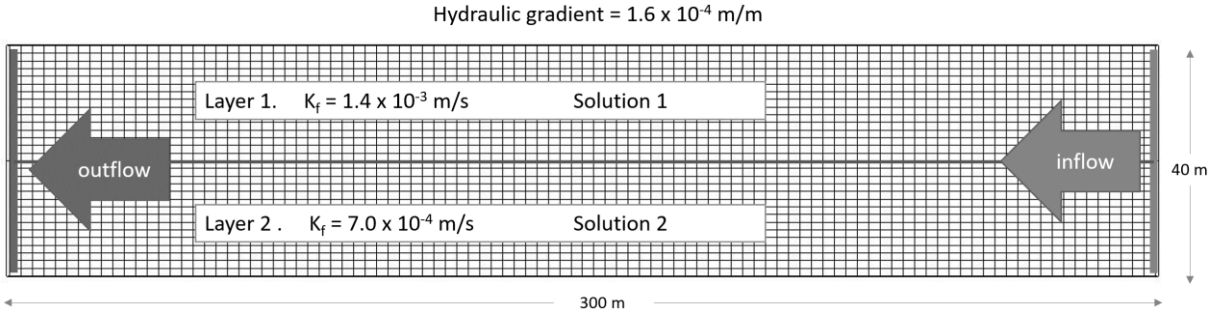

Figure 5. Numerical 2D reactive transport model for the Van Phuc aquifer, Vietnam. Model grid. Hydraulic conductivity values from Wallis et al. (2020)

Modelled initial hydrochemical compositions of solution 1 and 2 are listed in Table A-3. The model grid comprises 4,500 cells formed by 150 columns and 30 rows. The temporal discretization is 1 day. The model is run for 50 years corresponding to the simulation time by VAN GEEN ET AL. (2013). Based on WALLIS ET AL. (2020), the hydraulic gradient was linearly increasing over last 60 years, starting from 0 in 1950 to 2.7 x 10^{-4} m/m in 2010. The mean value calculated over last 50 years (1.6 x 10^{-4} m/m) is implemented via the constant head boundary conditions.

The groundwater flow model incorporates the transport parameters given by the authors (VAN GEEN ET AL., 2013; WALLIS ET AL., 2020). Table 3 represents main flow and transport parameters incorporated into the model.

Table 3. Groundwater flow and transport parameters used in the reactive transport model (based on data from Wallis et al. (2020)).

Parameter	unit	value
Model dimensions x * y	[m]	300 * 40
Discretization Δx	[m]	2
Discretization Δy	[m]	2
Hydraulic conductivity K_f x	[m/s]	1.1 x 10^{-3}
Effective porosity	[%]	20
Longitudinal dispersity	[m]	1
Horiz./Vert. transversal dispersivity	[m]	0.1

In agreement with WALLIS ET AL. (2020), a vertical anisotropy of 10 for hydraulic conductivity and homogeneous conditions for porosity is implemented.

The reactive transport model incorporates the mineralogical data from EICHE (2009) and VAN GEEN ET AL. (2013) along with the observed hydrochemical groundwater compositions (Table A-1 and Table A-2). The hydrochemical compositions that are used to define the initial concentrations in the model are based on the data collected by EICHE (2009) (Table A-3).

The most important process governing the major ion and redox chemistry is oxidation of DOC, coupled to the reduction of electron acceptors, mainly NO_3^- and SO_4^{2-}. Calcite and $Fe(OH)_3$ are included in the reaction network as the main phases controlling hydrogeochemical situation in the aquifer.

The reaction network controlling As mobility in groundwater is developed with a focus on three key processes: (1) the sorption of As onto Fe oxides, (2) the sorption of As onto newly formed and also existing calcite, and (3) competitive sorption effects of PO_4^{3-} and HCO_3^-. The conceptual model is presented graphically in Figure 6.

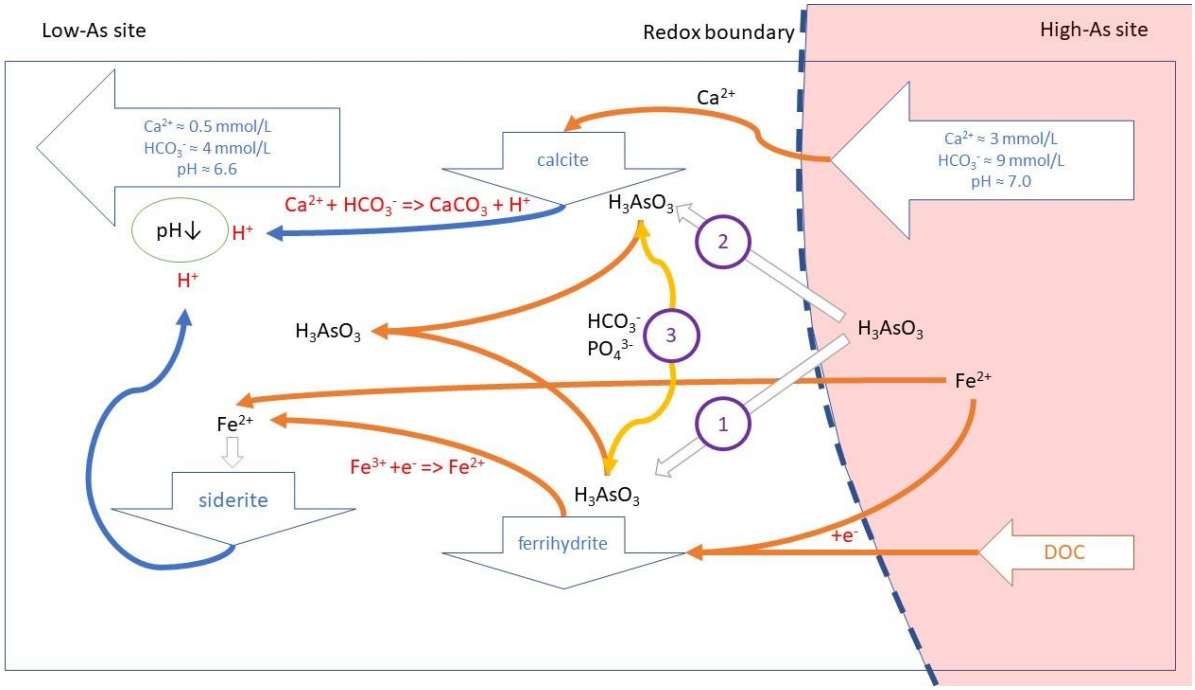

Figure 6. Conceptual model. Hydrogeochemical processes controlling the groundwater composition and arsenic distribution.

The sorption of As is assumed to occur on the surfaces of calcite and $Fe(OH)_3$. Ferrihydrite and calcite are chosen as principal adsorbents, because they are relatively abundant in the sediment samples and widely reported by former studies. Adsorption reactions are controlled by the total amount of reactive sites. The dynamic changes in the sorption capacity that result from the precipitation and dissolution of the minerals play a key role in explaining the observed As distribution. Total number of sorption sites on the surfaces of these minerals is stoichiometrically linked with simulated mineral concentrations. In the model, precipitation/dissolution processes lead to the changes in sorption capacities.

In the current study one of the most difficult aspects is to identify and describe the sequence and combination of the hydrogeochemical processes at the redox boundary. Organic matter degradation at the high-As site increases the CO_2 partial pressure. The changing redox state from Fe-reducing at the high-As site to Mn-reducing at the low-As site leads to the reduction of CO_2 partial pressure through the mixing of the water at the boundary, which accelerates the precipitation of carbonate minerals, especially calcite, at the redox boundary. The sharp drop of dissolved Ca^{2+} concentration suggests that calcite precipitation takes place at the redox boundary. The conceptual model is extended to calcite as a sorption site for As.

The construction of models is based on the hydrogeochemical conceptualization of the processes identified in the study aquifer, which contains a significant degree of

uncertainty. Therefore, the conceptual model is investigated through varying the contributions of each process. Different scenarios are simulated. To quantify the impact of each process on the As distribution in the aquifer, three numerical models of different complexity are created (Table 4).

Table 4. Numerical models including primary hydrogeochemical processes. Scenarios analysed in the case study.

	(1) Adsorption onto ferrihydrite	(2) Adsorption onto calcite	(3) Competition processes with HCO_3^- and PO_4^{3-}
Model 1	x		
Model 2	x	x	
Model 3	x	x	x

2.2.2.2 Model 1. Adsorption of As onto Fe oxide

Initial modeling considers only adsorption processes of As^{3+} onto ferrihydrite. The surface complexation reactions that are implemented into the model are based on the model of STOLLENWERK ET AL. (2007) and RAWSON ET AL. (2017). The equilibrium constants for each surface complexation process are listed in Table 5. Surface complexation reactions also include the protonation as well as deprotonation of the surface.

Table 5. Reaction network implemented into the model. (Formulas for adsorption reaction of As^{5+} and As^{3+}). Hfo_wOH represents weak sorption onto Fe oxides.

Reaction	Log K	Reference
$Hfo\_wOH + H^+ = Hfo\_wOH_2^+$	7.43	Stollenwerk et al. (2007)
$Hfo\_wOH = Hfo\_wO^- + H^+$	-7.03	Stollenwerk et al. (2007)
$Hfo\_wOH + AsO_3^{3-} + 3H^+ = Hfo\_wH_2AsO_3 + H_2O$	37.65	Rawson et al. (2017)
$Hfo\_wOH + AsO_3^{3-} + 2H^+ = Hfo\_wHAsO_3^- + H_2O$	31.52	Rawson et al. (2017)
$Hfo\_wOH + AsO_3^{3-} + H^+ = Hfo\_wAsO_3^{2-} + H_2O$	30.01	Stollenwerk et al. (2007)
$Hfo\_wOH + AsO_4^{3-} + 3H^+ = Hfo\_wH_2AsO_4 + H_2O$	30.66	Stollenwerk et al. (2007)
$Hfo\_wOH + AsO_4^{3-} + 2H^+ = Hfo\_wHAsO_4^- + H_2O$	22.34	Stollenwerk et al. (2007)
$Hfo\_wOH + AsO_4^{3-} + H^+ = Hfo\_wAsO_4^{2-} + H_2O$	8.70	Stollenwerk et al. (2007)
$Hfo\_wOH + PO_4^{3-} + 3H^+ = Hfo\_wH_2PO_4 + H_2O$	31.03	Rawson et al. (2017)
$Hfo\_wOH + PO_4^{3-} + 2H^+ = Hfo\_wHPO_4 + H_2O$	22.00	Rawson et al. (2017)
$Hfo\_wOH + PO_4^{3-} + H^+ = Hfo\_wPO_4 + H_2O$	19.55	Rawson et al. (2017)
$Hfo\_wOH + CO_3^{2-} + H^+ = Hfo\_wCO_3^- + H_2O$	12.78	Appelo et al. (2002)
$Hfo\_wOH + CO_3^{2-} + 2H^+ = Hfo\_wHCO_3 + H_2O$	20.37	Appelo et al. (2002)

The density of weak sites on the Fe oxides is from RAWSON ET AL. (2017) and equals to 1.31 x 10^{-2} mol of sites per mol of Fe. Iron oxides are thermodynamically stable under oxidizing conditions. The reductive dissolution of Fe oxides leads to a diminishing number of sorption sites. Microbially induced reduction of Fe oxides is most widely accepted as a key step in the mobilization of As in groundwater (NICKSON ET AL., 2000; SMEDLEY & KINNBURG, 2002; HARVEY ET AL., 2002; DIXIT & HERING, 2003; SWARTZ ET AL., 2004; POSTMA ET AL., 2007).

At the low-As site, Fe oxides reduce As mobility through the adsorption processes of As^{3+} and the generation of new sorption sites on the neo-formed minerals. However, the reductive dissolution of Fe oxide, mainly ferrihydrite, is the main process mobilizing freshly adsorbed As from the sediment. Ferrihydrite is the main electron acceptor considered in this approach (PONNAMPERUMA ET AL., 1967):

$$Fe(OH)_3\ (s) + 3H^+ + e^- => Fe^{2+} + 3H_2O \qquad (1)$$

The reaction couples the oxidation of organic carbon to the reduction of Fe oxide while releasing As. In the present model the degradation of organic matter is equilibrium

controlled. The newly released As^{3+} can be adsorbed onto minerals (calcite, ferrihydrite and goethite) also as described with the surface complexation model.

Like in RAWSON ET AL. (2017), two types of Fe oxides are incorporated into the model: easily reducible (ferrihydrite) and non-easily reducible, more crystalline (goethite) phases. Ferrihydrite is an ubiquitous mineral in deltaic sediments and is abundant in the study aquifer (EICHE, 2009). It has a very high specific surface area (around 600 m^2/g), so it has a very high adsorption capacity for As (STOLLENWERK ET AL., 2007). Arsenic is adsorbed more readily to amorphous rather than crystalline Fe minerals, due to a larger surface area. Goethite is more crystalline than ferrihydrite and has an about 10 times smaller surface area (APPELO & POSTMA, 2005). While the reductive dissolution of ferrihydrite leads to Fe^{2+} release, it can also be considered as possibility of Fe^{2+} for precipitation of siderite and goethite (HANSEL ET AL., 2003; HORNEMAN ET AL., 2004). At an aquifer storage and recovery site in Florida, WALLIS ET AL. (2011) showed that the mobilized Fe^{2+} forms preferentially complexes with carbonate and precipitated as siderite. Most of the samples in the Holocene aquifer show pH values around 7.0 indicating the neutral characteristic of the groundwater. The samples from the Pleistocene aquifer have pH below 7.0, which could be maintained by siderite and goethite precipitation. The sampled data do not exclude a contribution of goethite to As retention, but its role is most likely secondary.

2.2.2.3 Model 2. Adsorption of As onto calcite

The second model extends model 1 by addition of the adsorption processes of As onto calcite.

Despite the widespread presence of carbonate minerals in aquifers, knowledge about sorption of As on these minerals is limited. The possible role of calcite in sequestering As has been considered only by a few studies (ROMAN-ROSS ET AL., 2006; BI BENEDETTO ET AL., 2006; ALEXANDRATOS ET AL., 2007; SØ ET AL., 2008; YOKOYAMA ET AL., 2009; BARDELLI ET AL., 2011; RENARD ET AL., 2015). YOKOYAMA ET AL. (2009) showed that calcite adsorbs mainly As^{5+}. However, several studies have pointed out that calcite can also adsorb As^{3+} or co-precipitate (ROMAN-ROSS ET AL., 2006; JONES ET AL., 2013). On the other hand, it remains controversial whether calcite can immobilize As^{3+} (SØ ET AL., 2008; YOKOYAMA ET AL., 2009). SØ ET AL. (2008) observed in their batch experiments little or no As^{3+} sorption on calcite at low (< 5 μmol/L) dissolved As^{3+} concentrations.

Calcite has been implicated as playing an important role in the retention of As^{3+} where Fe oxides have lost their adsorbing capabilities, especially when groundwater is supersaturated with respect to calcite (DI BENEDETTO ET AL., 2006; RENARD ET AL., 2015). SADIQ (1997) suggested that carbonates play an important role for As adsorption at pH between 7.5 and 9. The point of zero charge (PZC) of calcite has been shown by MISHRA

(1978) to be near pH of 8.2. Below the PZC the positively charged calcium-hydroxyl species (>$CaOH^{2+}$) are dominant at the surface of the mineral. At higher pH the adsorbing effect of calcite should be minor, due to the PZC of calcite that changes to neutral or even negative values. Concentrations of As^{3+}in synthetic calcite can exceed 2 g/kg (ROMAN-ROSS ET AL., 2006). In natural calcite As concentrations vary between 120 - 190 mg/kg (COSTAGLIOLA ET AL., 2007). WINKEL ET AL. (2013) measured 913 mg As /kg in travertine.

At the study site, the measured drop of Ca^{2+} concentration along the groundwater flow gives information about calcite precipitation at the redox boundary. An increasing calcite amount can significantly enhance As retention and probably does markedly contribute to the observed distribution of As in the study site. The consequences of As uptake by calcite are of considerable relevance because of the ubiquity of this mineral in the study aquifer and its stability, especially under reducing condition. Therefore, calcite can represent an effective agent for As retention. The immobilization of As^{5+} by calcite can also occur by complexation with Ca^{2+} (BOTHE & BROWN, 1999; YOKOYAMA ET AL., 2012). In the study aquifer, As is mainly present as As^{3+}. Therefore, the complexation processes with Ca^{2+} observed by the authors (BOTHE & BROWN, 1999; YOKOYAMA ET AL., 2012) are neglected.

Unfortunately, WATEQ4F database does not comprise constants for the sorption of As onto calcite. Freundlich isotherms for the adsorption of both As^{3+} and As^{5+} on calcite have been reported for As concentration range of 1 - 100 µmol/L (JONES ET AL., 2013). The authors showed that the adsorption of As^{5+} was over 80% of the initial concentration compared to 50% for As^{3+}. To calculate As adsorption on calcite, these sorption rates are incorporated into the model.

Dynamic changes in the sorption capacity of ferrihydrite and calcite during precipitation and dissolution processes play a key role in the mobility of As. These interactions are modeled by coupling the amount of the surface complex sites to the mass of ferrihydrite in the model. The number of sorption sites on the minerals is used as a fitting parameter.

2.2.2.4 Model 3. Competitive sorption

The third model extends model 2 through addition of competition processes for the sorption sites on ferrihydrite.

The As retention capabilities of the Pleistocene deposits are reduced through the reductive dissolution and transformation of Fe minerals towards more stable phases. Furthermore, competition processes cause mobilization of As.

Competitive ion displacement can represent an important process by which As is mobilized. The influence of competing ions, mainly PO_4^{3-} and HCO_3^-, on the sorption of

As has been observed in different studies (KIM ET AL., 2000; APPELO ET AL., 2002; SWARTZ ET AL., 2004; ANAWAR ET AL., 2003). Both ions show strong affinity for the potential competition with both As^{3+} and As^{5+}. The high measured concentrations of HCO_3^- (8.6 mmol/L) and PO_4^{3-} (4.2 µmol/L) in the high As groundwater is the major argument to include both in the conceptual model.

2.3 RESULTS

In the first step, the model calibration is performed using the observed hydrochemical composition at both sites.

Reducing conditions establish due to organic matter degradation at the high-As site, which explains the presence of As^{3+} and Fe^{2+}. The model results illustrate how reduced groundwater penetrates the aquifer. Consequently, reducing conditions enhance the As mobilization. A possible source of As at the high-As site are Fe oxides that dissolve (EICHE, 2009). The model results for both sites are presented as full lines together with the field data in Figure 7.

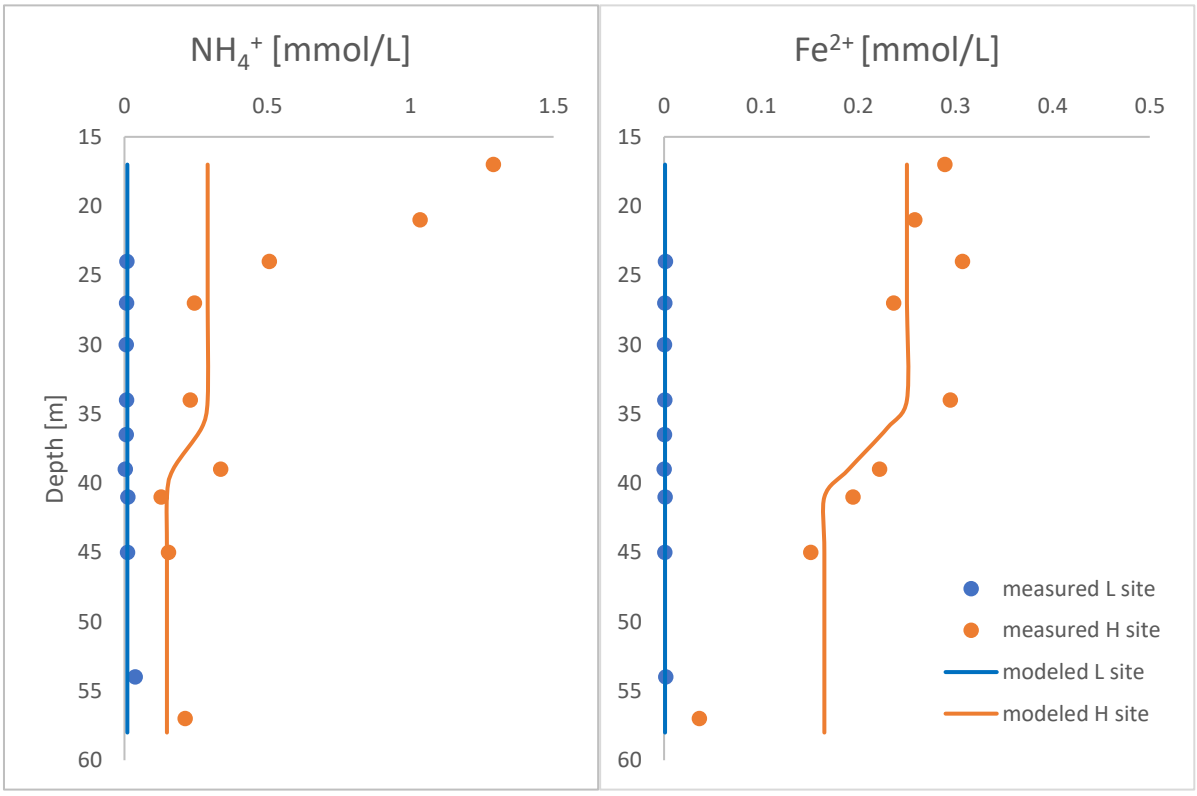

Figure 7. The groundwater hydrochemistry at both sites. The depth distribution of Fe^{2+} and NH_4^+ concentrations in the groundwater. The solid lines reflect model predictions (measured data from Eiche (2009)).

Elevated NH_4^+ concentrations are simulated at the high-As site, while N_2 dominates at the low-As site. Organic rich intervals at depths between ~15 m and ~20 m within the

upper silty layer are not implemented in the model. Therefore, the quantitative agreement between the observed results and model predictions for NH_4^+ in this section is lower. Concentrations of NH_4^+, Fe^{2+} (Figure 7) and HCO_3^- (Figure 8) all suggest microbial degradation of organic matter that is most pronounced in the upper part of the profile at the high-As site and decreases in intensity with depth.

These changes in the hydrochemistry are combined with the oxidation of organic matter coupled to the reduction of Fe oxide (APPELO & POSTMA, 2005):

$$CH_2O + 4FeOOH + 7H^+ => 4Fe^{2+} + HCO_3^- + 6H_2O \quad (2)$$

Ferrihydrite acts as main electron acceptor at the low-As site. The influence of other electron acceptors is small due to the low concentrations. The reaction increases the Fe^{2+} concentrations in the aquifer. The simulated reduction of Fe^{2+} concentration from 0.25 mmol/L to less than 0.1 mmol/L is the result of the reprecipitation of Fe minerals, especially siderite and goethite.

Significant changes in groundwater chemistry that are observed as a function of calcite precipitation comprise reduction in dissolved Ca^{2+} concentration from 3.0 mmol/L to 0.2 mmol/L in the upper part of the aquifer, as well as a decrease in HCO_3^- concentrations declining from 9.0 mmol/L to about 2.5 mmol/L (Figure 8). Concentrations of HCO_3^- reflect the degree of groundwater-sediment interaction as well as microbial mediated organic matter degradation.

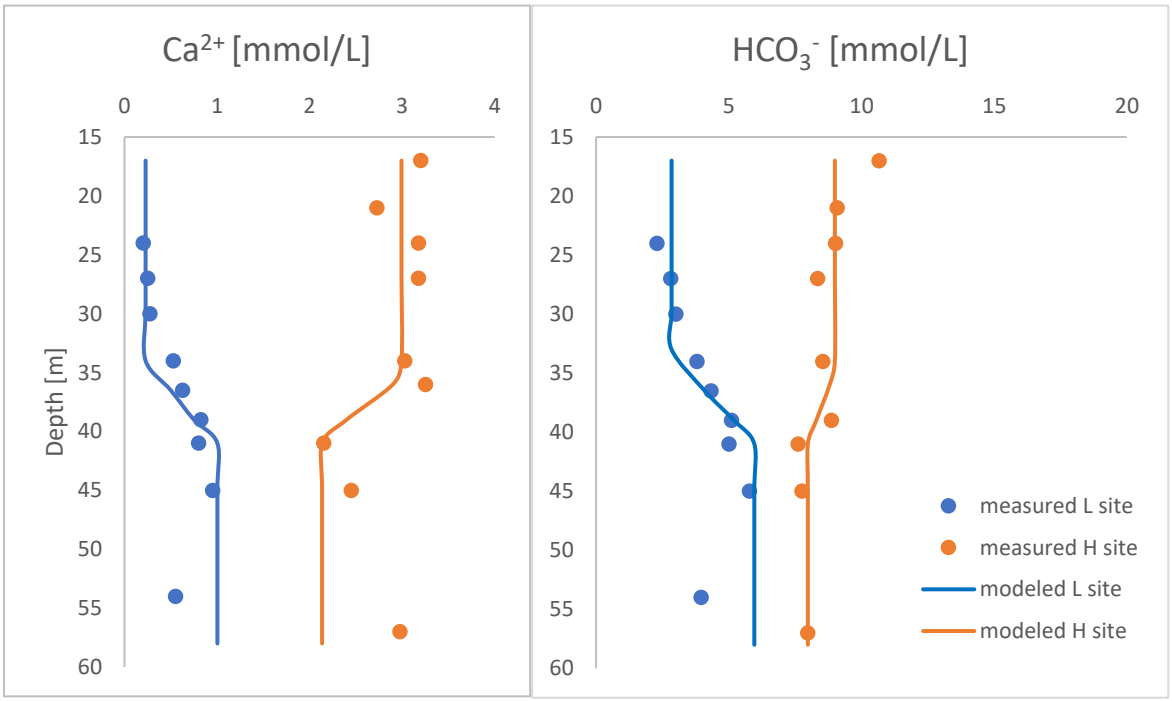

Figure 8. The groundwater hydrochemistry at both sites. The depth distribution of Ca^{2+} and HCO_3^- concentrations in the groundwater. The solid lines reflect model predictions (measured data from Eiche (2009)).

The increase in pH caused by the dissolution of Fe oxides induces calcite precipitation (Equation 3). On the other hand, the lowering in the CO_2 partial pressure, which is coupled to the reduction of Fe oxides, intensifies calcite precipitation. Calcite precipitation takes place at the redox boundary and explains the reduction of Ca^{2+} concentration. The formation of calcite from a saturated solution can be represented:

$$Ca^{2+} + HCO_3^{2-} = CaCO_3 + H^+ \quad (3)$$

Associated major changes are found also in the saturation indices of calcite (Figure 4). In contrast to the Low-As site, calculation of saturation indices showed that the groundwater at the high-As site is supersaturated with respect to calcite. Oversaturation of the groundwater with respect to calcite at the high As site can be attributed to the presence of inhibitors (PO_4^{3-} and a high CO_2 partial pressure). The distribution of Ca^{2+} and HCO_3^- concentrations shows larger amounts of $CaCO_3$ precipitations in the upper part of the aquifer (Figure 9).

Figure 9 shows the distribution of the redox boundary during the simulation time (t_0 and t_{50} – at the simulation start and after 50 years, respectively). In the model, for simulation of redox reactions the thermodynamic PHREEQC database is used. Therefore, the redox boundary represents sharp transition between reducing (pe<0) and oxic (pe>0) conditions. Significant differences in the As contamination movement are coupled to the depth variations of related hydrogeochemical composition of groundwater intruding the low-As site.

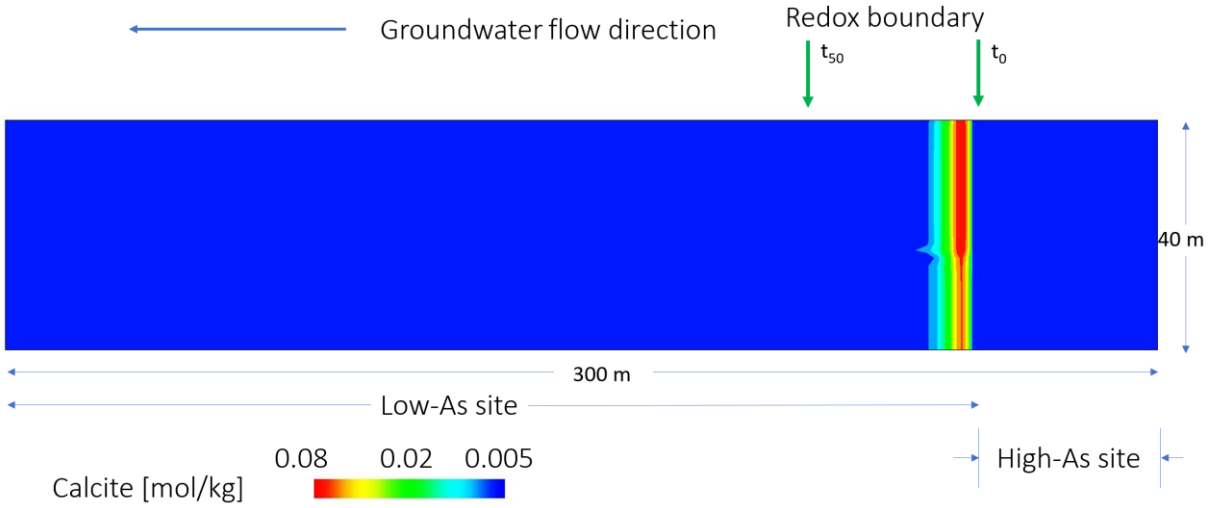

Figure 9. Modelled calcite distribution in a cross-section in the Van Phuc aquifer. The simulation time spans 50 years. The redox boundary position after 0 and 50 years is shown by arrows t_0 and t_{50}, respectively.

Groundwater As concentrations have a variable spatial distribution in the model (Figure 10), with concentrations ranging from 0.1 to 6.0 μmol/L. The model results show that As^{3+} is the dominant species. More than 90% of As in the groundwater is present as As^{3+}. The dissolved As concentrations is declining with depth, and so is the Fe^{2+} concentration.

This suggests that the processes that mobilize As and Fe^{2+} at the high-As site are coupled. Arsenic concentrations at the high-As site range between 3 µmol/L and 4 µmmol/L. The results provide a deeper understanding of the observed dissolved distribution of As and its evolution over a period of 50 years (Figure 10).

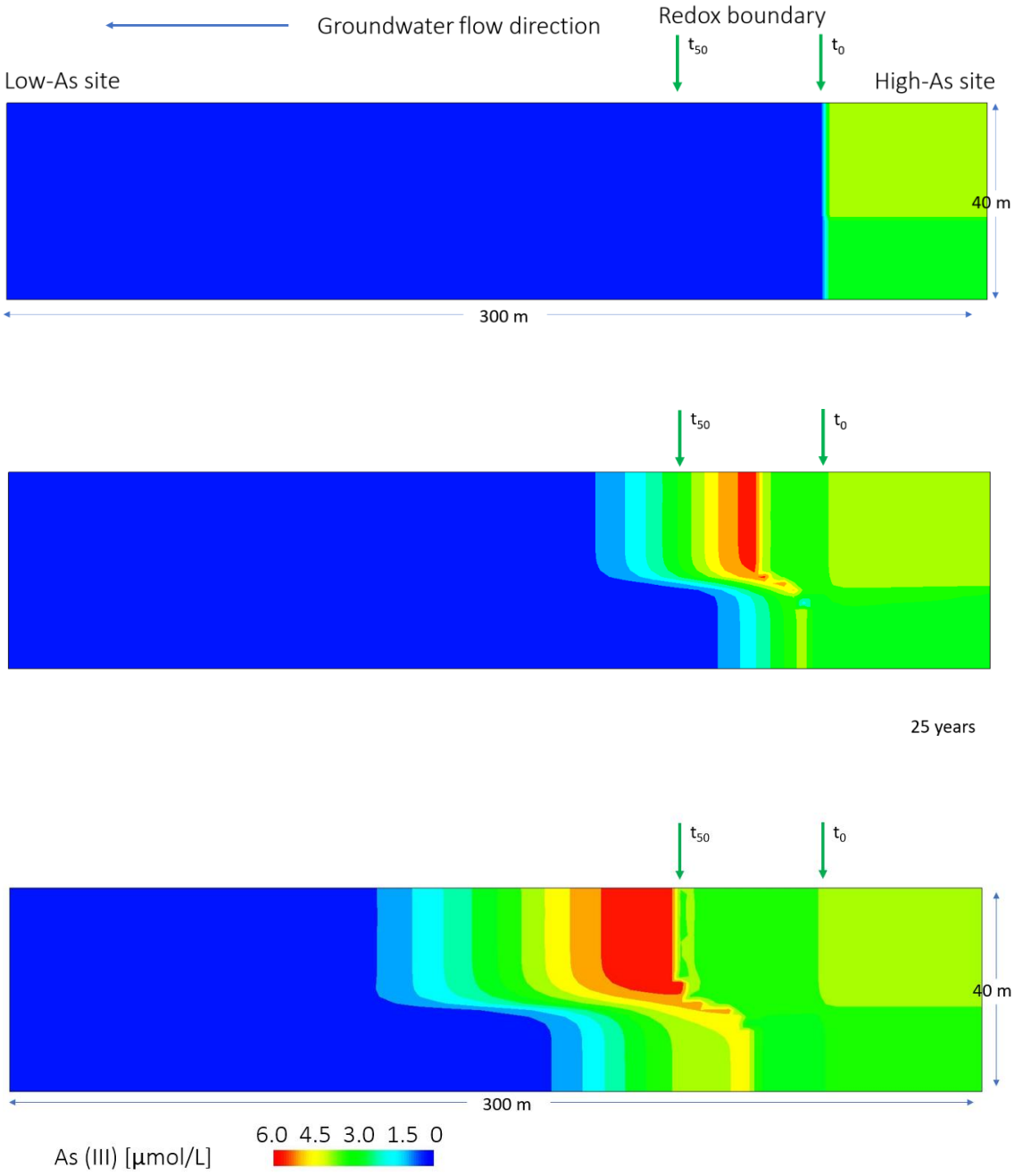

Figure 10. Arsenite distribution in a cross-section in the Van Phuc aquifer. The simulation results after 0, 25 and 50 years. The redox boundary position after 0 and 50 years is indicated by arrows t_0 and t_{50}, respectively.

The extent of As pollution in the aquifer is controlled by the distribution of Fe oxide reducing processes. When As-rich ferrihydrite undergoes reductive dissolution, As is mobilized along with Fe^{2+} and HCO_3^-. High As concentrations in Figure 10 allocate the zone of Fe oxide reduction and coupled As mobilization.

The dissolved As concentration is gradually decreasing along the groundwater flow path (Figure 11). The model results reflect a reduction along the flow path at the redox boundary induced by sorption processes. The comparison of the field measurements and model results show similar As levels.

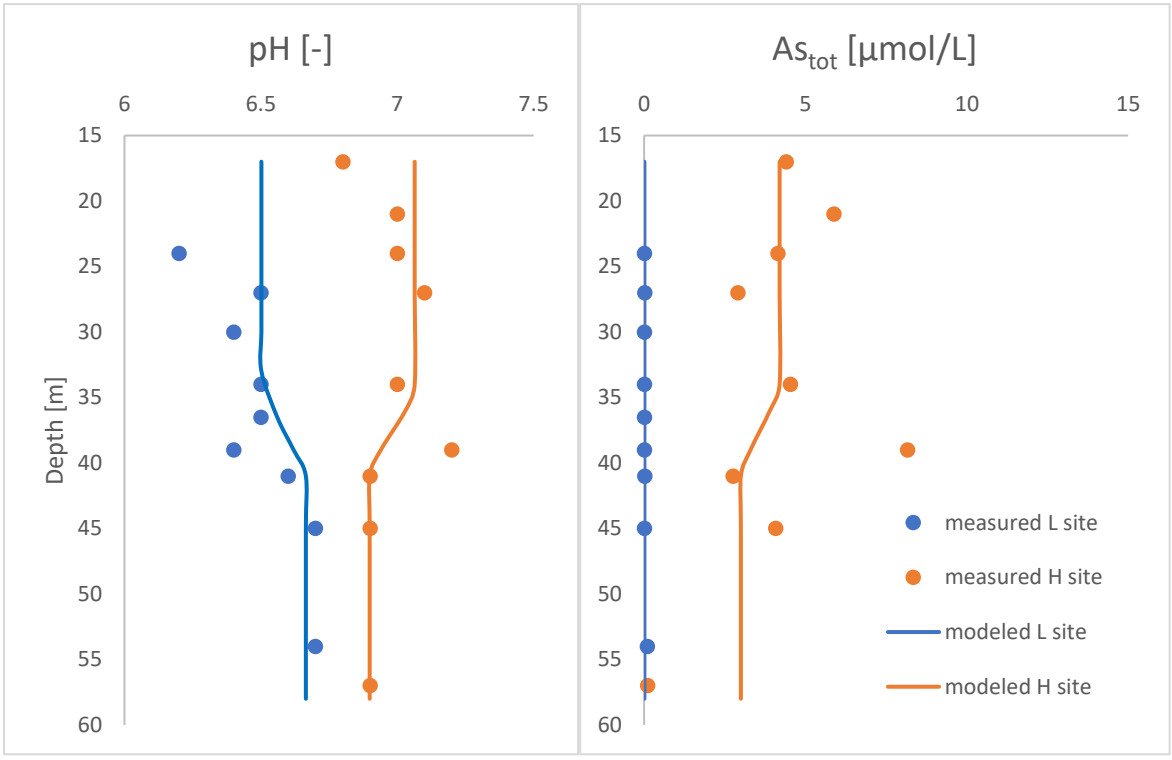

Figure 11. The groundwater hydrochemistry at both sites. The depth distribution of arsenic concentration and pH in the groundwater. The solid lines reflect model predictions (measured data from Eiche (2009)).

Precipitation of calcite, green rust, siderite and goethite lowers Ca^{2+} and Fe^{2+} concentration at the low-As site. The precipitation of Fe oxide leads to a sharp pH reduction at the area next to the redox boundary (Equation 1, 4 and Figure 12). In Figure A-1, Figure A-2 and Figure A-3 the simulated distribution of Ca^{2+}, NH_4^+ and pH over the past 50 years are presented.

$$FeOOH + 3H^+ + e^- = Fe^{2+} + 2H_2O \quad \text{(HASHIMOTO \& MISAWA, 1973)} \qquad (4)$$

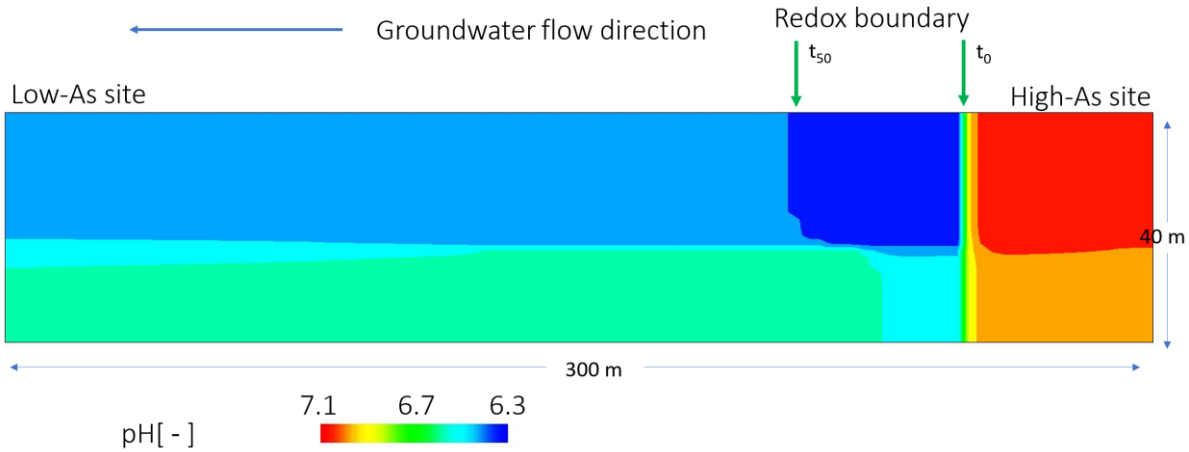

Figure 12. The distribution of pH in a cross-section in the Van Phuc aquifer. The simulation time equals to 50 years. The redox boundary position after 0 and 50 years is indicated by arrows t_0 and t_{50}, respectively.

The redox zonation varied as a result of the hydrogeochemical differences, which were described in detail by EICHE (2009) between the high-As and the low-As sites. The observed hydrochemical pattern suggests microbial degradation of organic matter as an important process, which is most pronounced in the upper part of the profile and decreases with depth. Iron oxide acts as electron acceptor by organic degradation. Microbial oxidation of organic matter and coupled reductive dissolution of Fe oxide are the important processes remobilizing As.

Quantitative agreement between the observed results and model predictions is high. Overall, the calibrated reactive transport model reproduced closely the observed hydrochemical patterns at both sites. The calibrated model serves as the basis for the scenarios.

Comparison of the conceptual models

In this part, the effects of previously hypothesized processes in the conceptual model on the As retention in Van Phuc are quantified. Numerical models of different complexity are used to assess the influence of each process on the As retention in the aquifer. Figure 13 illustrates the results of simulated As concentration profiles to varying hydrogeochemical conditions after 50 years. The results illustrate a strong impact of Fe oxide and calcite as well as a significant impact of the PO_4^{3-} and HCO_3^- concentrations on As retardation rates within the Pleistocene aquifer. The way to present the results of the conceptual models is to plot the As concentration as a function of space (Figure 13). The figure shows the distribution of dissolved As concentration in the upper part of the aquifer.

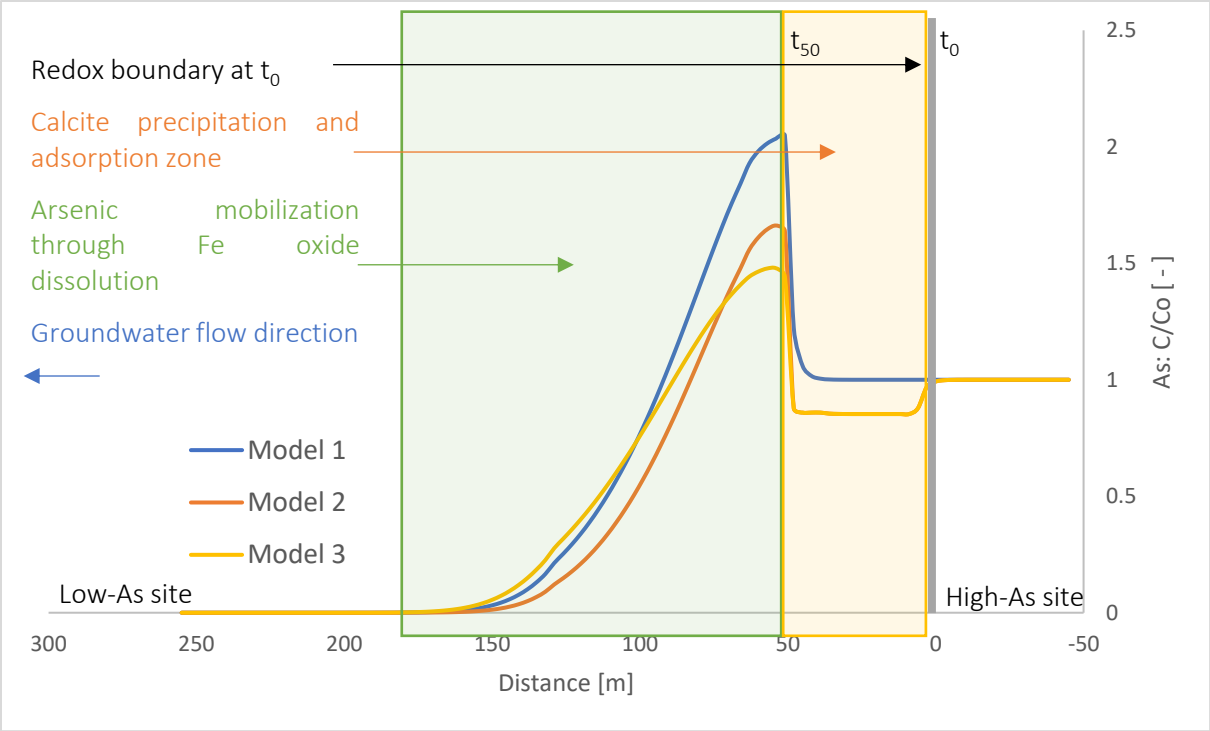

Figure 13. Arsenic concentration profile along the groundwater flow path. The As concentration is normalized to the concentration in the Holocene aquifer in the upper part (c_0 = 4 µmol/L). Model 1: sorption onto ferrihydrite; model 2: sorption onto ferrihydrite and calcite; model 3: sorption onto ferrihydrite and calcite including competition processes with PO_4^{3-} and HCO_3^-. In model 2 and 3, the reduction of As concentrations in the calcite precipitation zone by around 20 % is observed.

High As concentrations are mainly observed in the reductive zone near to the redox boundary. Induced by the organic matter degradation, the reductive dissolution of $Fe(OH)_3$ leads to a reduction of sorption sites and As mobilization. Protection against lateral migration of As into the Pleistocene aquifer is provided by the sorption onto Fe oxides and calcite. The transport of As is strongly retarded by sorption processes. The penetration distance of the As contamination after 50 years is equal to 150 m. Arsenic retention occurs upon a transition from reducing to oxidizing conditions.

Initial model simulations included only the adsorption of As onto Fe oxide. In the next model, As adsorption onto calcite is implemented. As a result, model 1 is revised to include the As adsorption onto calcite. In comparison to model 1, the results in model 2 shows increasing over time influence of calcite on As retention. The revised model showed the reduction of dissolved As concentration at the redox boundary. The results are consistent with a strong coupling between calcite precipitation and As retention. The precipitated minerals control the retention of As^{3+}, and newly released As into the aquifer as organic matter reduces Fe oxides. Calcite precipitation takes place at the moving towards redox boundary during the whole simulation period over 50 years.

Subsequently, the total mass of calcite and the associated sorption capacity successively increased over time. This resulted in increasing attenuation of As due to sorption onto calcite. Therefore, the reduction of As concentration in the groundwater during the first 15 years reflects the adsorption of As mainly onto Fe oxide. The effect of calcite on the As retention is more pronounced in the period between 15 and 50 years. In the calcite precipitation zone, As concentrations decline by 20 % from 4.0 μmol/L to about 3.2 μmol/L in the calcite precipitation zone as well as in the peak at the redox boundary from 8.0 μmol/L to about 6.4 μmol/L. Therefore, ferrihydrite adsorbs about 80 % of As. In this period Fe oxides get reduced while calcite remains stable. The rate of precipitation and spread of the precipitation zone depend on the transport velocities of the reactants into the Pleistocene aquifer. In comparison to model 2, the results in model 3 show that PO_4^{3-} and HCO_3^- strongly compete with As for surface site and have been shown to inhibit As adsorption by Fe oxides. The competition processes caused a decrease in As adsorption and resulted in lower dissolved As concentrations at the redox boundary.

All three models show a sharp increase of dissolved As concentration at a distance of around 50 m. This peak in dissolved As concentration is due to the release of As coupled to the reduction of ferrihydrite. Iron oxide reduction induced through DOC oxidation caused the release of newly adsorbed As. The modeling results imply that the hydrogeochemistry of the aquifer system is not in steady-state. Shifts in the redox state arising from the reduction of Fe oxides are responsible for rapid chemical changes in groundwater.

2.4 DISCUSSION

The approach presented here extends previous works (VAN GEEN ET AL., 2013; RATHI ET AL., 2017), which considered As retention in the Pleistocene aquifer in Van Phuc, by examining the adsorption of As onto calcite. VAN GEEN ET AL. (2013) derived the adsorption properties by determining the in-situ retardation using a conceptual site model. In their model, the obtained intrusion distance of the As plume into the Pleistocene aquifer over the last 50 years is equal to about 150 m. RATHI ET AL. (2017) performed modelling approach to simulate the results of laboratory experiments. In the next step, the model was used to estimate the As retention in the village Van Phuc. RATHI ET AL. (2017) found that the As adsorption onto Fe oxides can explain the measured retardation of the As contamination in the Pleistocene aquifer documented by VAN GEEN ET AL. (2013). In general, the results obtained in these studies are comparable to the presented results (Figure 14).

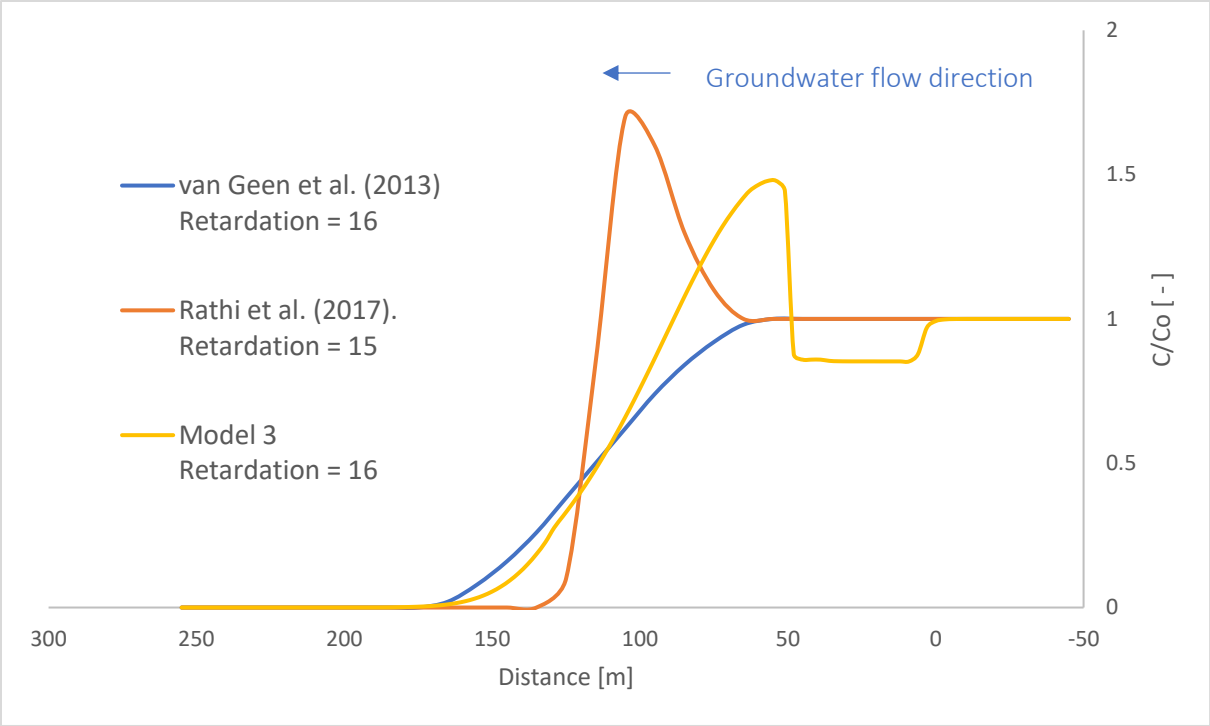

Figure 14. The comparison of the arsenic concentration profiles produced using the present model and the approaches of van Geen et al. (2013) and Rathi et al. (2017).

In comparison to the more dispersed plumes by VAN GEEN ET AL. (2013) and in model 3, the As front in the model by RATHI ET AL. (2017) has steep slope. The shape of the front is controlled by high adsorption rates. The neglection of calcite as sorption surface by RATHI ET AL. (2017) led to an overestimation of the Fe oxides sorption capabilities resulting in the rapid drop of the As concentrations. The simulated As concentration using model 3 that peaks near the plume fronts is related to the reductive dissolution of Fe oxides. The competition processes between As^{3+} and PO_4^{3-} are used by RATHI ET AL. (2017) to explain this peak. However, model 2 (without competitive processes) shows the same distribution with smaller amplitude.

In the model 3, a competitive effect of PO_4^{3-} and HCO_3^- on the adsorption of As^{3+} decreases the adsorption of As onto ferrihydrite. Thus, competitive sorption of PO_4^{3-} and HCO_3^- onto Fe oxide surface contribute to the intrusion of As into the low-As site. The simulations imply that a displacement of the adsorbed As by HCO_3^- and PO_4^{3-} is relevant.

Both As^{3+} and As^{5+} were shown to be efficiently removed from aqueous solutions by Fe oxide, especially ferrihydrite (APPELO ET AL., 2002; ANAWAR ET AL., 2003; AMIRBAHMAN ET AL., 2006; JESSEN ET AL., 2012; MAI ET AL., 2014; RAWSON ET AL., 2016; POSTMA ET AL., 2017) and calcite (ROMAN-ROSS ET AL., 2006; BARDELLI ET AL., 2011; JONES ET AL., 2013). Most model studies analyzing the spatial variations of the As concentrations in groundwater in terms of microbiological and hydrogeochemical processes have focused on the adsorption of

As onto Fe oxides. The results of the current model confirm this suggestion. In the model, a significant amount of As adsorbed onto Fe oxide is confirmed by the finding of EICHE (2009). Ferrihydrite adsorbs over 80 % of As^{3+}. In agreement with WILKIE & HERING (1996), the model results show that the sorption processes onto Fe oxide could be adequately described by considering only a single adsorption site. The simulated As/Fe ratio of 0.25 mmol/mol in the sediments is in agreement with the reported values by KOCAR & FENDORF (2009) (0.2 mmol/mol). An appreciable fraction of As^{3+} forms weak complexes on Fe oxides. Therefore, the reductive dissolution of Fe oxides is a primary factor remobilizing As.

However, in general, there is a poor correlation between dissolved Fe^{2+} and As concentrations. Thus, this process does not fully explain the patchy As distribution in contaminated aquifers (APPELO ET AL., 2002; YOKOYAMA ET AL., 2012). EICHE (2009) showed that dissolved As concentrations were poorly correlated with dissolved Fe^{2+} concentration at the study site in Van Phuc. For a long time, the retention capabilities of calcite were largely ignored. The neglection of calcite as sorption surface leads to an overestimation of the Fe oxides sorption capabilities. Therefore, capturing the behavior of As in groundwater by only considering adsorption onto Fe oxides is insufficient and a more comprehensive approach is needed including major processes controlling hydrogeochemistry. At the study site, Holocene groundwater is oversaturated with calcite. The model results show that most calcite precipitation proceeds at the redox boundary. Precipitated calcite, which is primarily a result of a CO_2 pressure drop and pH increase, acts as a sorption surface for mobilized As from Fe oxides in the aquifer. Arsenic adsorption onto calcite at the redox boundary explains the remarkable reduction in dissolved As concentration along the whole intrusion path. Due to a higher stability calcite retains As for a longer time. The adsorbed As onto calcite could not be easily released, because calcite is unaffected by redox changes unlike Fe minerals (YOKOYAMA ET AL., 2012). The amount of precipitated calcite increases over time. Hence, in the simulation period between 35 and 50 years, the impact of calcite on the As retention process grows up to 20%. HARVEY ET AL. (2002) and SWARTZ ET AL. (2004) showed that calcite dissolution is accompanied by As release. The authors observed a correlation between dissolved As and Ca^{2+}.

Another aspect of the data presented in this study is that it provides an explanation for the low correlation between As and Fe observed in several researches (APPELO ET AL., 2002; ANAWAR ET AL., 2003; BERG ET AL., 2008; EICHE ET AL., 2009; WANG ET AL., 2012; GUO ET AL., 2013; GUO ET AL., 2017). In agreement with GUO ET AL. (2013), precipitation of siderite and goethite is expected to attribute to this inconsistent trend. At the study site, goethite and hematite are much more common in the Pleistocene aquifer (EICHE, 2009). ZACHARA ET AL. (2002) and HORNEMAN ET AL. (2004) suggests that the reduction of

ferrihydrite induces an alteration of more stable minerals such as goethite without the release of Fe^{2+} into groundwater. Therefore, the release of As is delayed relative to Fe^{2+}. The model results show a clear pattern of conversion of Fe oxides towards siderite and goethite, however, only through dissolution/precipitation processes. Kinetically controlled transformation of Fe oxide into more stable crystalline phases presented by POSTMA ET AL. (2016) are not implemented. Transformation of ferrihydrite to goethite decreases the available surface area (APPELO ET AL., 2002; APPELO & POSTMA, 2005). In agreement with the results of ZACHARA ET AL. (2002), As^{3+} shows reversible sorption onto goethite. In model simulations that did not consider goethite and siderite precipitation, dissolved Fe^{2+} concentrations are considerably overestimated compared to the measured concentrations. The impact of the newly precipitated goethite on the As retention is relatively low and therefore is not presented in more details.

The competition processes for sorption surfaces play an important role in the spatial distribution of As. Some researchers have explored the competitive adsorption between AsO_3^{3-} or AsO_4^{3-} and HCO_3^- or PO_4^{3-} using surface complexation model (APPELO ET AL., 2002; JESSEN ET AL., 2012; MAI ET AL., 2014; RATHI ET AL., 2017). According to the DZOMBAK & MOREL (1990) model, ferrihydrite and goethite have significantly different adsorption capabilities. In contrast to goethite, ferrihydrite strongly adsorbs HCO_3^-. On the other hand, the authors observed stronger adsorption of PO_4^{3-} on goethite than on ferrihydrite. MAI ET AL. (2014) also showed that only PO_4^{3-} seems to have an effect on As adsorption and only at PO_4^{3-} high concentrations, while HCO_3^- had little or no effect. RATHI ET AL. (2017) investigated the retardation of As onto the Van Phuc aquifer sediments and found that As adsorption depends on the PO_4^{3-} concentration in the groundwater. In the present model, the effect of both processes on the As retention is relatively low and lies under 10 %. Due to the large scale of the model, the documented differences by DZOMBAK & MOREL (1990) in the competition capabilities of HCO_3^- and PO_4^{3-} cannot be quantified.

2.5 CONCLUSION

According to PHAST and PHREEQC modelling results, possible mechanisms for As retention in Van Phuc are explored. Adsorption of As by several minerals, organic matter oxidation, as well as other possible chemical reactions like precipitation/dissolution and oxidation/reduction are considered in the simulations. The redox boundary marks an important hydrogeochemical interface controlling the speciation and mobility of As. As shown by BERG ET AL. (2008), the large groundwater extraction in Hanoi resulting in the intrusion of the reduced Holocene groundwater into the Pleistocene aquifer has changed the distribution of the hydrogeochemical processes in the region.

The redox state of the aquifer has a major impact on the chemical composition of groundwater in Van Phuc. The microbiological degradation of organic matter plays an important role for the distribution of redox conditions. Under predominantly reduced conditions in the Holocene aquifer, dissolved As is transported dominantly as As^{3+}. In the Pleistocene aquifer, its migration is strongly affected by sorption onto ferrihydrite and calcite. Calcite is the more stable mineral under changing redox conditions and, therefore, presents an appropriate mineral trap for As, whereas the reductive dissolution of Fe oxides is responsible for the remobilization of As. Although As adsorption onto calcite initially provided a negligible influence on the As distribution, its overall contribution increased over time up to 20 %. Overlooking the critical role of calcite as sorption sites explains the absence of a relationship between sediment-bound and dissolved As concentrations. The formation of calcite that adsorbs As in the aquifer helps to explain inconsistencies in the relation between dissolved As and Fe^{2+} concentrations in groundwater.

The process of As adsorption onto calcite is applicable for the part-explanation of the As retention in Van Phuc. Calcite can play an important role for As retention where Fe and Mn oxides have low concentrations or lost their adsorbing effectiveness due to e.g. reductive dissolution.

Many As contaminated aquifer are supersaturated with respect to calcite, suggesting that calcite can play an import role also there. Thus, As retention by calcite must be investigated in the systems with varying redox conditions like at the current study site.

Chapter 3. Field assessment of the impact of water mixing processes on As dynamics in the vicinity of pumping and infiltration wells at a pump-and-treat site in South-West Germany

3.1 INTRODUCTION

Extraction activities usually are essential in (1) drinking water production, (2) pump-and-treat remediation techniques, (3) and aquifer thermal energy storage systems. The extraction of groundwater triggers a series of hydrogeochemical and microbiological reactions that modify the chemical quality of groundwater and mineralogical composition in an aquifer. Chemical compositions of groundwater often show concentration gradients with depth as well as in lateral context (APPELO & POSTMA, 2005; BONTE ET AL., 2015). The expected impact of induced mixing processes depends on the type (redox, pH or temperature) and magnitude of the gradient (APPELO & POSTMA, 2005). Therefore, the understanding of the hydrogeochemical zonation is required to predict and reduce environmental risks such as the mobilization of As in groundwater.

Pump-and-treat systems include groundwater extraction of contaminated and infiltration of treated water as a part of the remediation strategy (KEELY & BOULDING, 1989). Groundwater extraction wells are often susceptible to clogging (HOUBEN & TRESKATIS, 2003). In extraction wells, physical and hydrogeochemical processes, sometimes in combination with microbiological activity cause well clogging (DE ZWART, 2007; POSSERMIERS, 2014). Well clogging due to Fe minerals and calcite precipitation is a widespread problem in aquifers with varying chemical conditions (DE ZWART, 2007; HOUBEN & WEIHE, 2010; WEIDNER, ET AL., 2012; HENKEL ET AL., 2012; MEDINA ET AL. 2013; SHTIRKIN, 2013). The formation of clogging material is generally a result of mixing waters with different chemical compositions. HOUBEN (2003) recognized the mixing of oxic and anoxic groundwater due to extraction well operation as the primary cause of well clogging by Fe minerals. The common problem associated with water infiltration as well as in the case of extraction wells is reduction of permeability due to well clogging (COHEN ET AL., 1997). Calcite precipitation can be caused by infiltrating water with different temperature and CO_2 partial pressure than the ambient water in the aquifer, which occurs for ASR and pump-and-treat systems (PROMMER & STUYFZAND, 2005; WALLIS ET AL., 2011; SHTIRKIN, 2013).

The behaviour of As under laboratory conditions has been observed and successfully discussed by several numerical modelling approaches (DZOMBAK & MOREL, 1990; APPELO ET AL., 2002; POSTMA ET AL., 2007). Well-documented examples of As mobilization exist for managed aquifer recharge (WALLIS ET AL., 2010), aquifer storage and recovery (WALLIS ET AL., 2011; LAZAREVA ET AL., 2015) and aquifer thermal energy storage systems (BONTE ET AL., 2013A). However, numerical models in three-dimensional context are still missing, which allows to assess the lateral groundwater movement in aquifers. In contrast to previous studies observing mixing processes only in vertical and horizontal 1D/2D orientations (BONTE ET AL., 2014; POSSEMIERS, 2014), a three-dimensional approach is used in this study.

The present study aims to identify the hydrogeochemical processes induced by altering groundwater extraction and infiltration and their effect on the precipitation of Fe minerals and calcite, and the As enrichment process on clogging material. The study uses reactive transport modelling, which is based on the hydrogeochemical data from a pump-and-treat system in South-West Germany. For reasons of data, the exact location of the study site is not published.

3.2 MATERIALS AND METHODS

The development of the model includes the following steps:

- the development of a conceptual model;
- translation of the conceptual model into a numerical model;
- calibration of the numerical model to observed field conditions;
- application of the numerical model to better understand the distribution of As in the aquifer.

3.2.1 STUDY SITE. DATA SET DESCRIPTION

The study is performed at a former manufactured gas plant site located near Mannheim, in South-West Germany. The site offers a comparably comprehensive hydrogeochemical database (ARCADIS, 2016), well-defined site hydrogeology and a regional groundwater flow model (ARCADIS, 2012).

The impact of bombing of the site during World War II as well as continued leakages led to various contaminations of the sediments and groundwater in the subsurface. The contaminants are typical for gasworks, such as BTEX, PAH, phenols and NSO-HET. The primary pollutants are BTEX and PAH (Figure 15).

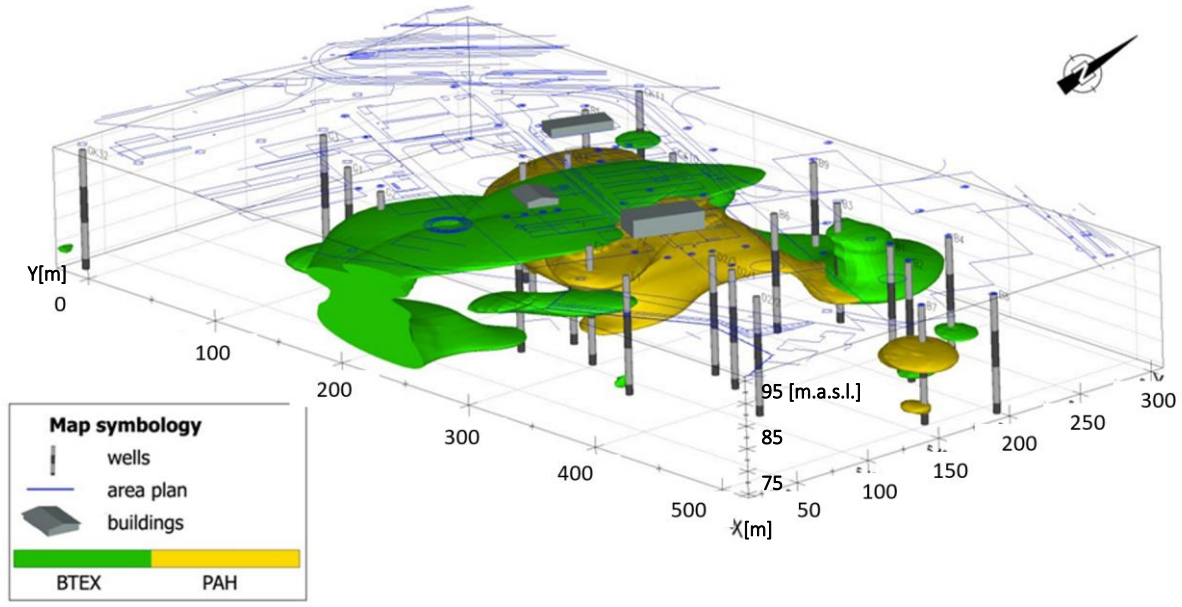

Figure 15. Spatial distribution of the NAPL bodies (PAH and BTEX) in the subsurface based on data from ARCADIS (2012).

The contaminants are found as NAPL bodies as well as dissolved in groundwater. Naphthalene, acenaphthene and benzene are the most prominent compounds in the plume. The spatial distribution of PAH compounds in the groundwater is shown in Figure 16. The measured concentrations are also listed in Table A-4.

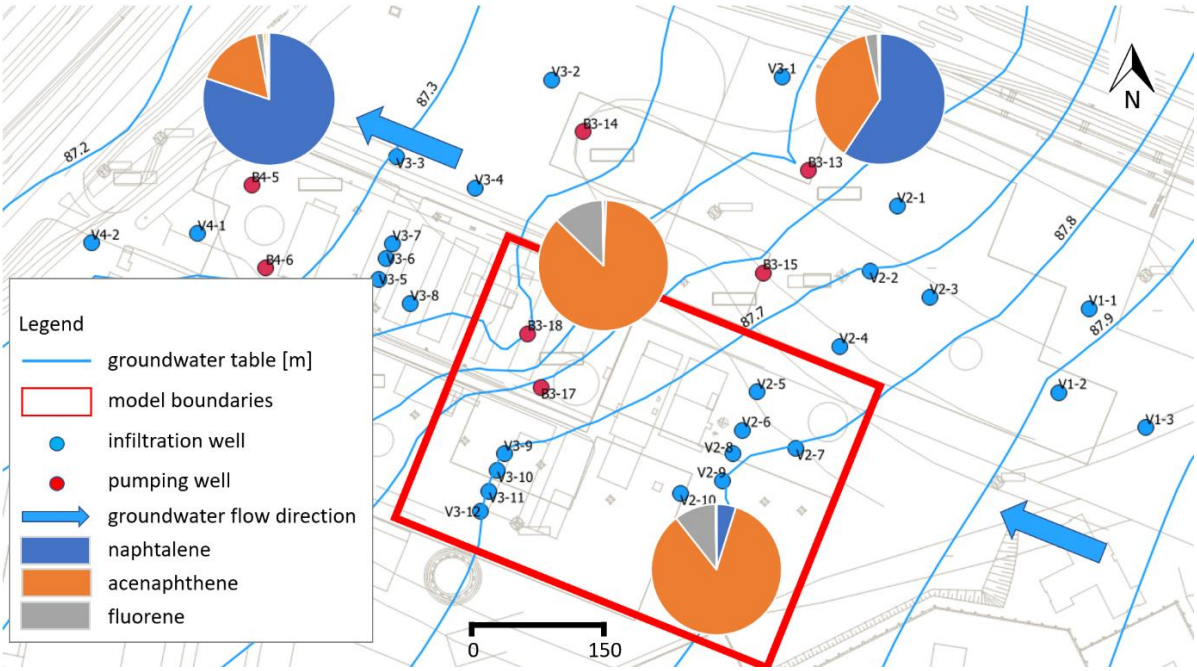

Figure 16. Spatial distribution of PAH compounds in the groundwater based on data from ARCADIS (2016). The pie charts display the main contaminants.

The pump-and-treat system under investigation was constructed in 2011. According to the remediation concept, 11 pumping wells extract contaminated groundwater from different depths. The total extraction rate is equal to 40 m^3/h and depends on infiltration capabilities of the infiltration wells. The extracted water after treatment is infiltrated into the aquifer using 31 infiltration wells. The infiltration and extraction activities markedly affect the groundwater flow path in the research area. The boundary conditions are described in detail in the following paragraphs.

Hydrogeology

The gasworks site is flat and located in the Upper Rhine Valley on the lower terrace formed in the last ice age (Würm). Hydrogeological conditions at the site intensively have been investigated over the previous fifteen years. Based on the gathered data, a three-dimensional hydrogeological and hydrogeochemical site model was developed. The porous aquifer is approximately 30 m thick. At the bottom, the aquifer is delimited by the clays. The aquifer can be divided into three layers with respect to hydraulic permeability (ARCADIS, 2012) (Figure 17).

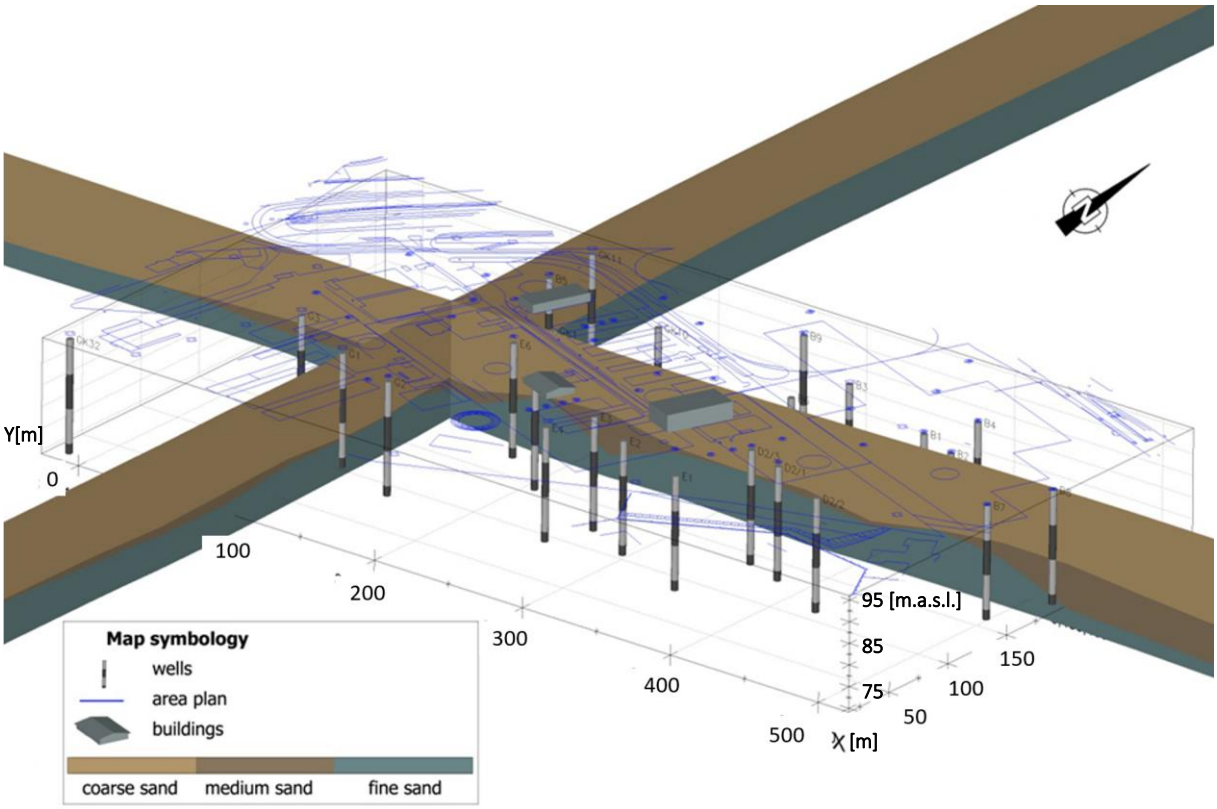

Figure 17. Schematic three-dimensional hydrogeological site model. The hydrogeological model based on data from ARCADIS (2012).

Hydraulic permeability in the first layer is determined within the range 3×10^{-3} - 2×10^{-4} m/s. Pumping tests yielded for the second and the third layer a relatively small hydraulic conductivity between 5×10^{-5} m/s – 6×10^{-6} m/s. The wells are mainly screened in the first high permeable layer. For the entire aquifer, effective porosity of 15 Vol-% is assumed. The overall hydraulic gradient is found to be 0.002 with a main flow direction to the north-west. Recharge was estimated to occur over most of the study area at around 210 mm/year (ARCADIS, 2012).

Hydrogeochemistry

Groundwater sampling was performed in three different depths (7-12 m, 15-19 m and 24-28 m) using a multiple-level packer sampling method. The sampling campaign was carried out by ARCADIS in November 2014 (ARCADIS, 2016).

The hydrogeochemistry of the uncontaminated aquifer part is characterized by aerobic conditions with the measured dissolved O_2 concentrations up to 0.13 mmol/L. The ambient groundwater also contains both, NO_3^- and SO_4^{2-} at concentrations up to 0.18 mmol/L and 3.4 mmol/L, respectively. The pH ranges between 6.8 and 7.1. The contaminated site of the aquifer due to BTEX and PAHs microbiological degradation is mainly characterized by reducing conditions as indicated by the respectively high Fe^{2+} and Mn^{2+} concentrations and low O_2 (< 0.003 mmol/L) and NO_3^- levels (< 0.01 mmol/L). Sulfate concentrations within the plume are found to be lower than the background concentrations, approximately 2.7 mmol/L (Table 6) (ARCADIS, 2016). The pump-and-treat system infiltrates oxygenated treated water into the reduced aquifer. In the contaminated site, the main source of NO_3^- and O_2 (up to 1.1 mmol/L and 0.14 mmol/L, respectively) is the treated infiltration water (Table 6).

Table 6. The hydrochemical composition of the background (measured in GK17), infiltration (measured in the treatment plant outlet) and contaminated water (mean measured concentrations in B3-16, B3-17, B3-18) (based on data from ARCADIS (2016), measured July 2015). The location of the wells showed in Figure 16.

Component	Unit	Background/Inflow	Infiltration	Contaminated
EC	[µS/cm]	1920	1750	1890
Temp	[°C]	13	17	15
pH	[-]	6.8	7.0	7.1
As_{tot}	[µmol/L]	<0.01	<0.01	0.35
PO_4^{3-}	[µmol/L]	<0.6	<0.6	<0.6
Na^+	[mmol/L]	2.6	2.4	2.7
Ca^{2+}	[mmol/L]	4.1	3.9	4.5
K^+	[mmol/L]	0.1	0.1	0.1
Mg^{2+}	[mmol/L]	1.4	1.2	0.9
Fe^{2+}	[mmol/L]	0.007	0.003	0.057
Mn^{2+}	[mmol/L]	0.011	0.002	0.012
Cl^-	[mmol/L]	3.1	2.6	2.9
NO_3^-	[mmol/L]	0.18	1.12	<0.01
NH_4^+	[mmol/L]	<0.003	4.2	5.3
O_2	[mmol/L]	0.13	0.14	<0.003
SO_4^{2-}	[mmol/L]	3.4	2.5	2.7
S^{2-}	[mmol/L]	<0.0006	<0.0006	0.01
HCO_3^-	[mmol/L]	8.7	8.4	9.9

The measured pH values are nearly neutral. The As concentrations in the groundwater samples are below detection limit, except pumping well B3-17 (0.35 µmol/L).

The dominant minerals in the aquifer are quartz (59 wt-%), mica (18 wt-%) and k-feldspars (12 wt-%) (SHTIRKIN, 2013). Calcite and Fe minerals such as ferrihydrite, hematite and goethite are also present. However, their concentrations are below 5 % and therefore could not be quantified. Except for the clogging material in well B3-17, the As concentrations in the solid phase are under detection limit. In the clogging

material consisting mainly of Fe sulfide and calcite, the measured As concentration is 9.6 ppm (SHTIRKIN, 2013).

3.2.2 CONCEPTUAL MODEL AND REACTION NETWORK IMPLEMENTATION

The model is based on the regional flow model created using MODFLOW 2005 (ARCADIS, 2012). The hydrogeological parameters are adopted unchanged. The reactive transport model is cut out from the regional groundwater model. The cut is performed so that the path lines between the infiltration and pumping wells do not extend beyond the boundaries. The model extension is chosen based on the distribution of the remediation areas (Figure 20). The axes are oriented parallel and orthogonal to the general groundwater flow direction (Figure 18).

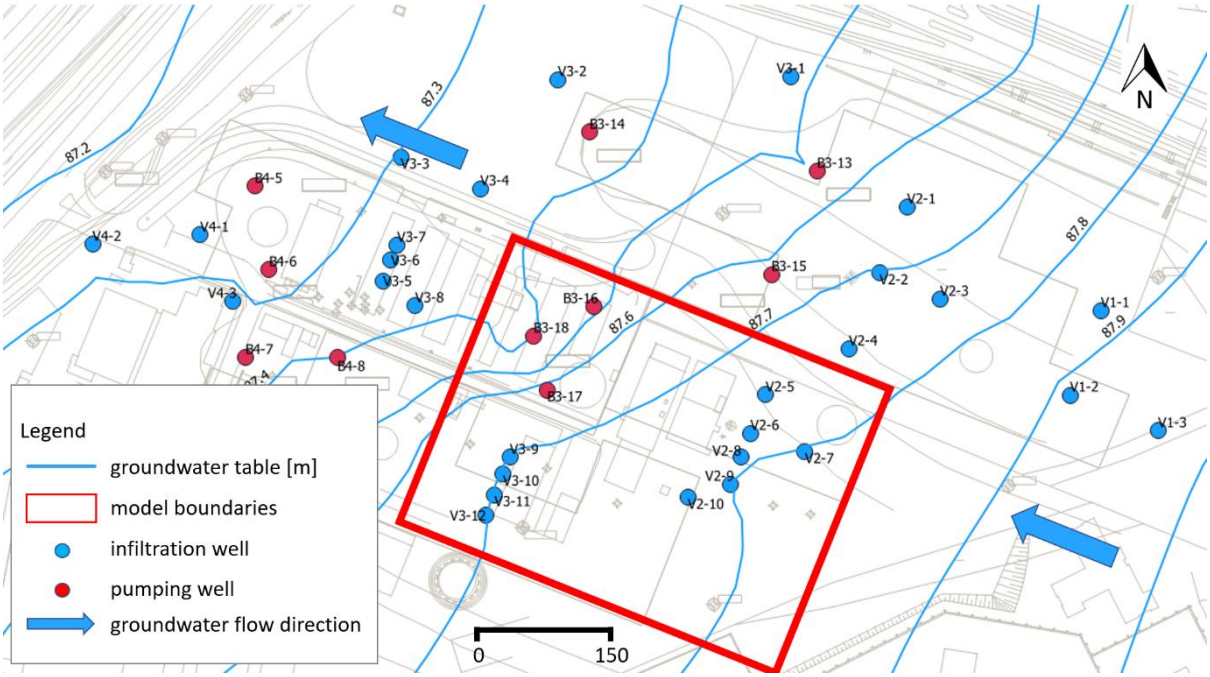

Figure 18. The groundwater water flow path. The boundaries of the reactive transport model (blue isolines are result from ARCADIS (2012)).

The ambient flow field simulated by constant boundaries at east and west boundaries of the mode domain. The measured extraction rates vary considerably depending on the infiltration capabilities of the wells. Mean extraction and infiltration rates from the year 2016 are implemented into the model (ARCADIS, 2016) (Table 7).

Table 7. Mean extraction and infiltration rates from the year 2016 implemented in the model (ARCADIS, 2016).

Well	Extraction/Infiltration rate (m^3/h)
B3-16	1.88
B3-17	2.89
B3-18	1.35
V2-5	0.30
V2-6	0.43
V2-7	0.16
V2-8	0.89
V2-9	0.53
V2-10	1.02
V3-9	0.87
V3-10	1.33
V3-11	1.69
V3-12	1.49

The model grid is depicted in Figure 19 and includes 13 wells (10 infiltration wells and three pumping well). The current model area is discretized into a finite-difference grid of 116 columns and 96 rows. The grid has a lateral extension of 330 m in x and 280 m in y direction. The grid cell sizes change from 5 m at the model boundaries (first 40 m) to 2.5 m at the center of the model. For this model, a fine vertical discretization (Δz = 2.0 m) is used.

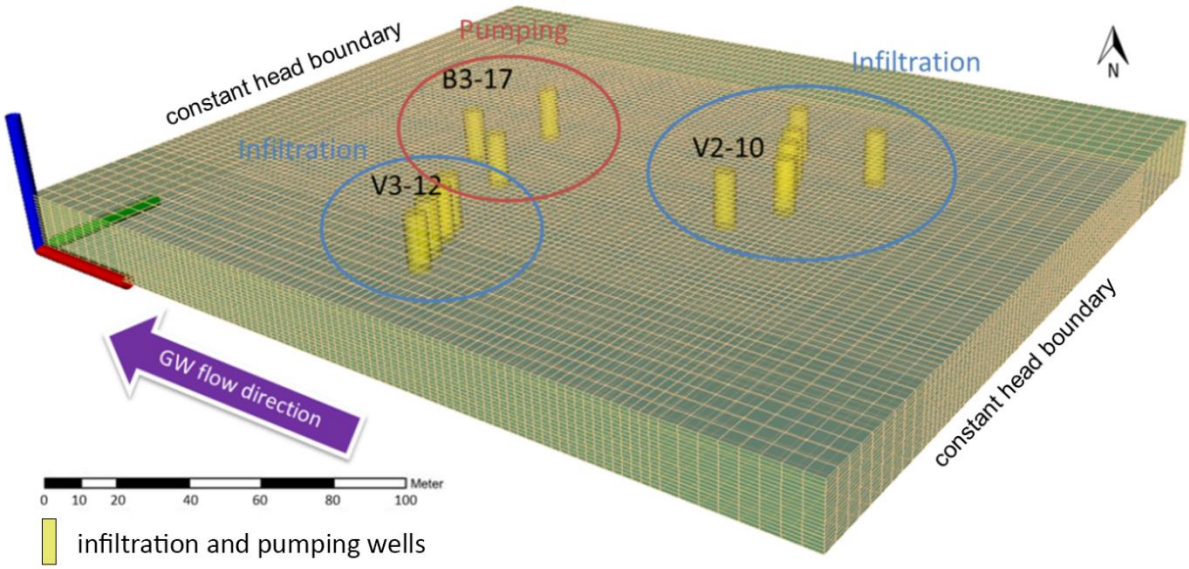

Figure 19. The model grid with the extraction and infiltration wells. The arrow shows preferred flow direction of groundwater.

The temporal discretization is 0.2 days. Recharge is kept constant at 210 mm/year. Table 8 provides details on the model discretization and initial conditions.

Table 8. Summary of discretization, model parameters and initial conditions used for modelling (ARCADIS, 2012).

Model parameters	Unit	Value
Model dimensions x * y * z	[m]	330 * 280 * 26
Discretisation Δx	[m]	5 (outside) and 2.5 (inside)
Discretisation Δy	[m]	5 (outside) and 2.5 (inside)
Discretisation Δz	[m]	2
Hydraulic conductivity	[m/s]	$3 \times 10^{-3} - 6 \times 10^{-6}$
Effective porosity	[%]	15
Longitudinal dispersivity	[m]	1
Horizontal transversal dispersivity	[m]	0.1
Vertical transversal dispersivity	[m]	0.1

Longitudinal α_L, transverse horizontal α_{TH} and transverse vertical α_{TV} dispersivities are initially assumed to be 1 m, 0.1 m and 0.1 m, respectively. To estimate the horizontal

transverse dispersivity α_{TH} the commonly used relationship of α_{TH} = 0.1 x α_L is used (BLUM ET AL., 2009).

The following boundary conditions in the groundwater flow model are determined:

- the Dirichlet (first-type) boundary conditions: groundwater inflow in the southeast and outflow in the northwest,
- inner boundary conditions: 3 extraction and 10 infiltration wells,
- groundwater recharge: the average groundwater recharge of 210 mm/year.

Figure 20 shows an overview of the boundary conditions of the groundwater model and also the distribution of the calibrated hydraulic conductivity values in the first layer.

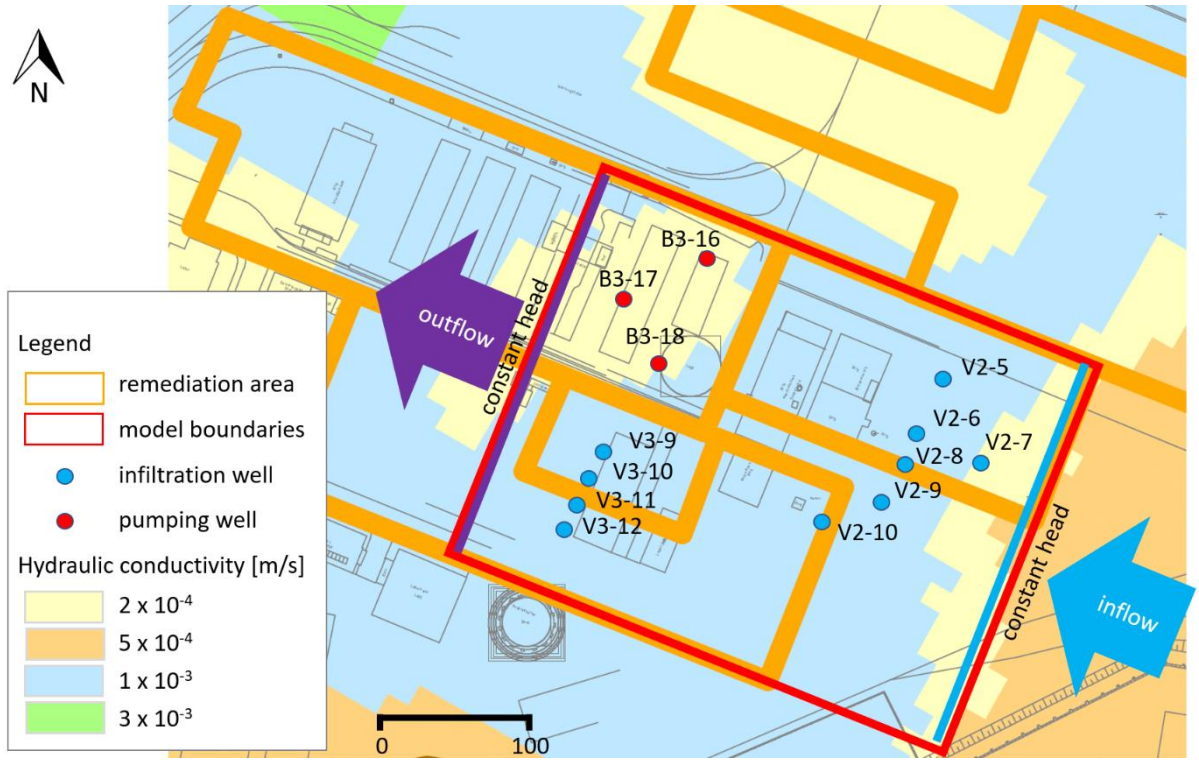

Figure 20. Boundary conditions. Hydraulic conductivity distribution in the first layer (the distribution based on the data from ARCADIS (2012)).

To provide confidence that the model is representative, a steady-state calibration was conducted using the measurement collected in November 2016. The mean absolute error has only limited applicability for assessing the quality of the model calibration. The calculated model error should be therefore set in relation to a measured range. To quantify the model error, the difference between the highest and lowest measured groundwater level ($h_{max,mea}$ -$h_{min,mea}$) is included:

$$f = \frac{1}{n(h_{max,mea} - h_{min,mea})} \sum_{i=1}^{n} (|h_{mea,\,i} - h_{cal,i}|)$$

where f = error

n = measurements number

$h_{max,mes}$ = max. measured groundwater level

$h_{min,mes}$ = min. measured groundwater level

The observed groundwater levels are plotted against the simulated water levels in a scatterplot (Figure 21). Deviations from the straight line indicating a perfect match between the observed and simulated values should be randomly distributed indicating that there is no bias towards over or under predicting the groundwater levels.

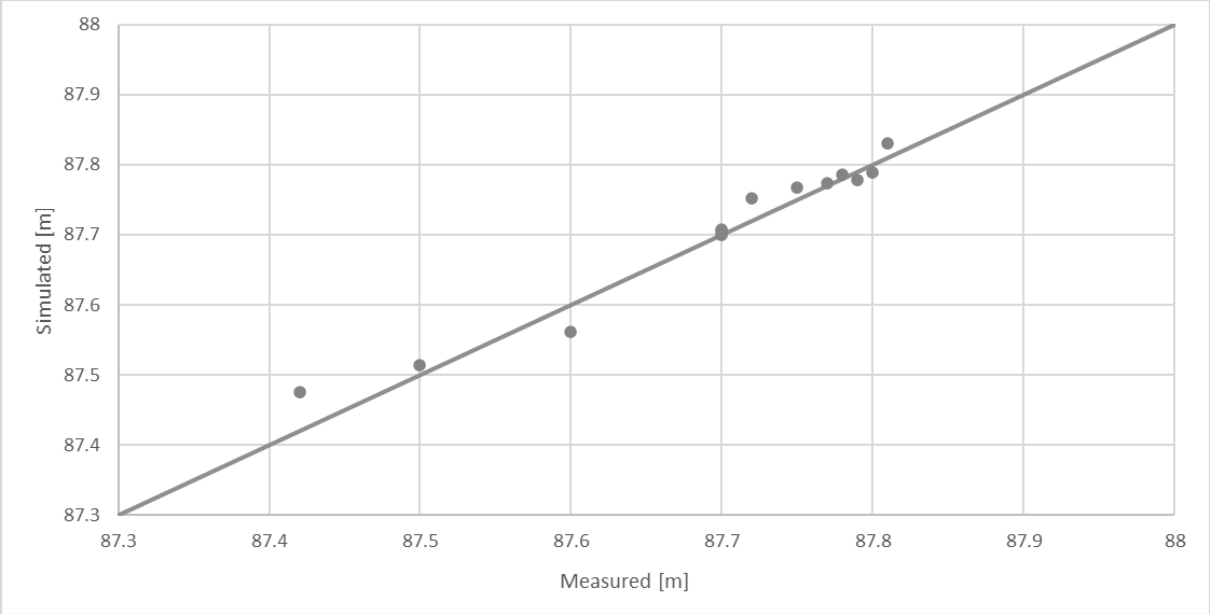

Figure 21. Steady-state situation. Scatter plot. Deviations between measured and simulated groundwater levels.

In the Figure, the points are evenly arranged around the diagonal, i.e., no tendency to shift can be observed. The mean absolute error is 0.02 m. The calculated model error of 4.4 % indicates a good model calibration. Typically, a model is considered as good calibrated with 5 % or less. The used data and the results are also presented in Table A-5.

Reaction network

The calibrated groundwater flow model represents the basis for a reactive transport model. The reactive transport simulations are performed to interpret the

hydrogeochemical observation at the study site. The reactive transport model incorporated the mineralogical data along with the observed groundwater compositions collected by SHTIRKIN (2013) (Table A-4). The site-specific reaction network included (1) immobile NAPL bodies, (2) the major ions and (3) the main minerals.

The initial groundwater concentrations of electron acceptors and major ions are based on the observed groundwater composition presented in Table 6. The concentrations are adopted from the measurements that were conducted toward the upstream boundary at GK17 (Table A-4). For simplicity initial (ambient) compositions are homogenously distributed in the model domain. The same composition is also used to define the inflow boundary and the recharge water composition. The PHREEQC code is used to define an equilibrated initial aqueous composition. Speciation of all major ions, mineral dissolution/precipitation and redox reactions are equilibrium-based.

The measured data indicate the presence of two NAPL bodies in the underground (Figure 22). The NAPL sources are represented in the model as a mass of immobile liquids. The initial mass of the NAPL bodies is assumed to be unlimited large to keep the dissolution rate constant over time. In the model, the NAPL bodies are considered at constant concentrations and homogeneously distributed in the source zone within the initially pristine aquifer.

Kinetically controlled dissolution from the NAPL bodies is implemented in the model to act as the sources of the dissolved hydrocarbon compounds. The dissolution of the contaminants is expressed through the first order mass transfer equation. The mass transport coefficient is determined during the model calibration.

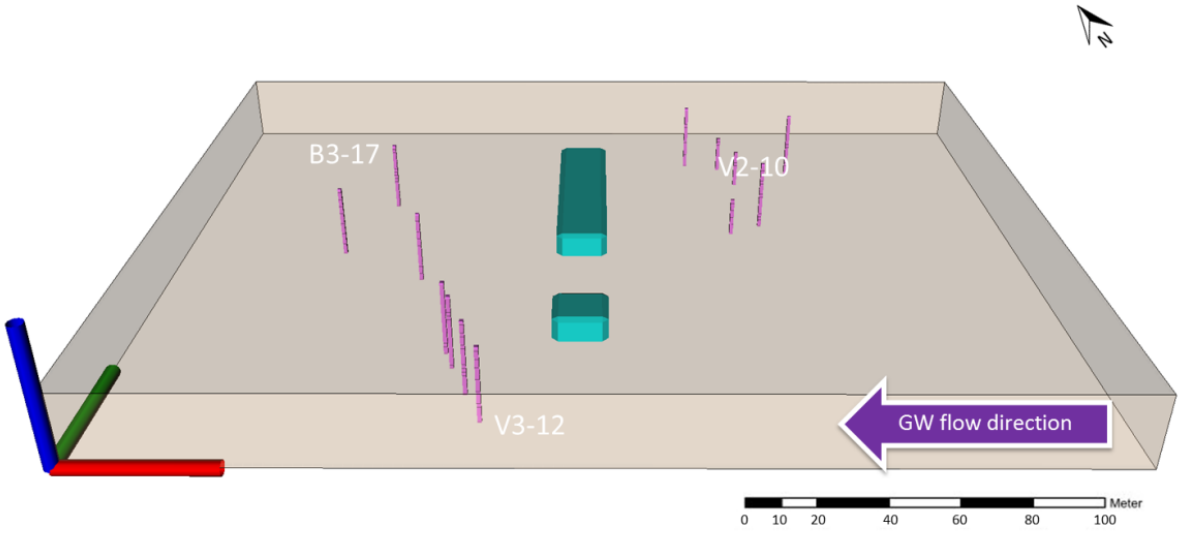

Figure 22. Spatial location of NAPL source areas (the turquois cubes) in the model for the entire area (the wells in pink).

The two-step partial equilibrium approach (BRUN & ENGESGAARD, 2002; JAKOBSEN & COLD, 2007) is considered in the simulation of the contaminant decomposition and redox processes. Kinetically controlled degradation is simulated by transforming conservative BTEX and PAH compounds into „reactive“ CH_2O, which is oxidized in the PHREEQC code according to the thermodynamic equilibrium (PROMMER ET AL., 1999; PROMMER ET AL., 2006; D'AFFONSECA ET AL., 2008). In the two-step approach the electron accepting step is modelled as an equilibrium reaction. In this approach the reactivity of the CH_2O determines the overall rates of the processes in groundwater. To represent the redox conditions, all compounds affecting the electron balance needed to be identified. The electron acceptors associated with the degradation of CH_2O are listed in Table 9.

Table 9. The main assumed reactions in the study area, which were considered for the model (Fetter et al., 1999; Appelo & Postma, 2005; Merkel & Planer-Friedrich, 2008).

Parameter	Reaction
Organic matter oxidation via O_2	$O_2 + \{CH_2O\} \Rightarrow CO_2 + H_2O$
Organic matter oxidation via NO_3^-	$4NO_3^- + 5\{CH_2O\} + 4H^+ \Rightarrow 2N_2 + CO_2 + 7H_2O$
Fe minerals dissolution/precipitation	$Fe^{2+} \Leftrightarrow Fe^{3+} + e^-$
SO_4^{2-} reduction	$SO_4^{2-} + 2\{CH_2O\} + H^+ \Rightarrow 2CO_2 + HS^- + 2H_20^-$

The model also accounts for the secondary reactions e.g. mineral precipitation and dissolution. The mineral assemblage including calcite, pyrite, and ferrihydrite, is based on the results of sediment analysis using X-ray diffraction (Figure A-7). Mineral precipitation/dissolution is included as equilibrium reactions based on the PHREEQC standard database. Due to the oxidizing ambient hydrogeochemical conditions, pyrite is assumed to be initially absent.

3.3 RESULTS

Redox Zonation

The reactive transport model is used to evaluate the factors that control the distribution of redox zones. This should form a basis for understanding the measured As enrichment on the clogging material in well B3-17.

In the first step, the reactive transport model is calibrated to precisely reproduce the hydrogeochemical conditions at the study site. The set of physical model parameters (hydraulic conductivity, porosity, and dispersion (Table 8)) is not further modified.

During the calibration phase of the model, it became clear that several hydrogeological factors affect the hydrogeochemical situation in the vicinity of the extraction wells. The most important factors are found to be (1) mixing processes and (2) altering extraction rates.

After the start of the simulation, reducing conditions develop within the source zone and penetrate the initially aerobic part of the aquifer. Figure 23 shows the simulated organic pollutant plume contours after 500 days. After 500 days in the area between infiltration and extraction wells, the concentration distributions of all main parameters reach steady-state.

The dissolution, transport and degradation of the organic contaminants are the main drivers for the hydrogeochemical changes in the aquifer. The groundwater samples allowed the delineation of contaminant plumes (Table A-4). The objective here is to determine the distribution of the redox zones knowing the distribution of the plume. To answer this question, the evolution of the plume must be modelled. In Figure 23 the simulated distribution of dissolved contaminants in the aquifer is presented.

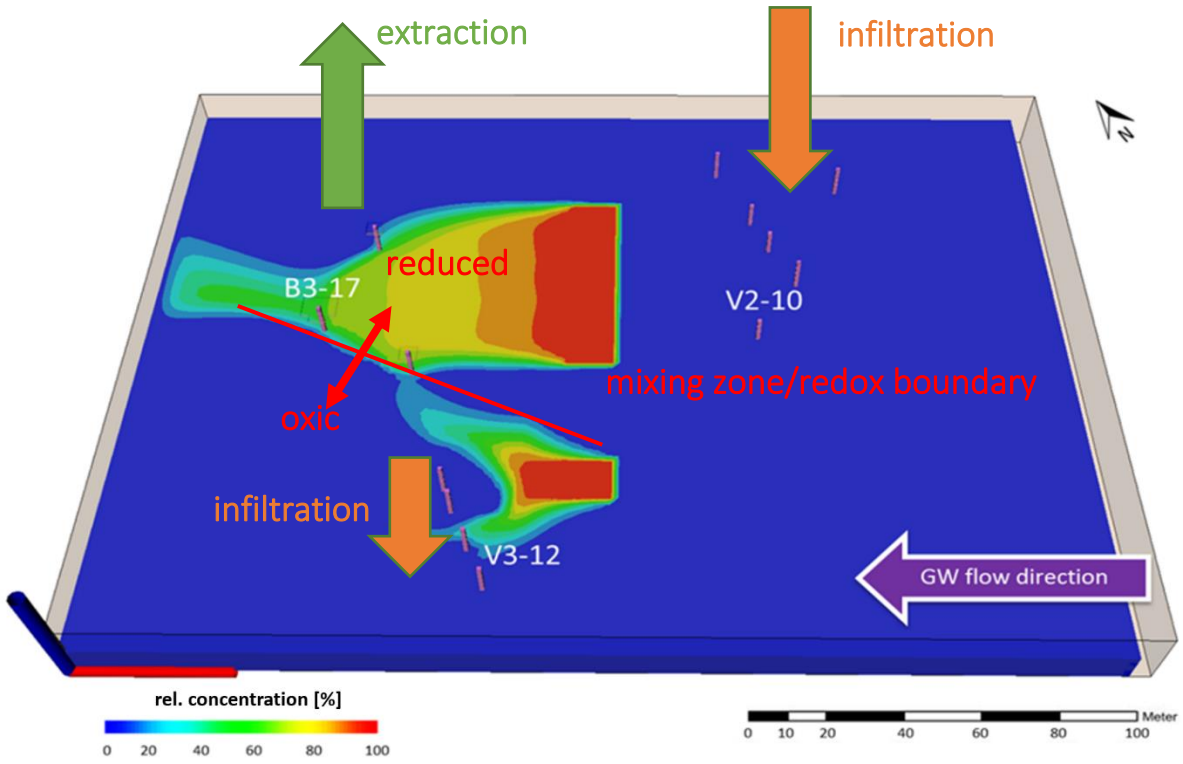

Figure 23. Calculated distribution of contaminant (C/C_o) in the aquifer after 500 days. Red line is mixing and redox boundary.

Background groundwater (Table 6) was found to be oxic with 0.18 mmol/L NO_3^-. Electron acceptors, mainly NO_3^- and SO_4^{2-}, are sequentially consumed during microbial

degradation of the pollutants. In fact, under these circumstances, it appears that the degradation of the contaminants leads to reduction of the concentrations in the plume.

Nitrogen compounds in the contaminated groundwater exist mainly as NH_4^+ (Figure A-4). Air stripping and granular activated carbon units are used in the treatment plant to remove organic compounds. After treatment, O_2, NO_3^- and SO_4^{2-} are present, while reduced species (Fe^{2+} and NH_4^+) are absent or occurred at very low concentrations. So, during the treatment process ammonium is oxidized to NO_3^- (Table A-4).

Treated groundwater is used as injectant. The controlling factor for denitrifying microbial degradation is the NO_3^- flux into the contaminated area. The main source of NO_3^- at the contaminated site is the treated infiltration water. In the model, the infiltration water is rich in NO_3^- and SO_4^{2-} with 1.12 mmol/L and 3.4 mmol/L, respectively. The water is passing through the NAPL source zone, where the organic contaminants dissolve into the aqueous phase (Figure 24).

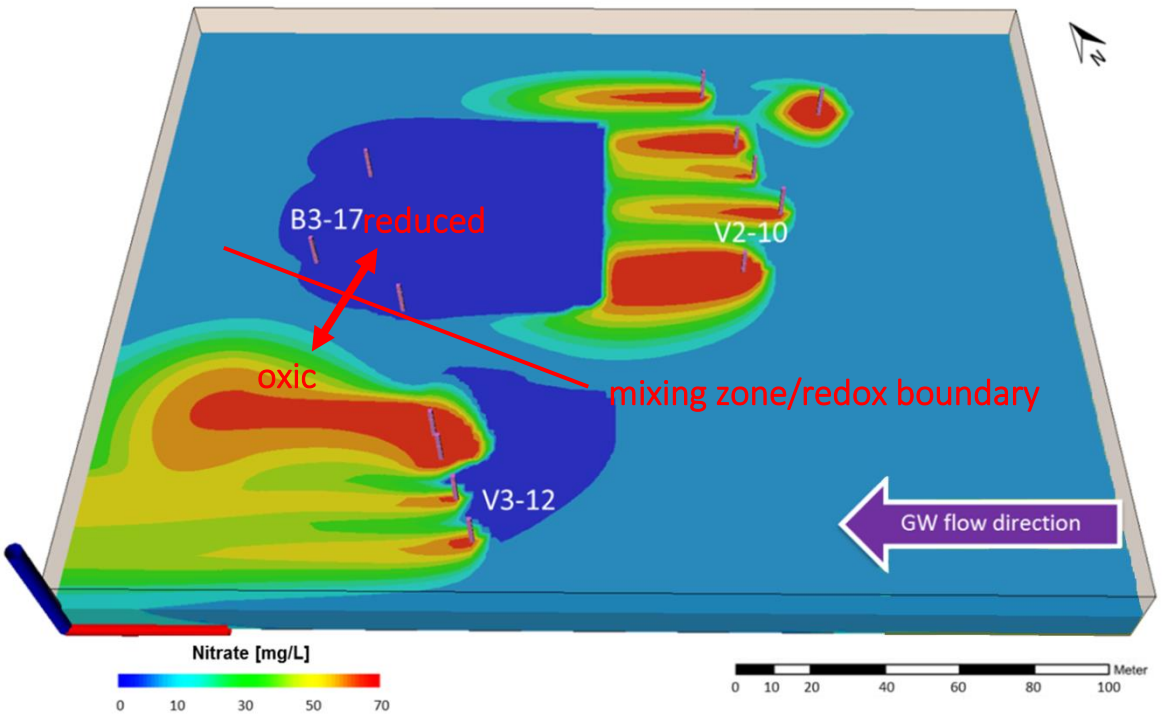

Figure 24. Calculated distribution of NO_3^- in the aquifer. Red line is mixing and redox boundary.

The distribution of NO_3^- is substantially affected by denitrification, leading to complete NO_3^- removal within short distances from the infiltration wells. Kinetically controlled redox reactions cause the sharp redox boundaries in the downstream of the infiltration wells. Within the zone between the infiltration and extraction wells, the redox

conditions become reducing, in the down-gradient direction. Dissolved O_2 and NO_3^- concentrations are below detection levels in B3-17. The calibrated model could reproduce the measured NO_3^- concentrations at most wells of the field site reasonably well (Figure 25).

Calcite

The contaminated groundwater has a higher HCO_3^- concentration of around 10 mmol/L due to contaminant degradation. Subsequently, the model shows that the contaminated groundwater reaches with a high CO_2 pressure the infiltration and extraction wells.

High CO_2 concentrations induce calcite dissolution in the contaminated part of the aquifer. The process leads to an increase of the dissolved Ca^{2+} concentrations (Figure 25).

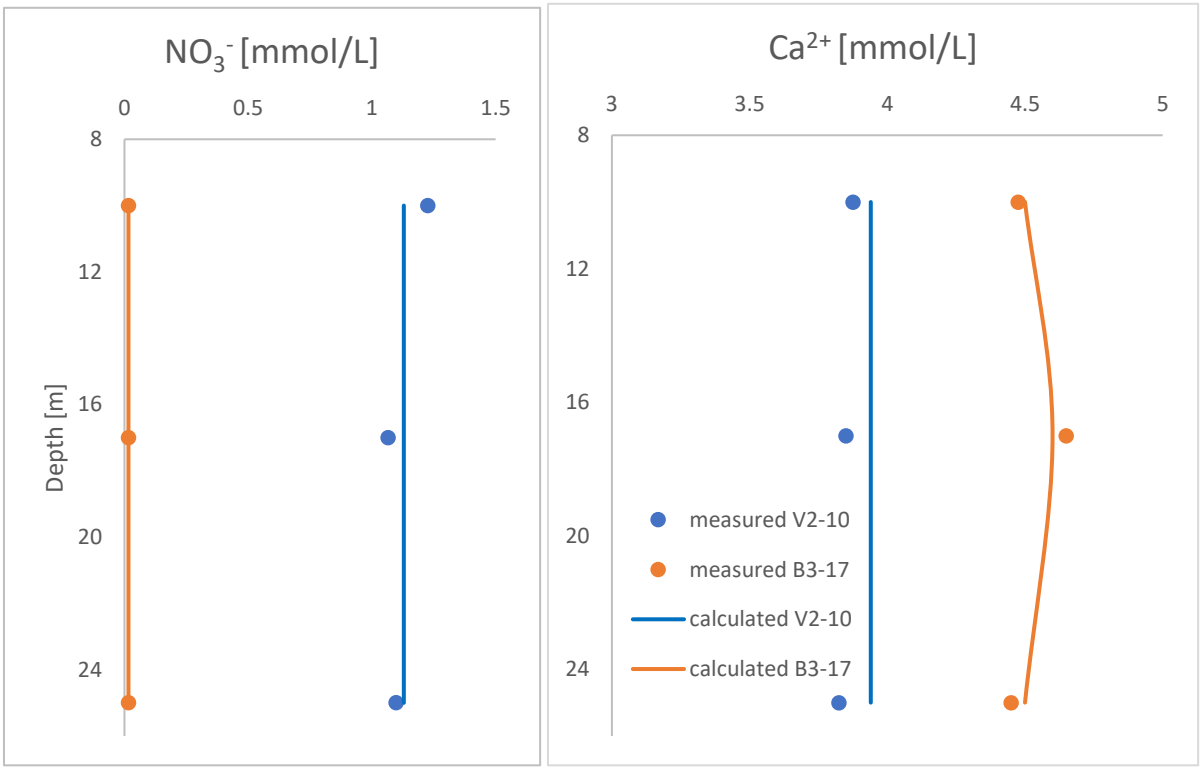

Figure 25. The groundwater hydrochemistry in V2-10 and B3-17. The depth distribution of NO_3^- and Ca^{2+} concentrations along the flow path. The solid lines reflect model predictions (measurements from ARCADIS (2016) (Table A-4)).

The contaminated groundwater is oversaturated with respect to calcite. Calcite precipitation is observed in the infiltration wells as well as in the extraction wells (Figure 26). However, the simulated calcite concentrations in the extraction wells are much lower in comparison to the infiltration wells.

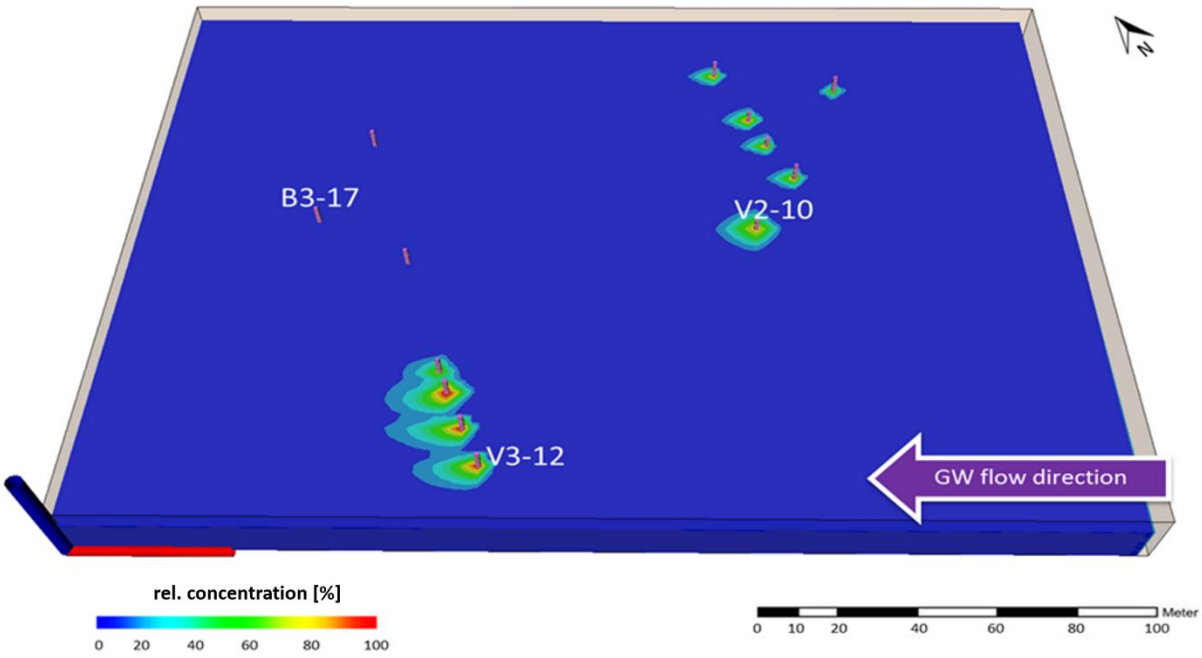

Figure 26. Calculated distribution of calcite precipitation (C/C_o) in the aquifer.

Main factor controlling the process is the partial pressure of CO_2. Before infiltration, the treated water is stored in tanks. During the storage time, the water equilibrates with ambient air, which has lower CO_2 pressure compared to the aquifer. During the infiltration, the differences in CO_2 pressure and pH induce calcite precipitation. The mixing between the contaminated groundwater and treated infiltration water at the redox boundary induce calcite precipitation through lowering the CO_2 partial pressure in the contaminated groundwater. This process was also observed by PALMER ET AL. (1992). In contrast to the extraction wells, the precipitation of calcite in the vicinity of the infiltration wells are more pronounced.

Fe minerals

Reduced conditions dominate in the zone between infiltration well V2-10 and extraction well B3-17. Sulfate concentrations in B3-17 are found to be higher than in the infiltration wells. The extracted groundwater contains between 2.6 and 2.9 mmol/L SO_4^{2-} (Figure 27). The results show that the reduced zone contains pyrite, which become oxidized and dissolved under the influence of the more NO_3^- rich water, providing additional dissolved Fe^{2+} in the groundwater (Figure 27) (APPELO & POSTMA, 2005). The comparison of the simulated redox zonation with measured concentrations shows a reasonable agreement.

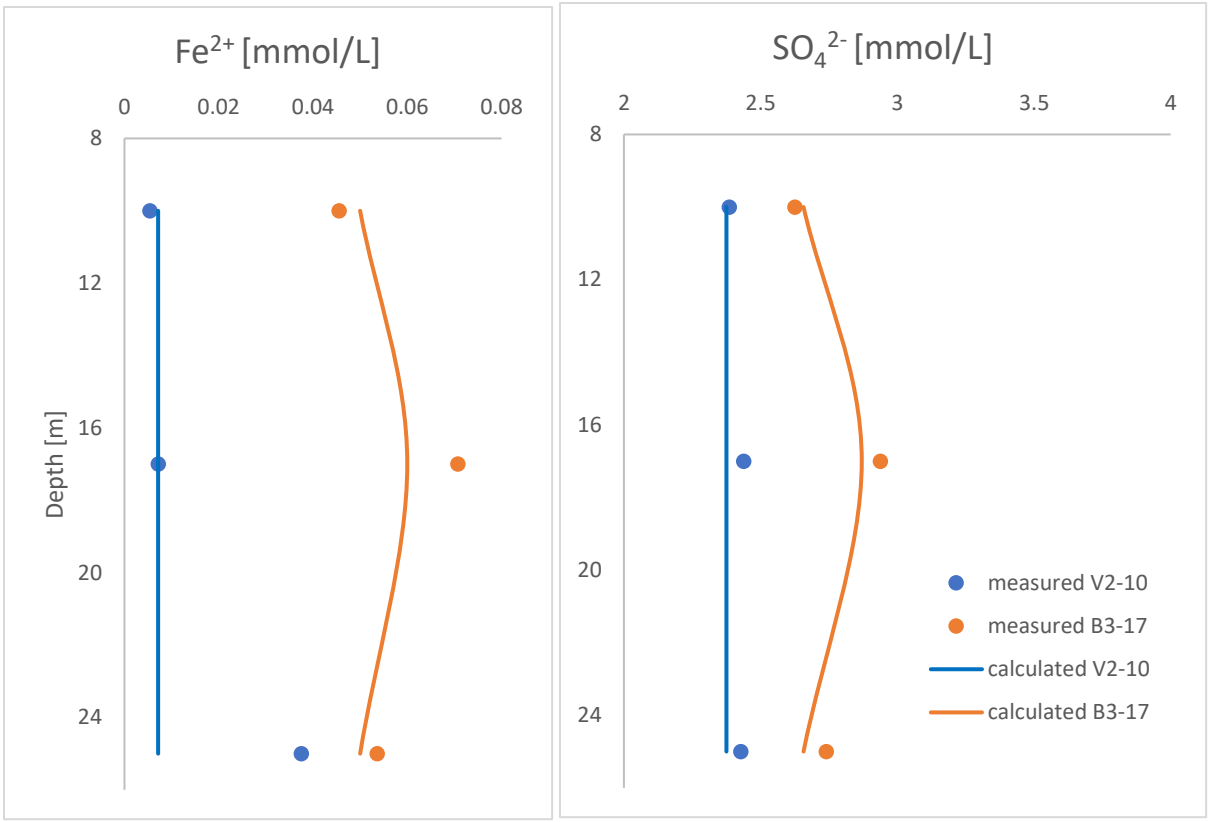

Figure 27. The groundwater hydrochemistry in V2-10 and B3-17. The depth distribution of Fe^{2+} and SO_4^{2-} concentrations in the groundwater. The solid lines reflect model predictions (measurements from ARCADIS (2016)).

Based on the calibrated model, tracer simulations are performed, which are used to deliver evidence on mixing processes. The model simulations illustrate how the infiltrated aerobic water penetrates the aquifer during infiltration phases, and thereby displaces the reduced contaminated groundwater. Chemical differences between ambient groundwater and injectant resulted from the applied water treatment.

The simulated tracer solutions consist of conservative/unreactive components. To increase the understanding of the system and the movement of waters with different redox states, several tracer simulations are carried out. The simulation results of tracer infiltration are exemplary displayed for well V3-12 in Figure 28.

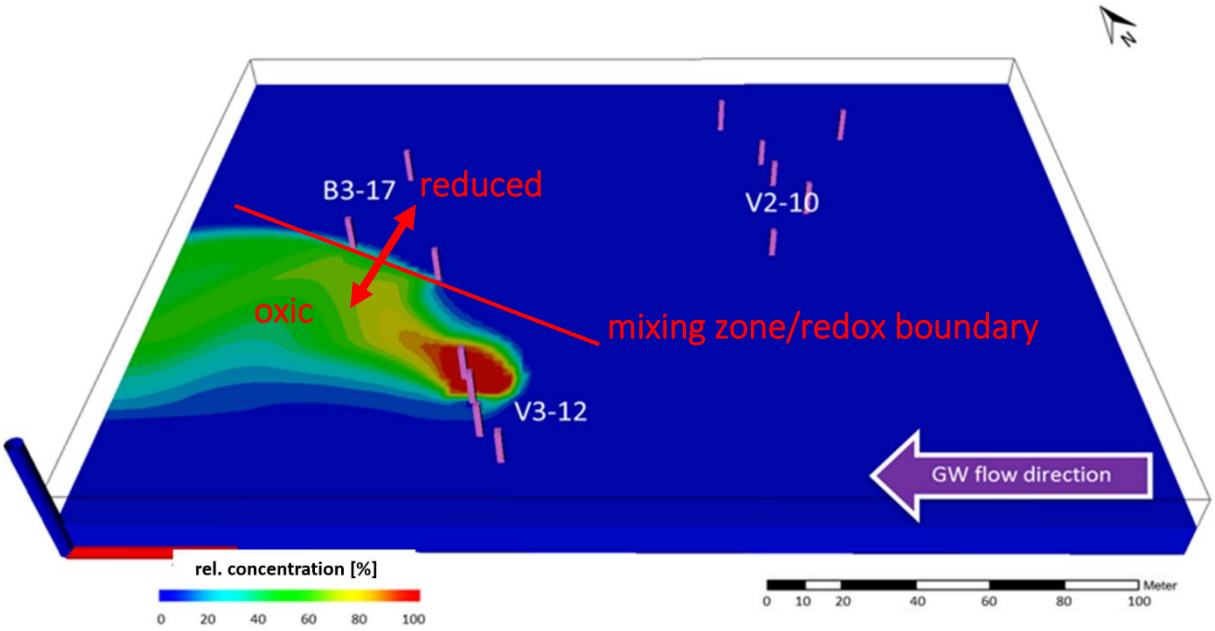

Figure 28. Tracer simulation in the well V3-12. Concentration (C/C_o) front of tracer representing the extent of the infiltrated water (the wells in pink). Red line is mixing and redox boundary (Figure 24).

The results showed that the infiltration water from V3-12 with high concentrations of the electron acceptors is captured by well B3-17. The hydrogeochemical composition in the vicinity of B3-17 is affected by lateral changes of the flow direction induced by the groundwater extraction. Transport of the infiltrated solute varies over time and depends mainly on extraction and infiltration rates. Figure 29 illustrates schematically the hydrodynamic situation in the model.

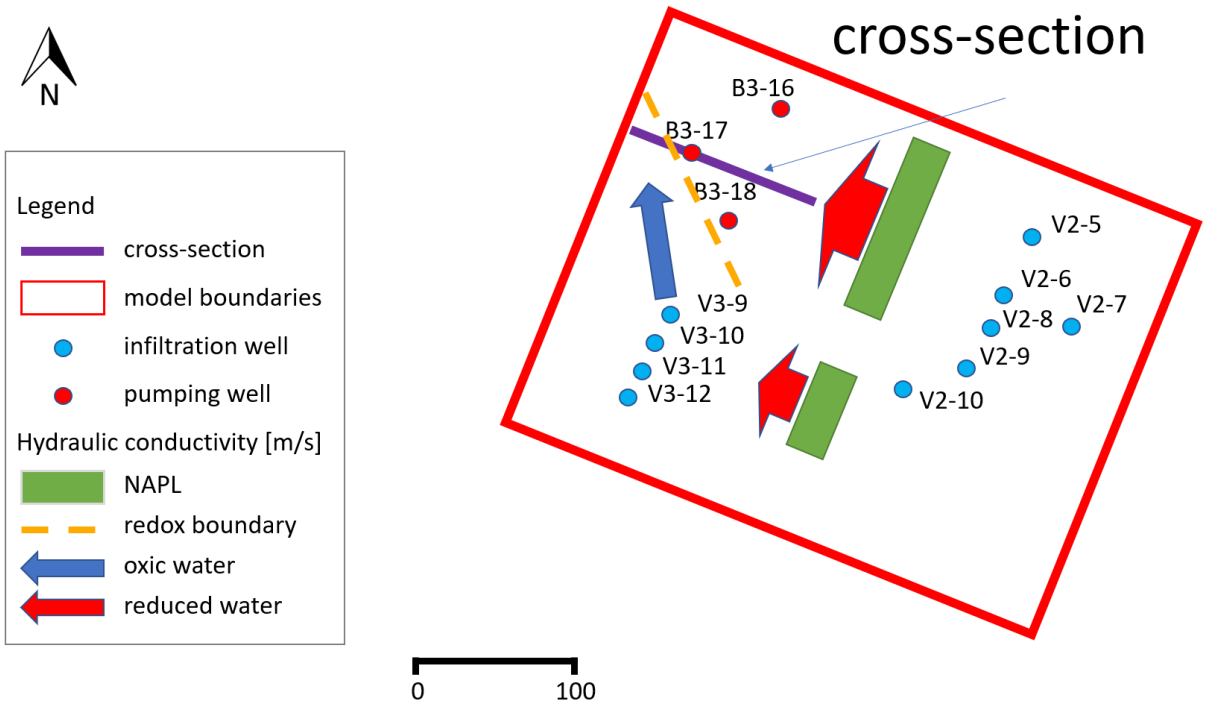

Figure 29. Main groundwater movements in the model. Position of the redox boundary and the cross-section in Figure 30 and 31.

In the next part, the results in the vicinity of the extraction well are presented. Based on the field data, two main extraction phases (2.0 m^3/h and 4.0 m^3/h) in well B3-17 are simulated. This modelling step is performed to understand to what extent the transient changes in extraction rates would induce the temporal changes of hydraulic conditions. The results allow to gain insight into the significant effects of altering pumping rates on hydrogeochemical processes in the vicinity of the extraction wells.

Low extraction rate (2.0 m^3/h)

In the initial periods with the lower extraction rate (2.0 m^3/h), increasing proportions of even more reduced groundwater migrate towards the pumping well (Figure 30). The reduction of extraction rates leads to more reduced conditions around the well.

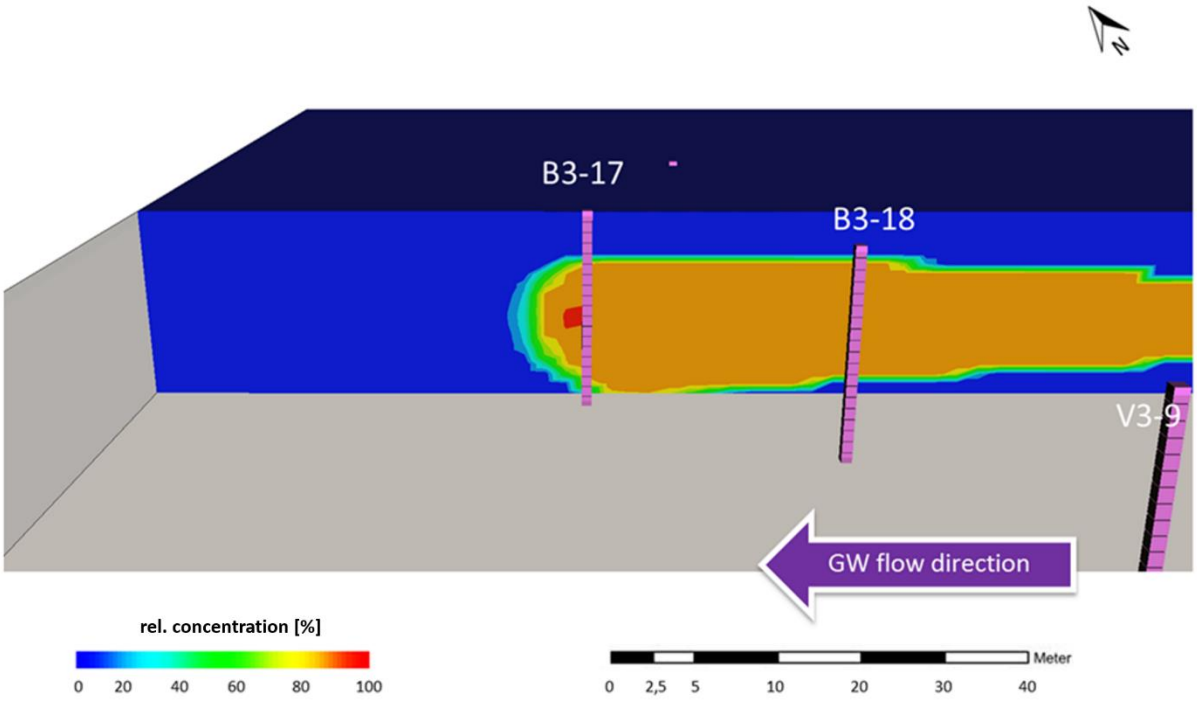

Figure 30. Calculated distribution of pyrite precipitation (C/C_o) in the vicinity of the pumping wells (extraction rate in B3-17 = 2.0 m^3/h). The location of the cross-section is depicted in Figure 29.

Intrusion of reduced groundwater from the contaminated site induces according to the model the reduction of ferrihydrite. During the reductive dissolution of ferrihydrite, Fe^{2+} is released into the groundwater. At these locations the S^{2-} produced during SO_4^{2-} reduction precipitates with Fe^{2+} as pyrite (Figure A-5).

High extraction rate (4.0 m^3/h)

In the initial periods (2.0 m^3/h), the pumping well extracted mainly reduced groundwater. In the next phase with the high extraction rate (4.0 m^3/h), the reduced groundwater from the contaminated site is displaced with the oxygenated infiltration water. Based on the results of the tracer test, the oxygenated groundwater comes from infiltration well V3-9. By the penetration of O_2 and NO_3^-, pyrite turns out to be oxidized.

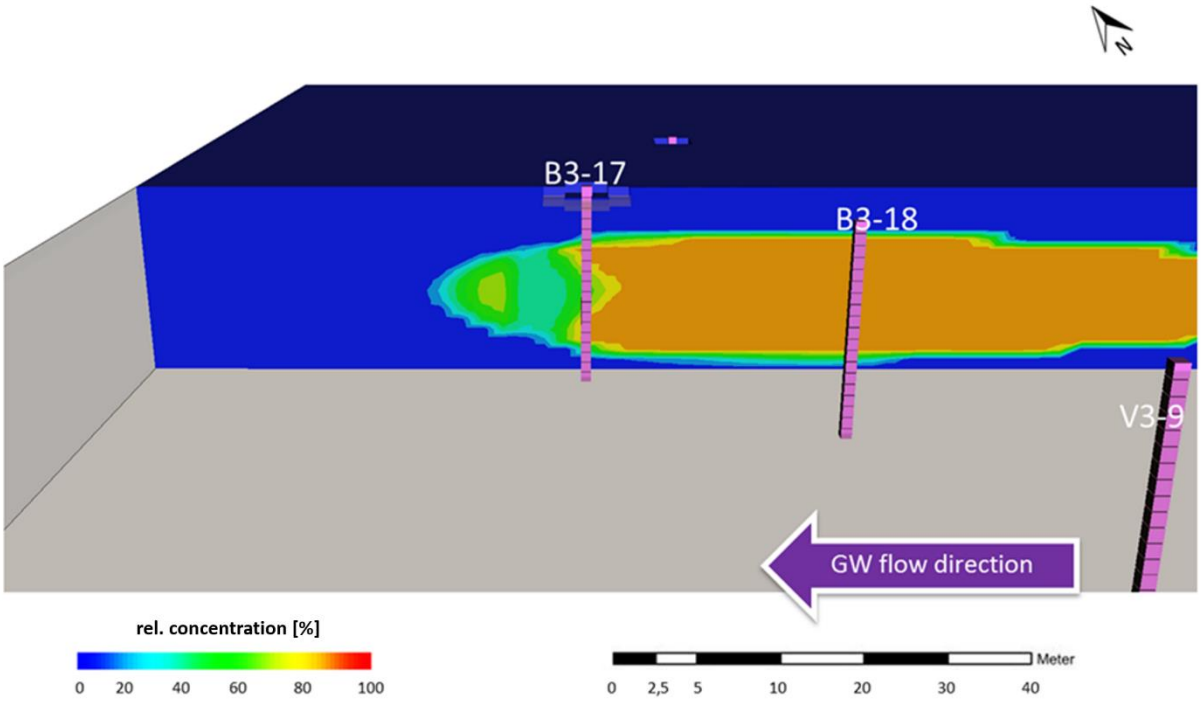

Figure 31. Calculated distribution of pyrite precipitation (C/C_o) in the vicinity of the pumping wells (extraction rate in B3-17 = 4.0 m^3/h). The location of the cross-section is in Figure 29.

Freshly dissolved Fe^{2+} becomes oxidized and precipitated as Fe oxides in the expanding oxidized zone of the aquifer. The reaction follows (APPELO & POSTMA, 2005):

$$FeS_2 + 3\ NO_3^- + 2\ H_2O \Rightarrow Fe(OH)_3 + 1.5\ N_2 + 2\ SO_4^{2-} + H^+ \quad (5)$$

On the other hand, lowering the water table gives atmospheric O_2 access to pyrite and thereby intensifies pyrite oxidation. The precipitation of Fe oxides occurs mainly around the reduced part of the well screen, with the highest precipitation just below the redox boundary (not shown).

The model simulation confirmed the expectation that the results are sensitive to the extraction rates. Figure 31 and Figure 30 show the effect of the different extraction rates on the distribution of pyrite precipitation. The cyclical variation of the extraction rates in B3-17 leads to the enrichment of Fe minerals in the vicinity of the well. In the case of the low extraction rates, reduced groundwater dominates in the vicinity of extraction well B3-17 and induces the precipitation of pyrite. The increase of the extraction rates in B3-17 leads to the dominance of oxic groundwater and the precipitation of Fe oxide.

3.4 DISCUSSION

The central question is why the relatively high As concentration (0.35 µmol/L) occurs in the extracted groundwater, while the groundwater samples in the whole study area have As concentrations below detection level. All results are combined in an effort to

develop an advanced concept explaining the distribution of As in the vicinity of the pumping wells, which is transferable to other remediation sites and As-affected regions in Asia. It is suggested that the observed mixing processes are the primary factor controlling As enrichment.

Currently, many theories have been advanced to explain the patchy As distribution in groundwater (NICKSON ET AL., 2000; APPELO ET AL., 2002; ANAWAR ET AL., 2003; NORRA ET AL., 2005; AMIRBAHMAN ET AL., 2006; HARVEY ET AL., 2006; BERG ET AL., 2007; MAI ET AL., 2014; LAZAREVA ET AL., 2015). However, all these theories observed only hydrogeochemical processes as key factors controlling As mobility. Besides the effects of hydrogeochemical reactions, mixing also has an influence on the As mobility in groundwater. It is complex to identify which physical or chemical processes take the lead in controlling the distribution of As in groundwater. Geochemical changes associated with the groundwater extraction and infiltration are observed and modelled in the context of aquifer storage and recovery systems (PROMMER & STUYFZAND, 2005; DESCOURVIÈRES ET AL., 2010; WALLIS ET AL., 2010; WALLIS ET AL., 2011) and aquifer thermal energy storage systems (BONTE ET AL., 2013; BONTE ET AL., 2014; POSSEMIERS, 2014). These studies showed that groundwater circulation induced by the systems impacted on hydrogeochemical conditions in aquifers. However, they observed mixing processes only in vertical and horizontal orientation. The assessment of mixing processes in lateral orientation allows to identify and quantify hydrogeochemical processes more precisely. In aquifers with redox zoning as in the observed case, these groundwater movements can induce or intensify hydrogeochemical processes at the redox boundary.

The simulation results are in agreement with BONTE ET AL. (2014) that hydrogeochemical reactions occur mainly at the boundaries of redox zones. At the study site, the redox boundary is defined as the transition between O_2/NO_3^- rich and Fe^{2+} rich groundwater. The extent to which extraction mixes different groundwater types depends on the pumping rate, screen length and distribution of redox zones (POSSEMIERS, 2014). The capture zones of extraction wells are often considered as a steady state feature. However, in reality the location and coverage vary due to the transient nature of groundwater extraction and infiltration. Therefore, the effect of alternating pumping should be precisely considered and integrated into the models.

The mixing of reduced and oxygenated waters increases clogging risks due to the potential precipitation of Fe oxides, Fe sulfides and calcite. Precipitation of these minerals is the main cause for chemical clogging (HOUBEN & TRESKATIS, 2003; HOUBEN & WEIHE, 2010). The model results show that not all of the freshly accumulated ferrihydrite and pyrite became dissolved during mixing. This results in a growth of mineral mass and sorption sites in the vicinity of the pumping wells over time. In this case, well age appears to reflect the amount of the clogging material around pumping well and

corresponding amount of sorbed As. This statement is checked at another study site and described in chapter 4.

The growth of clogging material is an explanation for the As enrichment process in the vicinity of the pumping well. The clogging material in the extraction well, which is presented mainly through Fe minerals and calcite, shows relatively high As concentration (9.6 ppm). The observed process is important for postulated statement by HARVEY ET AL. (2006) that irrigation pumping wells may remove As from aquifers and then apply to fields. In this case, time as a factor plays an import role in controlling As concentrations in extracted groundwater. The well documented As mobilization through the dissolution of minerals representing clogging material, mainly Fe minerals and calcite (APPELO ET AL., 2002; WALLIS ET AL., 2011; LAZAREVA ET AL., 2015), delivers a possible explanation for the high As concentrations in abstracted groundwater. The release is caused by a combination of pyrite oxidation and reduction of Fe oxide.

The observed system in the vicinity of extraction wells is similar to plant roots, especially rice roots. KRAMAR ET AL. (2017) and KIRK ET AL. (2015) showed in their studies that the enrichment of clogging minerals, Fe minerals and calcite, occurs in root zones. The diffusion of O_2 leads to precipitation of Fe oxides (KRAMAR ET AL.,2017). In the case of calcite, the uptake of NO_3^- by roots can cause calcite precipitation (KIRK ET AL., 2015).

It should be noted that minerals dissolution is not the only determining factor for high As concentrations. Competitive sorption of HCO_3^- and PO_4^{3-} onto the limited Fe oxide surface can also contribute to the release of As (NICKSON ET AL., 1998; APPELO ET AL., 2002; ZHENG ET AL., 2004; AZAM ET AL., 2008). At the study site, PO_4^{3-} concentration are under detection limit. Hence, competition processes between PO_4^{3-} and As are excluded from the conceptual model. The increased HCO_3^- concentrations are usually associated with reducing conditions (APPELO & POSTMA, 2005; HELD, 2007; MERKEL & PLANER-FRIEDRICH, 2008). Degradation of CH_2O results in increased HCO_3^- concentration. The model results show high HCO_3^- concentrations synchronously with the arrival of reduced groundwater from the contaminated site. Concentrations of dissolved HCO_3^- reflect the sediment-water interaction, especially calcite dissolution, as well as microbial degradation of pollutants. The displacing effect of HCO_3^- offers another explanation for high As concentrations in the extracted water.

3.5 CONCLUSION

Reactive transport modelling is used to obtain insight into the As enrichment onto clogging material. The developed numerical model based on the data collected at a pump-and-treat plant gives insight into the processes induced by groundwater extraction. The model explains high As concentrations in the well from which the water is extracted from the aquifer, which is generally characterized by dissolved As

concentrations under detection limit. While these conditions are comparable to drinking water extraction sites in Asia or ATES systems, differences in redox and hydrogeochemical conditions will determine the extent to which the model is transferrable to other sites. The most significant differences are expected for sites with low redox gradients, e.g., the aquifers with less nutrient and organic matter. In the case of ATES systems, the effect of temperature should also be considered.

The hydrogeochemical data and model results show that groundwater circulation induced by the pump-and-treat system have an important influence on groundwater quality. Extraction by the pump-and-treat system changes the lateral distribution of redox conditions. Mixing processes induce the precipitation of Fe minerals and calcite in the vicinity of the pumping and infiltration wells. Alternating extractions lead to the growth of clogging material over time, which is providing the sorption surface of As. This causes the As enrichment in the vicinity of the extraction wells. The modeling results show that the location of highest Fe minerals precipitation depends on the position of the extraction wells in relation with the redox boundary. The competition processes for sorption surface or the variation of hydrogeochemical conditions can cause temporal mobilization of As from clogging material.

Evidently, the extent and impact of mixing are location-specific. The extent to which mixing processes affect groundwater quality depends on the presence and type of hydrochemical gradients, pumping rates, location of NAPL concerning extraction wells and hydrogeological settings. The site-specific conditions can have an important impact on the groundwater quality. Therefore, an adjustment of each monitoring campaign taking into account the local conditions is indispensable. Furthermore, the groundwater should be observed in each operation phase of wells.

Chapter 4. Impacts of well operation on As distribution in extracted groundwater due to clogging material and temperature

4.1 INTRODUCTION

Arsenic is a persistent contaminant in groundwater and drinking water in the Bengal Delta Plain (BDP) (India) (BISWAS ET AL., 2014). Currently, the reductive dissolution of Fe oxide is the most widely accepted mechanism of As release in groundwater of the Bengal Basin (MCARTHUR ET AL., 2001; HARVEY ET AL., 2002; BERG ET AL., 2008; FAROOQ ET AL., 2011; FAROOQ ET AL., 2012; NEIDHARDT ET AL., 2012).

The results of chapter 2 and 3 show that the induced groundwater circulation by extraction activities impacts on chemical groundwater quality are leading to the As enrichment onto the clogging material in the vicinity of the pumping wells.

Based on a literature review and the results in chapter 2 and 3, three different factors affect the distribution of As in groundwater: (1) clogging material in extraction wells acts as enrichment surface for As, (2) temperature influences the velocities of reactions responsible for As mobilization in aquifers, such as those in South-East Asia, (3) the operation time of wells can give an information regarding the clogging material amount in the vicinity of wells.

Several studies (SUK & LEE, 1999; MCGUIRE ET AL., 2005; LEDESMA-RUIZ ET AL., 2015; ARMANUOS ET AL., 2016) used factor analysis to interpret groundwater chemical data. LIU ET AL. (2003) and HOSSAIN ET AL. (2013) adopted factor analysis to identify the processes governing the fate of As in groundwater.

To analyse the magnitude of previously described three processes on As dynamics in detail, a statistical analysis is set up on the basis of data produced by NEIDHARDT (2012). Multivariate analyses that considering a large set of physical (depth of wells and age of wells) and chemical parameters (including major cations and anions, DOC and pH) provide a better understanding of associations among biogeochemical and physical parameters. This chapter reveals the relations between well age, temperature and As concentration in extracted groundwater, and discusses how these chemical, physical parameters are related to the enrichment and mobilization of As in the vicinity of pumping wells.

4.2 MATERIAL AND METHODS

4.2.1 STUDY SITE

The study area is located in the Indian part of the Bengal Basin and is situated in the Himalayan foreland at the junction of the Indian, Eurasian and Burmese Plates. The region received mainly large volumes of sediments in two periods: between Oligocene and Late Pleistocene, and during the late Pleistocene-Holocene. The sediments were

brought by the Ganga and Brahmaputra from the Himalayas (ALAM ET AL., 2003; ROY & CHATTERJEE, 2015).

The BDP covers an area of about 10^5 km^2 (MUKHERJEE ET AL., 2009). The BDP is known as one of the worst affected areas worldwide by high As concentrations in groundwater (BUSCHMANN & BERG, 2009; NEIDHARDT, 2012).

In the Bengal Basin, groundwater is mainly of the Ca-HCO_3 type. Reducing conditions are dominant in the region, as demonstrated by high Fe^{2+} and CH_4 concentrations (HARVEY ET AL., 2005). In the BDP, As is found to be mainly associated with Fe oxides and Fe sulfides (VAN GEEN ET AL., 2003; AKAI ET AL., 2004).

4.2.2 SAMPLING, DATASET

In the time period between September and November 2007, private and governmental wells were sampled in an area of approximately 20 km^2 within a DFG project by MAJUMBER ET AL. (2015) (Table A-6). In Table A-6, all digits are listed in the measured concentrations for statistical purposes. During the sampling campaign, field parameters (electrical conductivity, pH, water temperature) were measured on-site with a multimeter (MultiLine F/SET-3, WTW). Only the existing wells with complete information (depth, well age, trace elements and major ion concentrations) were selected in this study as measuring points, which made up a total number of 174 wells. Fe^{2+} and total Fe concentrations were determined spectrophotometrically in the field (Lambda 20 UV-Vis Spectrophotometer, Perkin Elmer). ICP-MS was used to determine major and trace elements in the water samples. Detailed information regarding the sampling and analysis is given by NEIDHARDT (2012) and MAJUMBER ET AL. (2015).

In the current study for the description and interpretation of hydrochemical data, two methods are used: conventional techniques (interpretation of maps, plots and diagrams) and multivariate statistics.

Factor analysis is applied to a dataset that consists of 14 chemical (pH, HCO_3^-, As_{tot}, P_{tot}, Fe^{2+}, DOC, Na^+, Mg^{2+}, K^+, Ca^{2+}, Mn^{2+}, Cl^-, NO_3^-, SO_4^{2-}) and 2 physical (depth of wells and age of wells) parameters. Statistical methods are used to extract groups of correlated elements and support the interpretation of governing processes in the study aquifer. This association is identified by evaluating the variance within the whole bundle of the variables.

4.3 RESULTS

Generally, this groundwater belongs to the Ca-(Mg)-HCO_3 type. The measured temperatures range between 26.0 °C and 26.9 °C. The average groundwater

temperature is 26.4 °C. Table 10 shows the mean, minimum, maximum values, and standard deviation of the chemical and physical parameters.

Table 10. Summary of the field survey results (number of samples = 174) comprising respective mean, minimum, maximum, and standard deviation (based on measured data from Neidhardt (2012)).

Parameter	Units	Number	Mean	Min	Max	Std. Dev
Depth	[m]	174	39.5	6.7	271.0	42.6
Age of well	[year]	174	6.4	0.2	24	5.1
pH	[-]	174	7.1	6.0	8.0	0.4
Eh	[mV]	174	278	161	459	64
Temperature	[°C]	174	26.4	26.0	26.9	0.3
El. conductivity	[µS/cm]	174	707	200	1514	186
As_{tot}	[µmol/L]	174	0.69	0.01	4.44	0.82
P_{tot}	[µmol/L]	174	6.61	0.02	33.6	6.84
Fe^{2+}	[µmol/L]	174	67.3	0.2	834	98.2
Mn^{2+}	[µmol/L]	174	5.8	0.1	46.0	5.1
DOC	[mmol/L]	174	0.2	0.1	1.7	0.2
Na^{+}	[mmol/L]	174	1.0	0.2	4.9	0.6
Mg^{2+}	[mmol/L]	174	1.0	0.2	1.8	0.3
Ca^{2+}	[mmol/L]	174	2.5	0.5	4.4	0.6
HCO_3^-	[mmol/L]	174	3.6	1.3	6.4	0.8
Cl^-	[mmol/L]	174	0.6	<0.1	4.2	0.7
NO_3^-	[mmol/L]	104	0.2	<0.1	9.5	0.9
SO_4^{2-}	[mmol/L]	82	0.12	<0.01	0.52	0.11

The main part of the groundwater samples show concentrations of NO_3^- and SO_4^{2-} below the detection limit (0.1 mmol/L and 0.01 mmol/L, respectively). These values influence the results of statistical analyses. To obtain a large set of complete groundwater analyses, NO_3^- and SO_4^{2-} are excluded from further consideration as variables. The remaining dataset of 174 analyses with 14 parameters is assessed using multivariate statistical analysis.

The major cations in the sampled groundwater are Ca^{2+} and Na^+. Bicarbonate is the major anion in the study area, whereas Cl^- is the second dominant anion. Groundwater SO_4^{2+} concentrations range between 0.01 and 0.52 mmol/L.

Arsenic concentrations in 73 % of the groundwater samples are above the World Health Organisation standard for drinking water quality of 0.013 µmol/L As. The mean of As concentrations is 0.69 µmol/L, while concentrations reach up to of 4.44 µmol/L. The

proportion of wells that exceed 0.013 µmol/L As increases with depth from 14 % between 7 and 20 m up to 64 % between 20 and 30 m, then declines to less than 22 % between 30 and 270 m (Table 11).

Table 11. The depth distribution of the wells exceeding 0.13 µmol/L (based on measured data from Neidhardt (2012)).

Depth [m]	Proportion of wells [%]
7 - 20	14
20 - 30	64
30 - 270	22

The overall depth distribution of As is also remarkably similar to that reported by VAN GEEN ET AL. (2003) AND BY HARVEY ET AL. (2006). Although there is a considerable scatter in As over the entire depth range of the wells, concentrations greater than 1.3 µmol/L are largely restricted to the 20-30 m depth range. This pattern is also evident at a variety of specific study sites (VAN GEEN ET AL., 2003; EICHE ET AL., 2008).

Hydrochemical properties in groundwater samples vary spatially in a wide range, especially in respect to As and Fe^{2+} concentrations. The distribution of As concentrations is characterized by extremely horizontal as well as vertical heterogeneity. Arsenic concentrations vary within a couple of metres up to three orders of magnitude. The location of sampling points are shown in Figure 32.

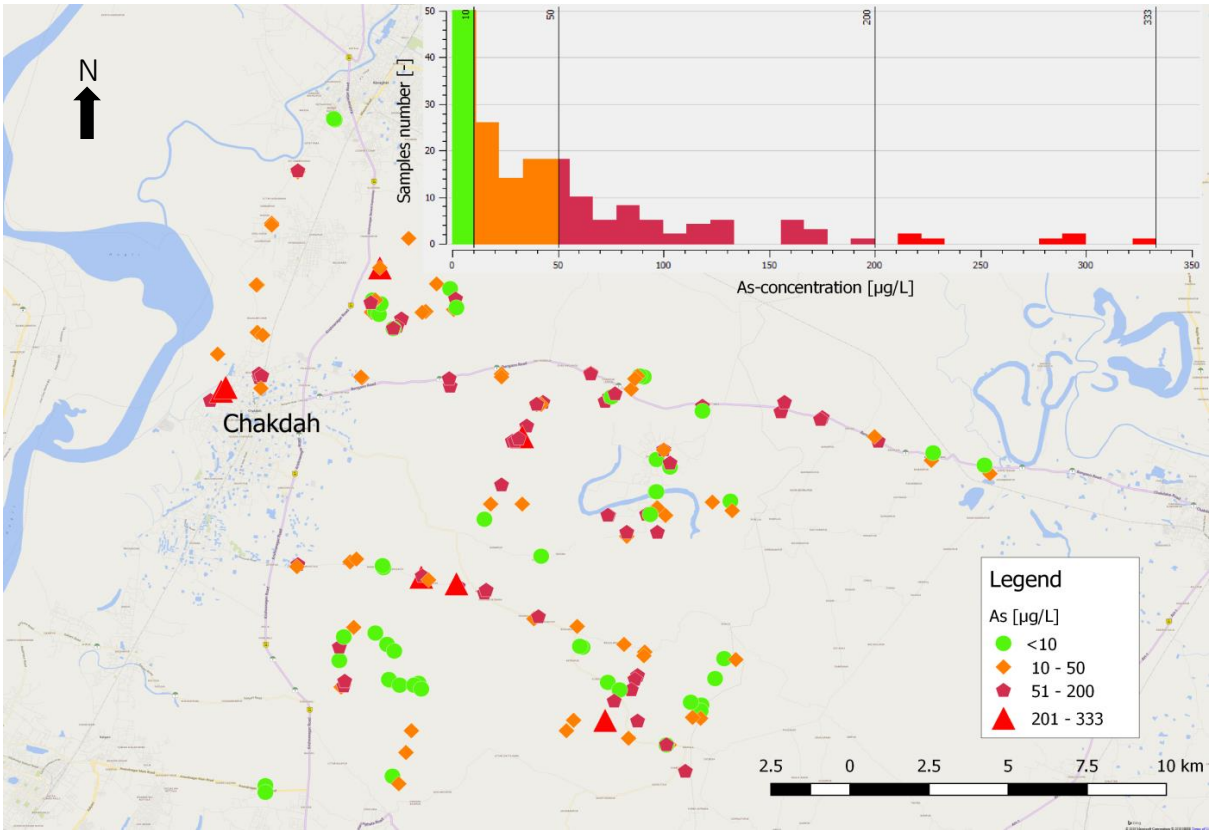

Figure 32. Locations and As concentrations of sampling points (n: 174) within the investigation area. Samples are grouped into four classes according to the As concentrations (background image from: bing.com) (based on measured data from Neidhardt (2012)).

Correlation matrix

The starting point of factor analysis is a correlation matrix. It is used to account for the degree of mutually shared variability between individual pairs of variables. Fourteen variables (depth of wells and age of wells, pH, HCO_3^-, As_{tot}, P_{tot}, Fe^{2+}, DOC, Na^+, Mg^{2+}, K^+, Ca^{2+}, Mn^{2+}, Cl^-) in groundwater from 174 wells are analysed using a correlation matrix.

To reject the null hypothesis, the significance level of 5 % is checked. In all cases, it is smaller than 5 %. The results show that specific electrical conductance strongly correlates with many other variables. Therefore, to avoid the impact of this variable on associations among other components, specific electrical conductance is eliminated from the datasets. Table 12 shows the correlation matrix of the variables after elimination of specific conductance.

Table 12. Correlation matrix of the 14 physicochemical variables (in red – strong correlation (r > ± 0.75), and in blue – significant correlation (r > ± 0.50)).

	Depth	Age	pH	HCO_3^-	As_{tot}	Fe^{2+}	DOC	Na^+	Mg^{2+}	K^+	Ca^{2+}	P_{tot}	Mn^{2+}
Age	-0.25	1.00											
pH	0.04	-0.01	1.00										
HCO_3^-	0.19	0.01	-0.20	1.00									
As_{tot}	0.03	0.10	-0.05	0.09	1.00								
Fe^{2+}	-0.22	0.14	-0.11	0.08	0.48	1.00							
DOC	-0.03	0.04	-0.17	0.05	0.05	0.14	1.00						
Na^+	-0.08	0.01	-0.02	0.36	0.04	0.09	0.07	1.00					
Mg^{2+}	-0.01	0.08	-0.14	0.60	0.05	0.13	0.08	0.58	1.00				
K^+	-0.10	-0.04	-0.01	0.11	-0.12	-0.06	0.01	0.25	0.30	1.00			
Ca^{2+}	-0.10	0.08	-0.16	0.40	-0.02	0.16	0.14	0.47	0.65	0.19	1.00		
P_{tot}	-0.31	0.12	-0.06	-0.03	0.51	0.77	0.10	0.04	0.01	-0.08	0.06	1.00	
Mn^{2+}	-0.22	0.06	-0.13	0.03	0.04	0.06	0.00	-0.06	-0.03	-0.01	0.11	0.00	1.00
Cl^-	-0.28	-0.01	-0.16	0.11	-0.13	0.07	0.22	0.58	0.52	0.27	0.54	0.09	0.04

Strong correlations between variables are not observed, except a correlation between Fe^{2+} and P_{tot}.

In the next step, relations between pairs of variables are analysed iteratively using a scatter plot. Despite the absence of any correlation between As and the age of wells in the correlation matrix, detailed analyses of the scatter plots revealed a positive correlation between the variables (Figure 33).

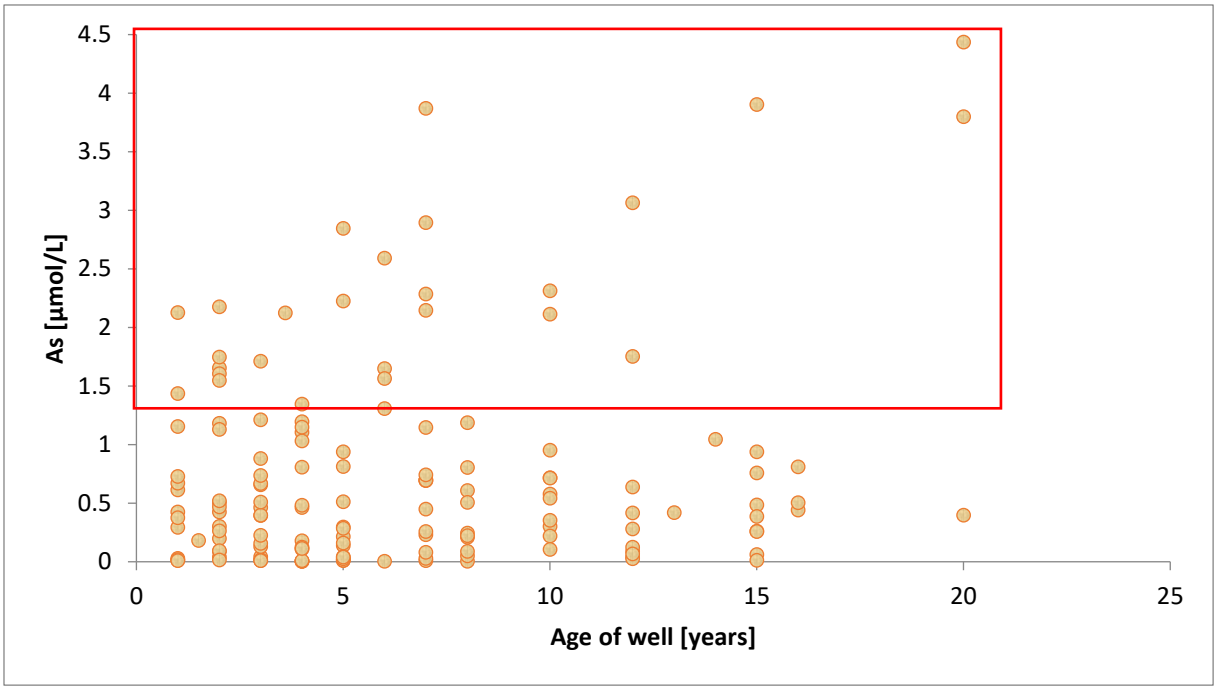

Figure 33. Relationship between As and well age (based on data from Neidhardt (2012)).

The samples with As concentration below 1.3 µmol/L are randomly distributed with respect to the age of wells. However, the samples above 1.3 µmol/L show a positive correlation. In Figure 34 this part of the scatter plot is cut out.

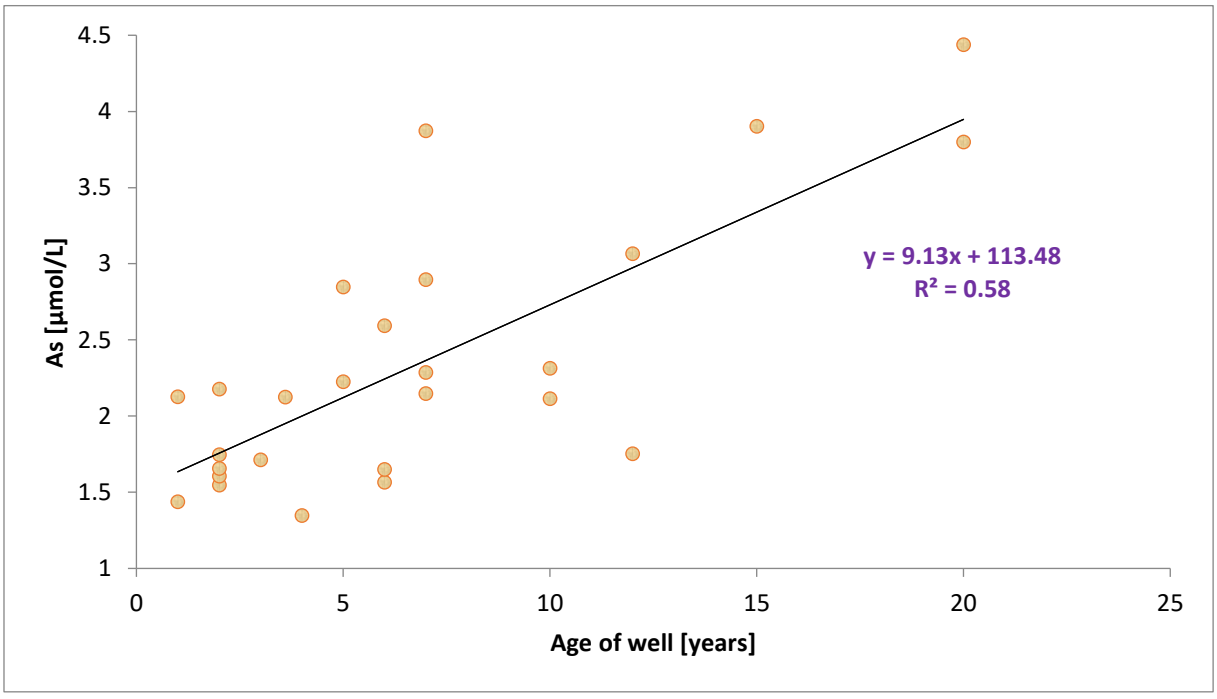

Figure 34. Relationship between As and well age. Arsenic concentration > 1.3 µmol/L (based on data from Neidhardt (2012)).

To analyse the hydrochemical evolution of groundwater, a stability diagram is used. The results show that 55 % of these samples are saturated or oversaturated with respect to calcite (Figure 35).

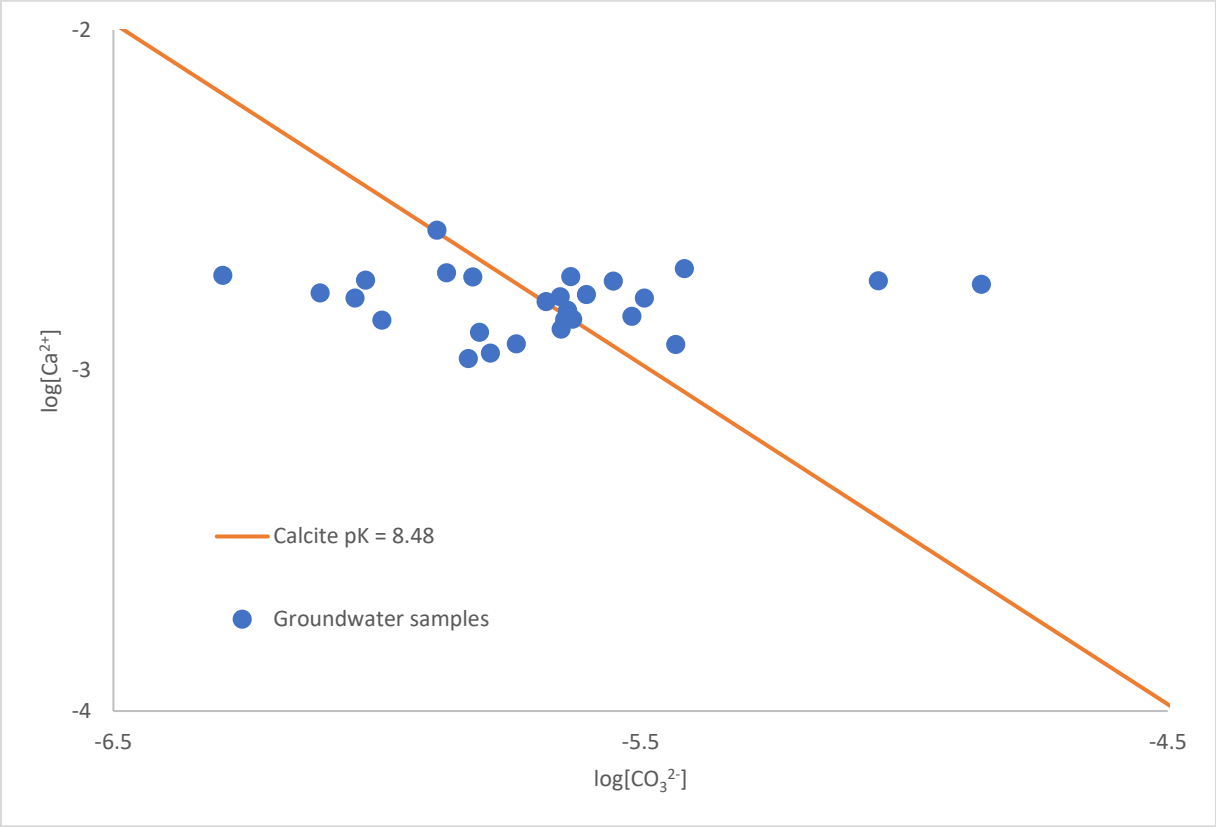

Figure 35. Calcite stability diagram at 25 °C for the samples with arsenic concentration over 1.3 µmol/L (based on data from Neidhardt (2012)).

The samples oversaturated with respect to calcite show potential for calcite precipitation and formation of the clogging material in the vicinity of wells.

The observed effect is pronounced and is easier distinguishable from other processes at high As concentrations. This fact confirms once again that the As distribution in groundwater is controlled by a group of processes.

In the next step, the reduced dataset consisting of 27 samples with As concentrations above 1.3 µmol/L is investigated using a factor analysis. Table 13 shows the correlation matrix of the reduced dataset.

Table 13. Correlation matrix of the 14 physicochemical variables (in red – strong correlation (r> ± 0.75), and in blue – significant correlation (r> ± 0.50)).

	Depth	Age	pH	HCO_3^-	As_{tot}	Fe^{2+}	DOC	Na^+	Mg^{2+}	K^+	Ca^{2+}	P_{tot}	Mn^{2+}
Age	-0.23	1.00											
pH	-0.16	0.19	1.00										
HCO_3^-	-0.02	0.41	-0.26	1.00									
As_{tot}	-0.38	0.70	-0.01	0.09	1.00								
Fe^{2+}	-0.33	0.06	-0.07	0.14	0.18	1.00							
DOC	-0.01	0.06	-0.41	0.46	-0.21	-0.09	1.00						
Na^+	-0.31	0.31	0.35	0.65	0.27	0.36	-0.06	1.00					
Mg^{2+}	-0.21	0.41	-0.32	0.74	0.17	0.34	0.35	0.49	1.00				
K^+	0.08	0.01	0.23	-0.17	0.25	-0.13	-0.25	0.03	-0.20	1.00			
Ca^{2+}	0.03	0.36	-0.15	0.80	0.02	0.27	0.50	0.58	0.81	-0.16	1.00		
P_{tot}	-0.56	0.12	0.00	0.13	0.30	0.77	-0.16	0.36	0.28	0.00	0.08	1.00	
Mn^{2+}	-0.33	0.33	-0.26	-0.10	0.55	0.38	-0.12	0.09	0.13	-0.08	0.05	0.24	1.00
Cl^-	-0.30	0.31	0.01	0.21	0.20	0.30	-0.06	0.28	0.58	-0.20	0.47	0.32	0.45

The examination of the correlation matrix shows the existence of a significant correlation between As concentration and age of wells. Dissolved Ca^{2+} has a strong positive correlation with Mg^{2+} and HCO_3^-. Phosphorus is positively correlated with Fe^{2+}, and shows a negative correlation with the depth of well. In the next step, the dimensionality of this matrix is reduced by gathering the variables with high intercorrelations into groups.

Factor analysis

Based on the eigenvalues > 1 criterion, four factors explain the variability of the variables at the study site (Figure 36).

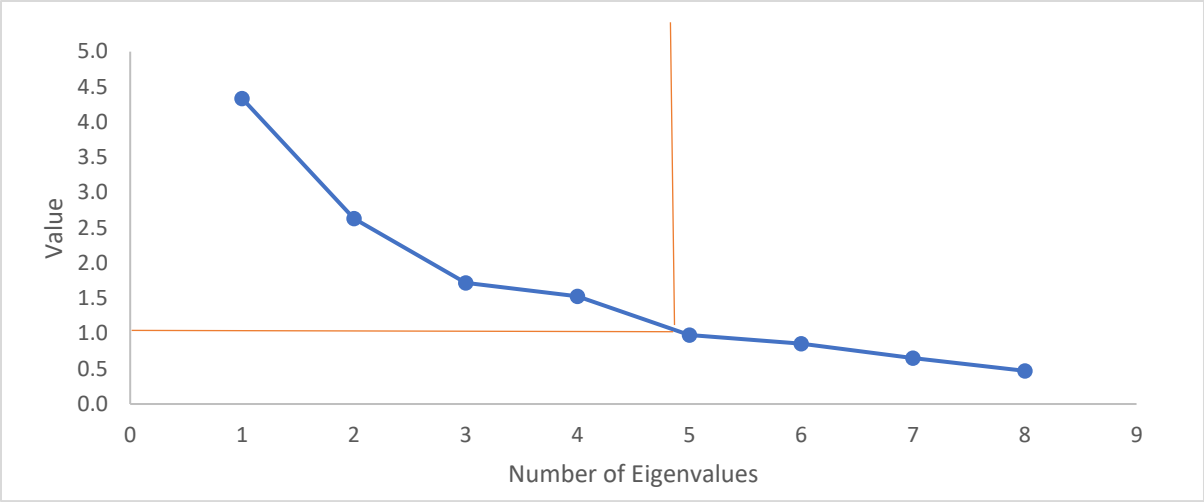

Figure 36. Scree plot. Identification number of factors.

Factor analysis is used to define hydrogeochemical processes in the groundwater. Table 14 shows the factor pattern of four factors. The table incorporates both, positive and negative loadings.

Table 14. Loading for varimax rotated factor matrix. Factor loadings and percentage of variance explained by the four factors (in red – high factor loading (r > ± 0.75), and in blue – significant factor loading (r > ± 0.50)).

Variable	Factor 1 mineralization	Factor 2 fertilizer	Factor 3 organic	Factor 4 As enrichment
Depth	-0.01	-0.65	0.12	-0.24
Age	0.39	0.02	0.02	0.80
pH	-0.10	0.09	-0.82	-0.19
HCO_3^-	0.93	0.00	0.08	0.07
As_{tot}	0.02	0.22	-0.19	0.89
Fe^{2+}	0.13	0.85	0.07	-0.03
DOC	0.49	-0.23	0.54	-0.15
Na^+	0.70	0.34	-0.53	0.06
Mg^{2+}	0.81	0.29	0.24	0.17
K^+	-0.15	-0.23	-0.56	0.28
Ca^{2+}	0.92	0.10	0.15	0.04
P_{tot}	0.07	0.86	-0.11	0.06
Mn^{2+}	-0.19	0.45	0.37	0.63
Cl^-	0.33	0.52	0.14	0.25
Prp.Totl [%]	25	20	13	15

The dataset is reduced to four factors, which explain 73 % of total variance in the analysed dataset. Factor 1 explains the highest percentage of variability within the dataset (25 %), factor 2 a lesser percentage (20 %), the third factor 13 %, and the last factor 15 %.

Each factor is considered as a process controlling chemical composition of groundwater. Factor 1 is characterized by high positive loadings of HCO_3^-, Na^+, Mg^{2+}, and Ca^{2+}; weaker positive loadings of the well age. A strong correlation between Ca^{2+} and Mg^{2+} can originate from carbonate or silicates weathering processes. These associations can be explained by water mineralization. Factor 2 has high positive loadings of Fe^{2+} and P_{tot}, and negative of well depth. The process describes PO_4^{3-} release through organic matter degradation and accompanying the reductive dissolution of Fe oxides (NEIDHARDT ET AL., 2018). Thus, Factor 2 is called the fertilizer factor. The relations between pH and DOC in Factor 3 can be described with CO_2 production coupled to the microbial degradation of organic matter. Factor 4 has high positive loadings of the age of well and As. This factor can be associated with the accumulation of As onto clogging material and can be referred to as the As enrichment factor. The results indicate the absence of a correlation between As and Fe^{2+}.

Cluster analysis

In the next step, a hierarchical cluster analysis is performed on the reduced dataset (27 samples). The cluster analysis classified the groundwater samples into four general classes, namely, C_1, C_2, C_3 and C_4. The result of the cluster analysis is shown in dendrogram (Figure 37).

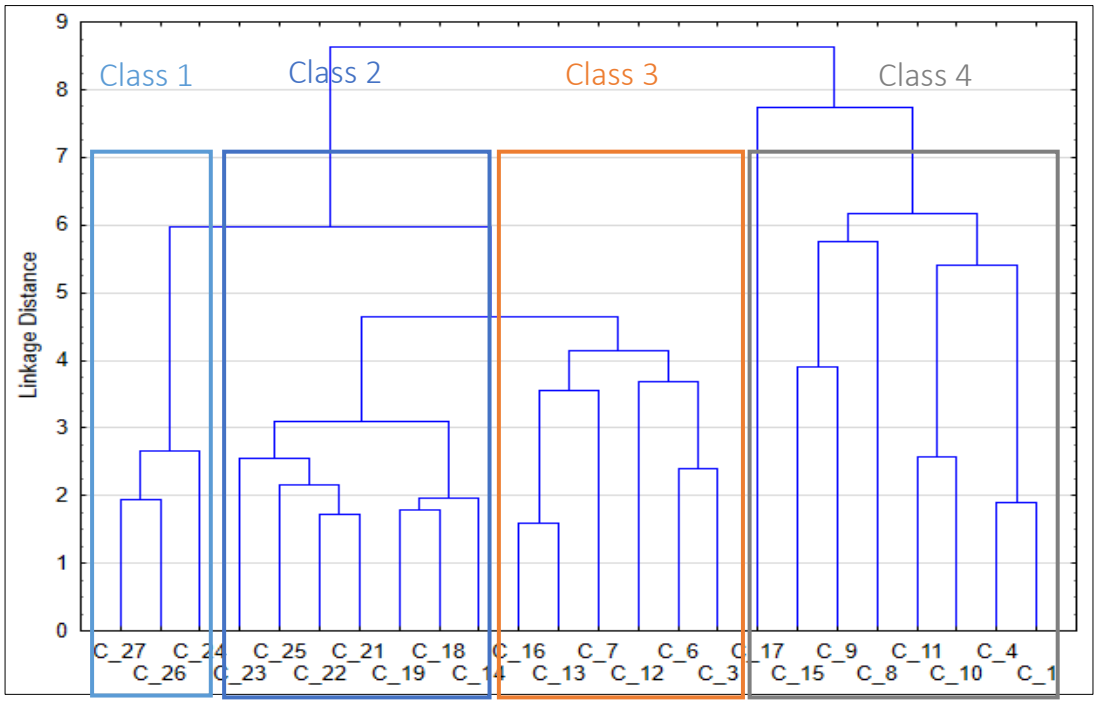

Figure 37. Dendrogram of the cluster analysis.

The piper diagrams in Figure 38 shows distinguishable hydrochemical features between these classes. The groundwater hydrochemical type is Ca-Mg-HCO_3. The samples are characterised by relatively low Cl^- and SO_4^{2-}concentrations and the predominance of Ca^{2+} and Mg^{2+}. Compared to other classes, Class 4 shows a higher ratio of Na^+.

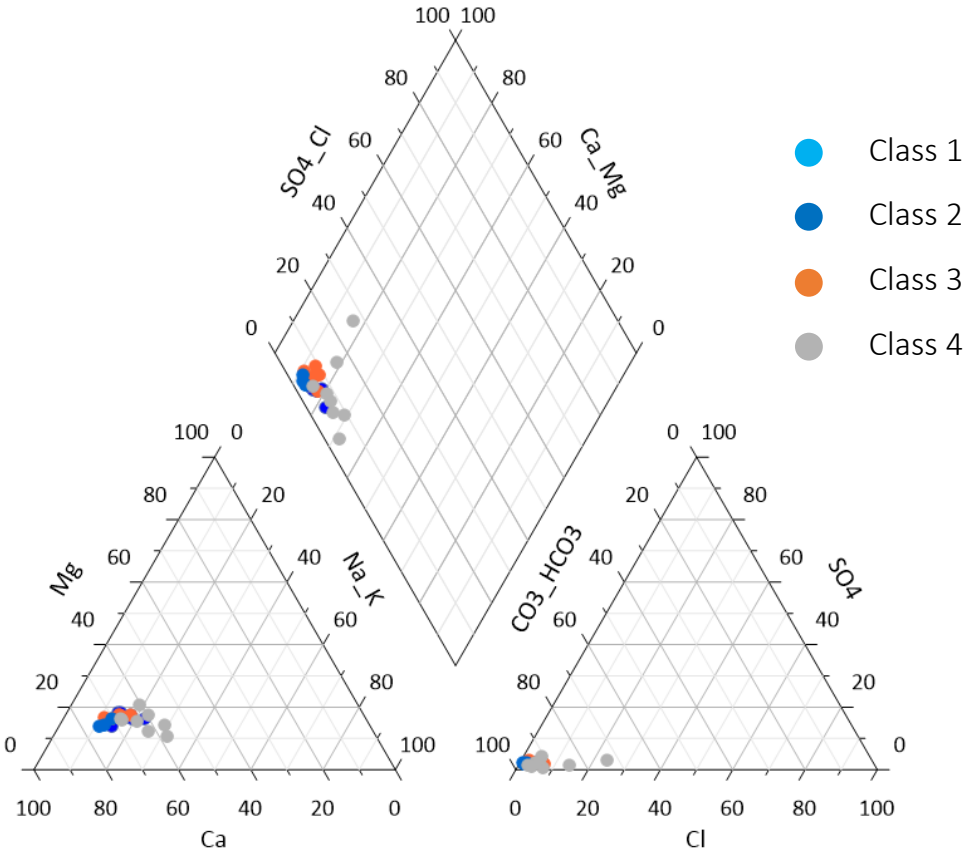

Figure 38. Piper diagram showing the main hydrochemical composition of the four classes.

It is difficult to visually distinguish between the hydrochemical distribution of the classes on a traditional piper diagram. The classes are also not related spatially to each other (Figure A-6). Therefore, relations between classes are analyzed in detail using scatter plots in Figure 39, Figure 40 and Figure 41. The graphs show differences among the classes according to relations between physical and hydrochemical parameters.

Figure 39 shows the relations between Ca^{2+} and As concentrations. The samples in C_3 and C_4 have mainly a higher As concentrations (> 2 µmol/L). In contrast to C_3 and C_4, C_1 and C_2 show relatively low As concentrations.

Class 2 and Class 3 have similar linkage distance, and therefore, have higher hydrochemical similarity. The classes differ slightly in Ca^{2+} concentrations (Figure 39). Similarity between C_1 and C_2 samples are also strong. Class 4 is distinct from other classes.

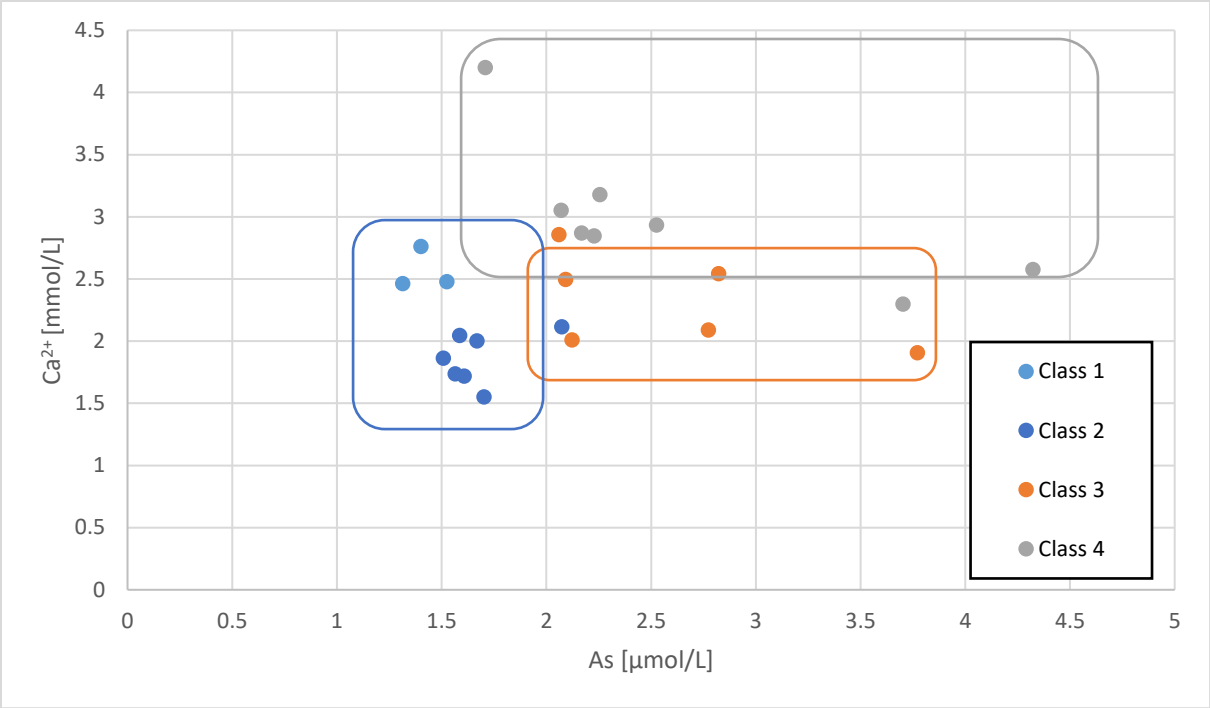

Figure 39. Cluster analysis. Relations between As and Ca^{2+} (based on data from Neidhardt (2012)).

Calcium concentrations in C_2 are below 2.15 mmol/L, and in C_3 are above. Low Ca^{2+} and Na^+ concentrations coincide with C_2 and high concentrations with C_4. The relations between Na^+ and As concentrations are presented in Figure 40.

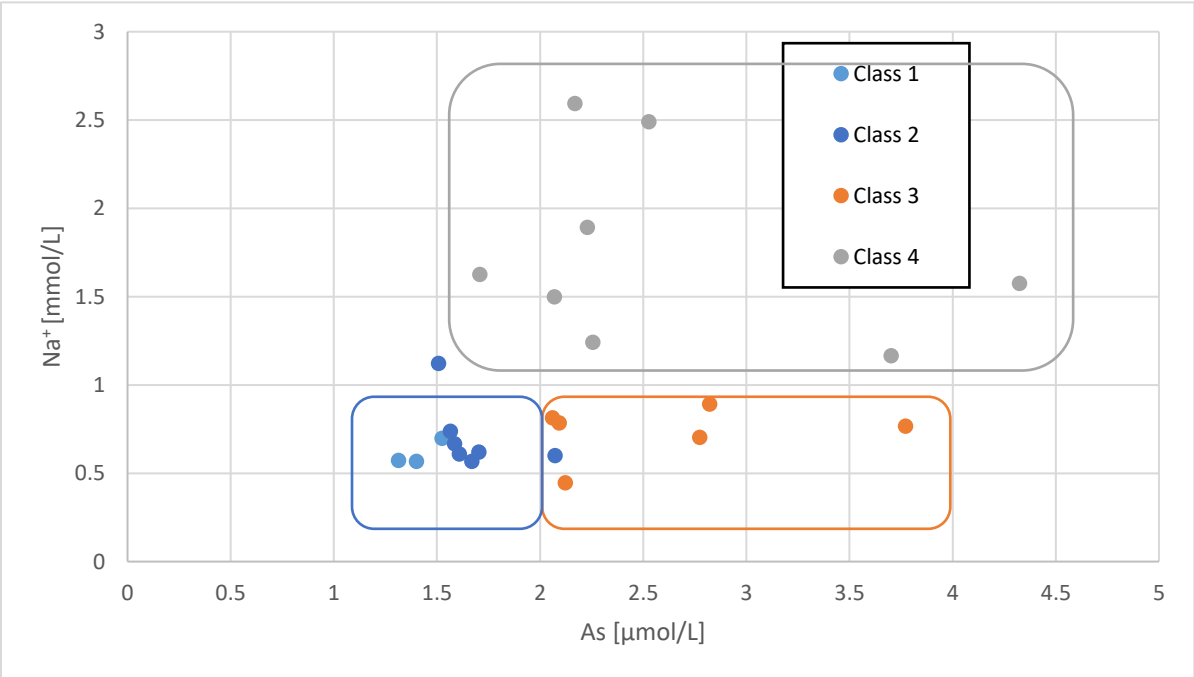

Figure 40. Cluster analysis. Relations between As and Na^+ (based on data from Neidhardt (2012)).

In C_4 As concentrations range between 1.7 and 4.3 µmol/L. Class 1 shows relatively low As concentrations among the classes. Depth of the wells delivers a possible explanation (Figure 41).

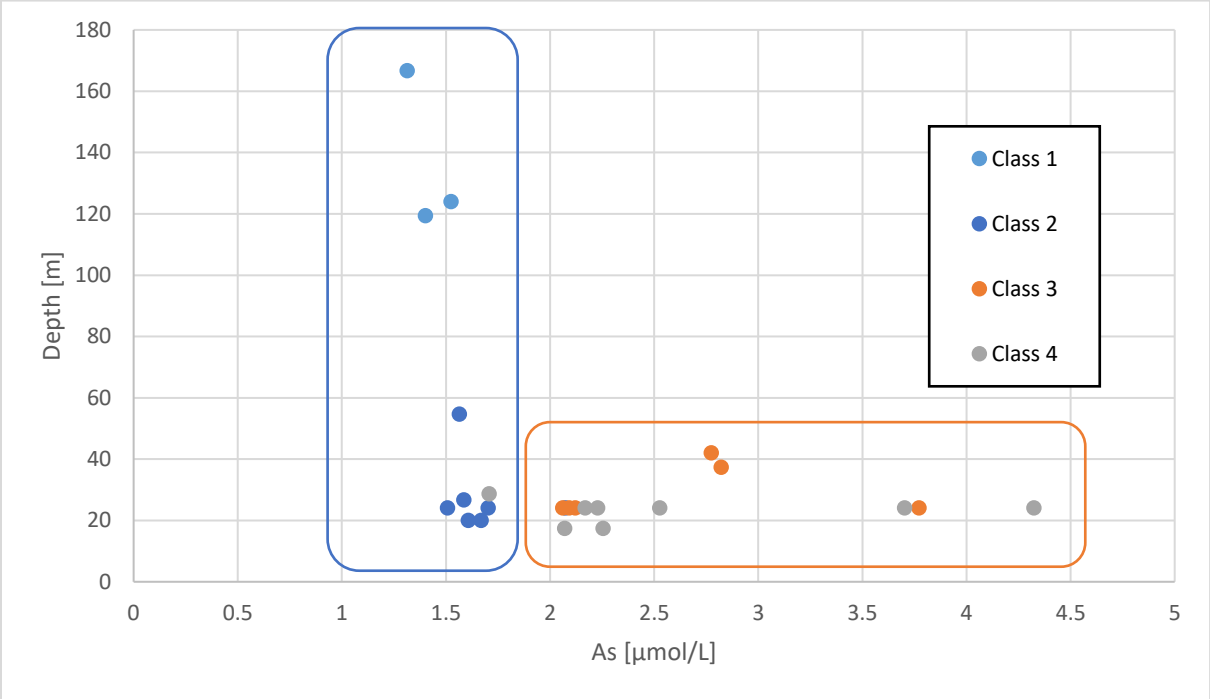

Figure 41. Relations between As and Depth of the well (based on data from Neidhardt (2012)).

The wells in C_1 are filtered between 120 m and 166 m. Other three classes extract groundwater below 60 m.

4.4 DISCUSSION

The results in chapter 2 and 3 show that clogging material, especially Fe minerals and calcite, controls the As enrichment in the vicinity of wells. Besides local hydrogeochemical conditions, the operation time of extraction wells also plays an important role. The aim of this chapter is to investigate the postulated thesis and modelling results of these two studies using multivariate statistical analyses on the data collected in the western part of the BDP.

The results provide that As concentrations correlate with the age of wells. This corresponds to an increase in As concentrations over time. Several studies (McArthur et al., 2001; Burgess et al. 2002; Kinniburgh et al., 2003; van Geen et al., 2003) also provide significant statistical evidence that As concentrations in extraction wells positively correlate with the age of wells. However, suggestions concerning the processes explaining the correlation were not formulated. The results in chapter 3 gives

an explanation how alternating extraction activities intensify the growth of clogging material in the vicinity of wells.

ISLAM ET AL. (2004) demonstrated that As is mainly mobilized in West Bengal from Fe oxides. A lack of correlation of between Fe^{2+} and As concentrations in groundwater can be explained by the relatively high concentrations of phosphate, which competes with As for sorption sites (APPELO ET AL., 2002; SWARTZ ET AL., 2004). However, the absence of a correlation between P_{tot} and As indicates that the ion competition process cannot fully explain the heterogeneous distribution of As. Therefore, it can be seen as only one of the processes describing As mobilization.

Factor 2 represents contamination of shallow aquifer with phosphorus fertilizers. The factor can explain movement of water from rice fields into subsurface. During recharge periods on rice fields, redox conditions become reduced. Therefore, Fe oxides dissolve and phosphorus is released and transported into groundwater. This process was discussed by HARVEY ET AL. (2006), KRAMAR ET AL. (2017) and NEIDHARDT ET AL. (2018). In general, the low concentrations of SO_4^{2-} indicate that Fe^{2+} has not been mobilized into groundwater from Fe sulfides (APPELO & POSTMA, 2005).

The important finding is that the correlation between the As concentrations and the age of wells is found in the wells with high As levels (> 1.3 µmol/L). The absence of a correlation between the samples with low As concentration shows that in these samples the distribution of As is controlled by a group of processes (i.e. Fe oxide reduction, Fe sulfide oxidation and competition processes for surface adsorption places). In the case of As concentrations below 1.3 µmol/L, the As enrichment process onto clogging material as factor describes relative small part of mobilized As in groundwater.

The results of cluster analysis show a correlation between the mineralization of groundwater and As concentration in the shallow aquifer. This effect is more pronounced for C_2, C_3 and C_4 as for C_1. In comparison to C_1, C_4 represents highly mineralized groundwater with high concentrations of Ca^{2+} and Na^{+}. Class 1 shows that the deeper aquifer appears to have lower As concentrations (Figure 41). This result is in agreement with the depth profiles of As presented by KINNIBURGH ET AL. (2003) and MCARTHUR ET AL. (2004).

Nevertheless, the well age alone is not a reliable indicator for the As enrichment process in the vicinity of the extraction wells. The well age corresponds to the possible amount of clogging material. Clogging material provides an increasing number of the sorption sites for As over time. The results of chapter 2 and 3 indicate that the enrichment process of As on clogging material is able to influence the observed heterogeneous As distribution in groundwater. However, both, hydrogeochemical settings and amount of clogging material are important prerequisites for As accumulation.

The second important finding is that, in contrast to aquifers in Europe, relatively high temperatures are found in the study area (Table 10). To explain the significantly different As levels in Europe and Asia, the various physical conditions of these regions must be considered. The average groundwater temperature in the study area is determined by 26.4 °C. In comparison to Asia, groundwater temperature in Europe ranges between 10 °C and 15 °C (BRIELMANN ET AL., 2009; BONTE ET AL., 2013A; BONTE, 2015). The differences in average aquifer temperature in Asia and Europe can explain discrepancies in As mobility in these regions. However, energy storage techniques are receiving a growing interest in Europe. The increasing number of such systems leads to local warming of groundwater up to 25 °C (BRIELMANN ET AL., 2011; BONTE, 2013). Besides energy storage systems, the temperature effects of climate change and urbanization on the aquifer system makes this parameter more pronounced for the distribution of As in Europe.

A number of studies looked in an integrated way at the temperature impacts on hydrogeochemical changes (HENNING & LIMBERG, 1995; BRIELMANN ET AL., 2009; BRIELMANN ET AL., 2011; ZUURBIER ET AL., 2013; HARTOG, 2011). Temperature was not intensively investigated as a factor controlling the behaviour of As in an aquifer. Temperature plays an important role in the solubility of minerals, reaction kinetics, oxidation of organic matter, redox processes and sorption-desorption (BRONS ET AL., 1991; GRIFFIOEN & APPELO, 1993; PROMMER & STUYFZAND, 2005; SOWERS ET AL., 2006; BRIELMANN ET AL., 2009). BONTE ET AL. (2013B) studied in laboratory experiments the temperature-driven changes in the behaviour of trace elements and heavy metals. The authors showed significant As mobilization at 25 °C from sediment cores in comparison to 5 °C and 11 °C. PROMMER & STUYFZAND (2005) illustrated that redox reactions in groundwater can be affected by temperature changes (2 – 23 °C). JESUßEK ET AL. (2012) reported the mobilization of organic carbon and an increase in microbial activity above 25 °C. The authors demonstrated also that temperature increase can stimulate the microbial reductive dissolution of Fe oxides.

The results of sequential extraction by NEIDHARDT (2012) showed that As is mainly adsorbed onto Fe oxides at the study site. Microbially mediated redox reactions, especially the reductive dissolution of Fe oxides, can be stimulated by a temperature increase (JESUßEK ET AL., 2013; POSSEMIERS, 2014). In the current results, however, there is relatively weak correlation between As and Fe^{2+}, suggesting that reductive dissolution is not solely process controlling As mobilization. Another explanation is the reprecipitation of dissolved Fe^{2+} in form of siderite and goethite (ZACHARA ET AL., 2002). The weak correlation between As and Fe^{2+} can be explained through the As readsorption process onto calcite and Fe minerals or removal of Fe^{2+} though the precipitation of Fe minerals. The reduction of ferrihydrite induces a formation of more stable minerals such

as goethite without the release of Fe^{2+} into groundwater (ZACHARA ET AL., 2002; HORNEMAN ET AL., 2004; BOSTICK ET AL., 2004). Released As could co-precipitate with freshly crystalized Fe minerals. Therefore, the release of As is delayed relative to dissolved Fe^{2+}.

4.5 CONCLUSION

The primary focus of this research is to investigate the postulated thesis and modelling results in chapter 2 and 3 on the data from the western part of the BDP. The investigation approach includes statistical analyses that provide insight into the As enrichment behaviour as a function of time and temperature.

Arsenic concentrations in the study area vary greatly over short distances. Some of this variation is caused by the As enrichment on the clogging material in the vicinity of extraction wells. The As enrichment on the clogging material can give an interpretation of the observed correlation between the age of wells and dissolved As concentration. The highest As concentrations occur in oldest and clogged wells. Therefore, well age plays an important role in determining the concentrations of soluble As.

Relatively weak correlation between As and Fe^{2+} corresponds to the readsorption of As on the clogging material or recrystallisation of ferrihydrite. Arsenic released from Fe oxides can be likely resorbed on Fe sulfides and calcite.

The study represents temperature as factor regionalising As contamination. The groundwater temperature around 25 °C is typical for Asia. In Europe the temperature of groundwater lies between 10 and 15 °C, where the effect of temperature on mineral equilibria and kinetics is smaller. However, the installation of aquifer thermal energy storage systems leads to local temperature increase up to 25 °C making temperature factor more pronounced for the distribution of As in Europe.

In summary, two factors can control As mobility in an aquifer: temperature and amount and chemical/mineralogical composition of the clogging material that can correlate with age in the extraction wells. Consequently, these factors should be considered for groundwater quality monitoring programs. The developed conceptual models should serve as hypotheses to be further tested and amended by future detailed field and laboratory investigations.

Chapter 5. Conclusion. Conceptual model

5.1 INTRODUCTION

In this chapter, the outcomes of this PhD thesis are summarized and discussed on the basis of the research questions postulated in chapter 1. Following this, the observed processes controlling the spatial As distribution are gathered into a conceptual model. Last, the perspectives for future research based on the results of this thesis are given.

5.2 SUMMARY

- What is the impact of calcite in contrast to Fe minerals on the As distribution in groundwater?

The results of the reactive transport model describing hydrogeochemical conditions in the Van Phuc aquifer in chapter 2 provide a potential explanation for the heterogeneous distribution of As in groundwater and considerable degree of decoupling between As and Fe observed in previous studies. A literature survey on the As adsorption and retention showed that most published research focused on Fe oxide, whereas the impacts of calcite on As distribution has been addressed to a limited extend. At the beginning of the simulation period, calcite has only a negligible influence on the retention of As due to low calcite content. The model shows the growth of calcite at the redox boundary over time. Therefore, its overall contribution has continuously increased over time up to 20%. In contrast to Fe minerals, calcite is stable under the fluctuation of redox conditions. That makes calcite a more persistent mineral trap for As. Calcite plays an important role in the retention of As in groundwater. The overlooking calcite role as sorption sites can result in an overestimation of other factors.

- What are the driving physical and hydrogeochemical processes determining the enrichment of As process in the vicinity of pumping and infiltration wells?

The simulation results in chapter 3 illustrate that both, physical (groundwater flow and mixing processes) and hydrogeochemical processes (redox and mineral dissolution/precipitation processes) are essential to improve the conceptual understanding of the As distribution in groundwater. The mixing processes induced by pumping and infiltration activities cause the hydrogeochemical changes on the boundary between reduced and oxidized conditions. Mixing of waters with contrasting redox conditions result in the precipitation of Fe minerals and calcite. Varying extraction rates result in a growth in the content of minerals and corresponding sorption sites in the vicinity of pumping wells. The sorption of As onto precipitated mineral phases leads to As enrichment over time.

Previous studies mainly concentrated on local hydrogeochemical conditions. The main contribution of the present study is a demonstration that the high concentrations of As in extracted groundwater partially is the result of As enrichment processes onto

clogging material. The study also describes the impact of extraction and infiltration activities inducing the mixing of waters with different hydrochemical compositions on the distribution of As in groundwater.

- What is the impact of extracting activities in the long term on chemical composition and As enrichment?

The results in chapter 4 provide significant statistical evidence that the As concentrations in extraction wells positively correlate with the age of wells. The operation time of wells corresponds to the amount of clogging material, which is increasing over time due to varying extraction rates. The age of wells gives indirect information about the risks of As contamination in each well. The correlation improves the simulation results obtained in chapter 2 and chapter 3.

The competition processes for sorption sites on mineral surfaces or the variation of hydrogeochemical conditions can lead to the short-term mobilization of significant As amount from clogging material and increase in dissolved As.

- What is the impact of temperature on As mobility?

The analysis of the data from different regions (Europe and Asia) combined with data from literature provides insight into the temperature dependence of the spatial As distribution. Temperature plays an important role in minerals solubility, redox and sorption-desorption processes. A higher temperature enhances microbial activity and increase the mineralization of organic matter. The distribution of As in an aquifer is strongly controlled by redox state. Redox reactions are sensitive to small temperature variations. Therefore, the mobility of As is significantly enhanced with a temperature increase. Considerable differences in groundwater temperature contribute to explain higher As mobility in the Asia region compered to Europe. In Europe, urbanization and thermal usage of aquifers can locally raise the issue of groundwater quality.

5.3 CONCEPTUAL MODEL

After having summarizing and discussing the observed principal effects and processes in chapter 2, 3 and 4, the next step is to create a synoptic conceptual model. High As concentration in extracted groundwater is the result of complex interaction between physical and hydrogeochemical processes in the vicinity of groundwater extraction wells. In the thesis three categories of effects are distinguished: (1) hydrogeological, (2) hydrogeochemical and (3) thermal. The conceptual model incorporates all of them. The conceptual model is presented graphically in Figure 42.

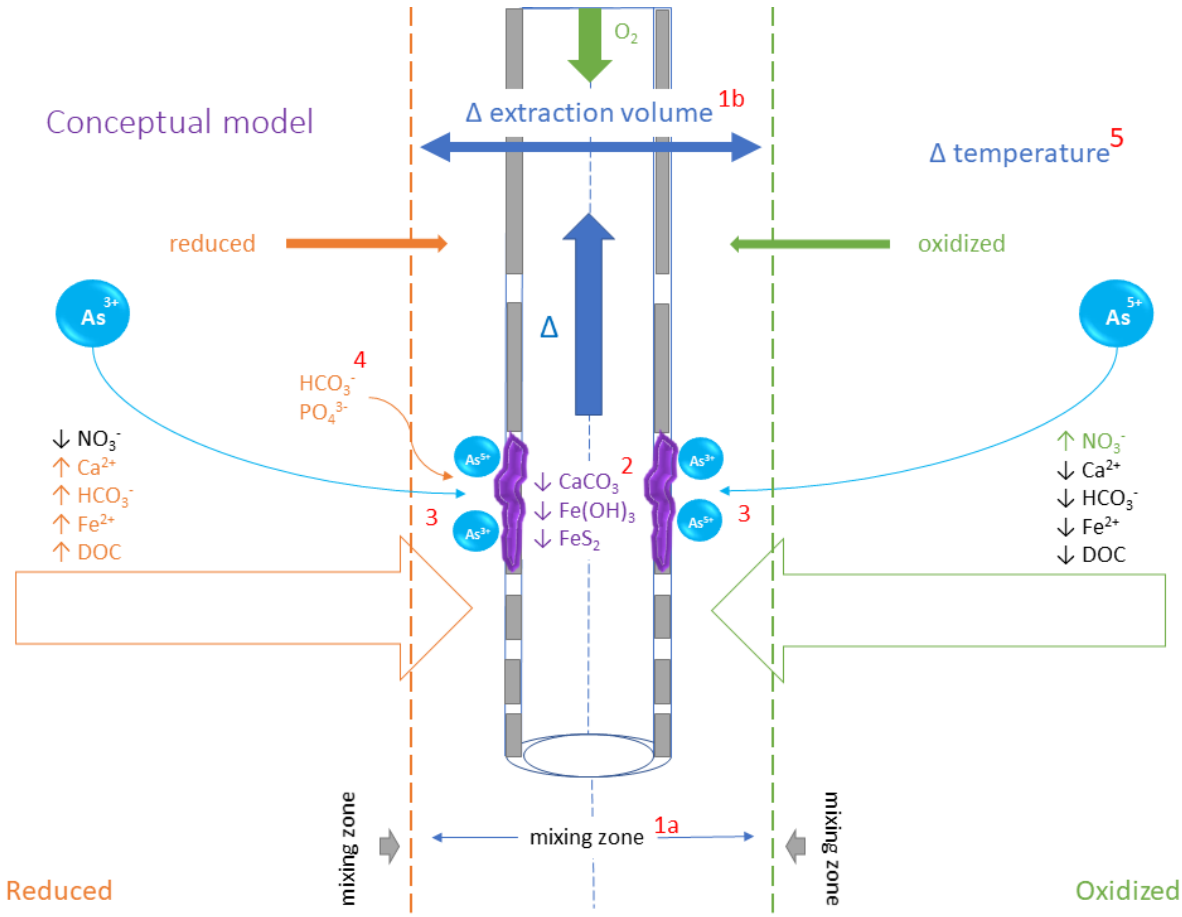

Figure 42. Conceptual model. Processes controlling the enrichment of As in the vicinity of the extraction well. Processes: (1a) mixing processes; (1b) alternating groundwater extraction; (2) precipitation of Fe oxide, Fe sulfide and calcite, and growth of clogging material; (3) arsenic adsorption; (4) competitive adsorption of HCO_3^- and PO_4^{3-}; (5) temperature effect.

The distribution of As in the vicinity of extraction wells is a function of five key processes. The first process **(process 1a)** is the physical mixing of water with different chemical compositions by extraction wells impacting on local redox conditions in an aquifer. The effect of this process on extracted water depends on mineralogical composition, pumping rates, the duration of each pumping activity, and the lateral and vertical distribution of hydrochemical zones. The mixing of groundwaters with different redox conditions and CO_2 partial pressure can lead to the precipitation of Fe oxide (HOUBEN, 2003; HOUBEN & TRESKATIS, 2003; STUYFZAND 2007; MEDINA ET AL., 2013; POSSEMIERS, 2014) and calcite (PALMER ET AL., 1992), respectively. The mixing of different groundwater types has already been described as the dominating process controlling hydrogeochemical changes in ATES (DE ZWART, 2007; BONTE, 2013), pump-and-treat (SHTIRKIN, 2013), ASR systems (PROMMER & STUYFZAND, 2005; DESCOURVIÈRES ET AL., 2010) and drinking water wells (POSSEMIERS, 2014).

It is further shown that pronounced temporal changes in As concentrations can occur, which are directly linked to fluctuation of the infiltration and extraction rates. The hydrochemical compositions of the groundwater depth profiles in the vicinity of extraction wells are a transient feature (BONTE, 2013). This factor complicates the impact assessment of extraction activities on the groundwater quality. The simulation results at the study site 2 illustrate that both, physical (groundwater flow and mixing processes) and hydrogeochemical processes (redox and mineral dissolution/precipitation processes) are essential for the understanding of As distribution and temporal and spatial variation of the redox zonation. Alternating extraction (process 1b) can lead to the precipitation and growth of clogging minerals (process 2), especially Fe minerals and calcite over time, as well as to physical well clogging (DE ZWART, 2007; HOUBEN & WEIHE, 2010; VAN BEEK, 2011; MEDINA ET AL., 2013).

The operation time of wells can give an information regarding the amount of clogging material in the vicinity of wells. This enables subsequent accumulation of dissolved As. The enrichment of As onto clogging material (process 3) becomes more pronounced and quantitatively remarkable over time. Several study cases (MCARTHUR ET AL., 2001; BURGESS ET AL. 2002; KINNIBURGH ET AL., 2003; VAN GEEN ET AL., 2003) observed a positive correlation between the age of wells and As concentrations. However, suggestions concerning the processes explaining the correlation were not formulated. The results at the study site 3 gives an explanation how the age of wells corresponds to the amount of clogging material. The mixing processes in the vicinity of extraction wells induce the precipitation of clogging minerals, especially Fe oxide and calcite. Alternating extractions lead to the growth of clogging material amount over time. The results provide significant statistical evidence that As concentrations in extraction wells positively correlate with the age of wells. The age of wells gives indirect information about the risks of As contamination in each well.

In pump-and-treat and aquifer thermal energy storage systems, the enrichment of As in groundwater occurs in the vicinity of extraction wells as well as infiltration wells (GRIFFIOEN & APPELO, 1993; SHTIRKIN, 2013). In contrast to Fe minerals, calcite precipitation is more pronounced around infiltration wells.

Arsenic migration can be strongly affected by sorption onto calcite, especially, where Fe and Mn oxides have low content or lost their adsorbing effectiveness. The results at the study site 1 show that in comparison to ferrihydrite overall contribution of calcite to the As retardation increased over time up to 20 %. Calcite is the more stable mineral under changing redox conditions (YOKOYAMA ET AL., 2012) and, therefore, presents an appropriate mineral trap for As. While the reductive dissolution of Fe oxides is responsible for the remobilization of As in groundwater.

The accumulation of As in the vicinity of wells is followed by mobilization processes. An important prerequisite of the mobilization of As is a competition process for sorption surfaces (process 4). PO_4^{3-}, OH^- and HCO_3^- show strong affinity for the potential competition with As (APPELO ET AL., 2002; NEIDHARDT, 2012; JESSEN ET AL., 2012; MAI ET AL., 2014; RATHI ET AL., 2017; WANG ET AL., 2019). A competitive effect of PO_4^{3-}, OH^- and HCO_3^- decreases the adsorption of As onto Fe minerals.

Temperature is another important aspect regionalising As contamination (process 5). In the current study, the data from Asia and Europe are presented. This allows to reveal the importance of temperature for the As distribution in an aquifer. Redox reactions are sensitive to small temperature changes (PROMMER & STUYFZAND, 2005). The increased availability of organic carbon combined with a higher microbial activity under increased temperature shifts groundwater towards more reducing conditions (JESUßEK ET AL., 2013). Furthermore, sorption of As complexes is consistently exothermic and decreases with increasing temperature (BONTE, 2013). In Europe, this parameter should be accounted in aquifers with thermal energy storage systems, which increase locally temperature up to 25 °C. The combination of the thermal energy storage systems induced temperature increase with mixing processes can result in a shift of As from the sorbed to aqueous phase.

To elucidate As mobility at each study site, a group of processes should be considered. Overlooking the role of these processes can lead to an overestimation of other factors. For this reason, an integrated design of the extraction wells taking into account local hydraulic, physical and hydrogeochemical conditions is indispensable.

This study has clearly shown that it is not only important to identify hydrogeochemical factors but also physical in order to delineate the heterogeneous distribution of dissolved As concentrations in groundwater. The following local conditions can induce and intensify the enrichment of As in the vicinity of extraction wells and cause As release into groundwater:

- Heterogeneous distribution of redox conditions in the vicinity of extraction wells;
- Alternating groundwater extraction rates;
- High concentration of HCO_3^- and PO_4^{3-} to inhibit or slow down the adsorption of As;
- High groundwater temperature to intensity microbiological activity.

In this study, a good understanding of the dependence of these conditions on the enrichment of As in the vicinity of extraction wells is obtained.

5.4 RESEARCH PERSPECTIVES

The last part of this thesis provides a short overview of relevant new research perspectives that follow from the results of this thesis. This study provides new insights with regard to the distribution of As in an aquifer. However, many questions still remain:

- The strong temperature dependence of As mobility is important to consider. A next step is to incorporate temperature dependences of adsorption rates onto calcite and Fe oxide.
- In this thesis, the mixing processes induced through groundwater extraction are qualitatively simulated and described. For a better understanding of the effects, the investigation of these interactions in a more quantitative way is required. This can be achieved by detailed clogging material analysis. The reactive transport modeling framework presented in chapter 2 can provides a good starting point.
- Arsenic forms with Ca^{2+} relatively insoluble aquatic complexes (BOTHE & BROWN, 1999; YOKOYAMA ET AL., 2012; RENARD ET AL., 2015) making As^{5+} more stable in the solution. The authors showed that the processes also induce the oxidation of As^{3+} to As^{5+}. This finding suggests more pronounced immobilization of As by calcite. Incorporation of this processes into the model can elucidate As adsorption onto calcite in more details.

Chapter 6. References

Akai, J., Izumi, K., Fukuhara, H., Masuda, H., Nakano, S., Yoshimura, T., Ohfuji, H., Anawar, H.M., & Akai, K. (2004). Mineralogical and geomicrobiological investigations on groundwater arsenic enrichment in Bangladesh. Applied Geochemistry, 19(2), 215-230.

Alam, M., Alam, M. M., Curray, J. R., Chowdhury, M. L. R., & Gani, M. R. (2003). An overview of the sedimentary geology of the Bengal Basin in relation to the regional tectonic framework and basin-fill history. Sedimentary geology, 155(3-4), 179-208.

Alexandratos, V. G., Elzinga, E. J., & Reeder, R. J. (2007). Arsenate uptake by calcite: macroscopic and spectroscopic characterization of adsorption and incorporation mechanisms. Geochimica et Cosmochimica Acta, 71(17), 4172-4187.

Amirbahman, A., Kent, D. B., Curtis, G. P., & Davis, J. A. (2006). Kinetics of sorption and abiotic oxidation of arsenic (III) by aquifer materials. Geochimica et Cosmochimica Acta, 70(3), 533-547.

Anawar, H.M., Akai, J., Komaki, K., Terao, H., Yoshioka, T., Ishizuka, T., Safiullah, S., & Kato, K. (2003). Geochemical occurrence of arsenic in groundwater of Bangladesh: sources and mobilization processes. Journal of Geochemical Exploration, 77(2-3), 109-131.

Appelo, C. A. J., & Postma, D. (2005). Geochemistry, groundwater and pollution. 2nd. Ed. Balkema, Rotterdam.

Appelo, C. A. J., & Rolle, M. (2010). PHT3D: A reactive multicomponent transport model for saturated porous media. Ground water, 48(5), 627-632.

Appelo, C. A. J., Van der Weiden, M. J. J., Tournassat, C., & Charlet, L. (2002). Surface complexation of ferrous iron and carbonate on ferrihydrite and the mobilization of arsenic. Environmental Science & Technology, 36(14), 3096-3103.

ARCADIS (2012). Aktualisierung Grundwassermodel. Sanierung Gaswerk, Fremdüberwachung, Organisation Arbeitskreise, sonstige fachgutachterliche Begleitung. Karlsruhe. (not published. The text will be sent on request).

ARCADIS (2016). Sanierung ehemaliges Gaswerk. Untersuchung der räumlichen Schadstoffverteilung und Redoxverhältnisse und hydrochemische Modellierung. Karlsruhe. (not published. The text will be sent on request).

Armanuos, A. M., Negm, A., & Valeriano, O. C. S. (2016). Groundwater Quality Investigation Using Multivariate Analysis-Case Study: Western Nile Delta Aquifer, Egypt. International Journal of Environmental Science and Development, 7(1), 1.

Azam, M. S., Shafiquzzaman, M., Mishima, I., & Nakajima, J. (2008). Measurement of soluble arsenic in soil of Bangladesh by acid-alkali sequential extraction. Journal of Scientific Research, 1(1), 92-107.

Bardelli, F., Benvenuti, M., Costagliola, P., Di Benedetto, F., Lattanzi, P., Meneghini, C., Romanelli, M., & Valenzano, L. (2011). Arsenic uptake by natural calcite: An XAS study. Geochimica et Cosmochimica Acta, 75(11), 3011-3023.

Berg, M., Stengel, C., Trang, P.T.K., Viet, P.H., Sampson, M.L., Leng, M., Samreth, S., & Fredericks, D. (2007). Magnitude of arsenic pollution in the Mekong and Red River Deltas—Cambodia and Vietnam. Science of the Total Environment, 372(2-3), 413-425.

Berg, M., Tran, H. C., Nguyen, T. C., Pham, H. V., Schertenleib, R., & Giger, W. (2001). Arsenic contamination of groundwater and drinking water in Vietnam: a human health threat. Environmental science & technology, 35(13), 2621-2626.

Berg, M., Trang, P. T. K., Stengel, C., Buschmann, J., Viet, P. H., Van Dan, N., & Stüben, D. (2008). Hydrological and sedimentary controls leading to arsenic contamination of groundwater in the Hanoi area, Vietnam: the impact of iron-arsenic ratios, peat, river bank deposits, and excessive groundwater abstraction. Chemical geology, 249(1-2), 91-112.

BGS, D. (2001). Arsenic contamination of groundwater in Bangladesh. British Geological Survey (Technical Report, WC/00/19. 4 Volumes). British Geological Survey, Keyworth.

Biswas, A., Gustafsson, J. P., Neidhardt, H., Halder, D., Kundu, A. K., Chatterjee, D., & Bhattacharya, P. (2014). Role of competing ions in the mobilization of arsenic in groundwater of Bengal Basin: insight from surface complexation modeling. Water research, 55, 30-39.

Blum, P., Hunkeler, D., Weede, M., Beyer, C., Grathwohl, P., & Morasch, B. (2009). Quantification of biodegradation for o-xylene and naphthalene using first order decay models, Michaelis–Menten kinetics and stable carbon isotopes. Journal of contaminant hydrology, 105(3-4), 118-130.

Bonte, M. (2015). Impacts of shallow geothermal energy on groundwater quality. Iwa Publishing.

Bonte, M., Röling, W. F., Zaura, E., van der Wielen, P. W., Stuyfzand, P. J., & van Breukelen, B. M. (2013b). Impacts of shallow geothermal energy production on redox processes and microbial communities. Environmental science & technology, 47(24), 14476-14484.

Bonte, M., Stuyfzand, P. J., & Breukelen, B. M. V. (2014). Reactive transport modeling of thermal column experiments to investigate the impacts of aquifer thermal energy storage on groundwater quality. Environmental science & technology, 48(20), 12099-12107.

Bonte, M., van Breukelen, B. M., & Stuyfzand, P. J. (2013a). Temperature-induced impacts on groundwater quality and arsenic mobility in anoxic aquifer sediments used for both drinking water and shallow geothermal energy production. Water research, 47(14), 5088-5100.

Bostick, B. C., Chen, C., & Fendorf, S. (2004). Arsenite retention mechanisms within estuarine sediments of Pescadero, CA. Environmental science & technology, 38(12), 3299-3304.

Bothe Jr, J. V., & Brown, P. W. (1999). The stabilities of calcium arsenates at 23±1 C. Journal of Hazardous Materials, 69(2), 197-207.

Brielmann, H., Griebler, C., Schmidt, S. I., Michel, R., & Lueders, T. (2009). Effects of thermal energy discharge on shallow groundwater ecosystems. FEMS Microbiology Ecology, 68(3), 273-286.

Brielmann, H., Lueders, T., Schreglmann, K., Ferraro, F., Avramov, M., Hammerl, V., Blum, P., Bayer, P., & Griebler, C. (2011). Oberflächennahe Geothermie und ihre potenziellen Auswirkungen auf Grundwasserökosysteme. Grundwasser, 16(2), 77.

Brons, H. J., Griffioen, J., Appelo, C. A. J., & Zehnder, A. J. B. (1991). (Bio) geochemical reactions in aquifer material from a thermal energy storage site. Water research, 25(6), 729-736.

Brun, A., & Engesgaard, P. (2002). Modelling of transport and biogeochemical processes in pollution plumes: literature review and model development. Journal of Hydrology, 256(3-4), 211-227.

Burgess, W. G., Burren, M., Perrin, J., & Ahmed, K. M. (2002). Constraints on sustainable development of arsenic-bearing aquifers in southern Bangladesh. Part 1: A conceptual model of arsenic in the aquifer. Geological Society, London, Special Publications, 193(1), 145-163.

Buschmann, J., & Berg, M. (2009). Impact of sulfate reduction on the scale of arsenic contamination in groundwater of the Mekong, Bengal and Red River deltas. Applied Geochemistry, 24(7), 1278-1286.

Buschmann, J., Berg, M., Stengel, C., & Sampson, M. L. (2007). Arsenic and manganese contamination of drinking water resources in Cambodia: coincidence of risk areas with low relief topography. Environmental science & technology, 41(7), 2146-2152.

Catelani, T., Perito, B., Bellucci, F., Lee, S.S., Fenter, P., Newville, M., Rimondi, V., Pratesi, G., & Costagliola, P. (2018). Arsenic uptake in bacterial calcite. Geochimica et Cosmochimica Acta, 222, 642-654.

Cohen, R. M., Mercer, J. W., Greenwald, R. M., & Beljin, M. S. (1997). Design guidelines for conventional pump-and-treat systems. Technology Innovation Office, Office of Solid Waste and Emergency, Response, US EPA, Washington, DC, EPA/540/S-97/504.

Cornell, R. M., & Schwertmann, U. (2003). The iron oxides: structure, properties, reactions, occurrences and uses. John Wiley & Sons.

Costagliola, P., Rimondi, V., Benvenuti, M., Chiarantini, L., Di Benedetto, F., Gasparon, M., Lattanzi, P., & Paolieri, M. (2007). Arsenic uptake by natural calcites: preliminary results from sequential extraction of Italian Travertines. In IMWA Symposium 2007: Water in Mining Environments (pp. 415-418). Universita degli Studi di Cagliari.

D'Affonseca, F. M., Blum, P., Finkel, M., Melzer, R., & Grathwohl, P. (2008). Field scale characterization and modeling of contaminant release from a coal tar source zone. Journal of Contaminant Hydrology, 102(1-2), 120-139.

D'Affonseca, F. M., Prommer, H., Finkel, M., Blum, P., & Grathwohl, P. (2011). Modeling the long-term and transient evolution of biogeochemical and isotopic signatures in coal tar–contaminated aquifers. Water Resources Research, 47(5).

Datta, B., Petit, C., Palliser, M., Esfahani, H. K., & Prakash, O. (2017). Linking a simulated annealing based optimization model with PHT3D simulation model for chemically reactive

transport processes to optimally characterize unknown contaminant sources in a former mine site in Australia. Journal of Water Resource and Protection, 9(05), 432.

Davis, K. J., Dove, P. M., & De Yoreo, J. J. (2000). The role of Mg2+ as an impurity in calcite growth. Science, 290(5494), 1134-1137.

De Zwart, A. H. (2007). Investigation of clogging processes in unconsolidated aquifers near water supply wells. Ponaen & Looyen BV, Delft.

Descourvières, C., Hartog, N., Patterson, B. M., Oldham, C., & Prommer, H. (2010). Geochemical controls on sediment reactivity and buffering processes in a heterogeneous aquifer. Applied Geochemistry, 25(2), 261-275.

Di Benedetto, F., Costagliola, P., Benvenuti, M., Lattanzi, P., Romanelli, M., & Tanelli, G. (2006). Arsenic incorporation in natural calcite lattice: Evidence from electron spin echo spectroscopy. Earth and Planetary Science Letters, 246(3-4), 458-465.

Dixit, S., & Hering, J. G. (2003). Comparison of arsenic (V) and arsenic (III) sorption onto iron oxide minerals: implications for arsenic mobility. Environmental science & technology, 37(18), 4182-4189.

Dzombak, D. A., & Morel, F. M. (1990). Surface complexation modeling: hydrous ferric oxide. John Wiley & Sons.

Eiche, E. (2009). Arsenic Mobilization Processes in the Red River Delta, Vietnam: Towards a Better Understanding of the Patchy Distribution of Dissolved Arsenic in Alluvial Deposits (Vol. 37). KIT Scientific Publishing.

Eiche, E., Berg, M., Hönig, S. M., Neumann, T., Lan, V. M., Pham, T. K. T., & Pham, H. V. (2017). Origin and availability of organic matter leading to arsenic mobilisation in aquifers of the Red River Delta, Vietnam. Applied Geochemistry, 77, 184-193.

Eiche, E., Kramar, U., Berg, M., Berner, Z., Norra, S., & Neumann, T. (2010). Geochemical changes in individual sediment grains during sequential arsenic extractions. water research, 44(19), 5545-5555.

Eiche, E., Neumann, T., Berg, M., Weinman, B., van Geen, A., Norra, S. & Stüben, D. (2008). Geochemical processes underlying a sharp contrast in groundwater arsenic concentrations in a village on the Red River delta, Vietnam. Applied Geochemistry, 23(11), 3143-3154.

Farooq, S. H., Chandrasekharam, D., Abbt-Braun, G., Berner, Z., Norra, S., & Stueben, D. (2012). Dissolved organic carbon from the traditional jute processing technique and its potential influence on arsenic enrichment in the Bengal Delta. Applied Geochemistry, 27(1), 292-303.

Farooq, S. H., Chandrasekharam, D., Norra, S., Berner, Z., Eiche, E., Thambidurai, P., & Stüben, D. (2011). Temporal variations in arsenic concentration in the groundwater of Murshidabad District, West Bengal, India. Environmental Earth Sciences, 62(2), 223-232.

Fendorf, S., Nico, P. S., Kocar, B. D., Masue, Y., & Tufano, K. J. (2010). Arsenic chemistry in soils and sediments. In Developments in soil science (Vol. 34, pp. 357-378). Elsevier.

Ferguson, G. (2006). Potential use of particle tracking in the analysis of low-temperature geothermal developments. Geothermics, 35(1), 44-58.

Fetter, C. W., Boving, T. B., & Kreamer, D. K. (1999). Contaminant hydrogeology (Vol. 500). Upper Saddle River, NJ: Prentice hall.

Ghosh, A., & Mondal, S. (2018). Application of multivariate statistics towards the geochemical evaluation of fluoride enrichment in groundwater at Shilabati river bank, West Bengal, India. Environmental Engineering Research, 24(2), 279-288.

Goldberg, S. (2002). Competitive adsorption of arsenate and arsenite on oxides and clay minerals. Soil Science Society of America Journal, 66(2), 413-421.

Griffioen, J., & Appelo, C. A. J. (1993). Nature and extent of carbonate precipitation during aquifer thermal energy storage. Applied Geochemistry, 8(2), 161-176.

Guo, H., Stüben, D., & Berner, Z. (2007). Removal of arsenic from aqueous solution by natural siderite and hematite. Applied Geochemistry, 22(5), 1039-1051.

Guo, H., Tang, X., Yang, S., & Shen, Z. (2008). Effect of indigenous bacteria on geochemical behavior of arsenic in aquifer sediments from the Hetao Basin, Inner Mongolia: Evidence from sediment incubations. Applied Geochemistry, 23(12), 3267-3277.

Guo, H., Zhang, B., Li, Y., Berner, Z., Tang, X., Norra, S., & Stüben, D. (2011). Hydrogeological and biogeochemical constrains of arsenic mobilization in shallow aquifers from the Hetao basin, Inner Mongolia. Environmental Pollution, 159(4), 876-883.

Guo, H., Zhang, D., Ni, P., Cao, Y., Li, F., Jia, Y., Li, H., Wan, L., & Wang, G. (2017). On the scalability of hydrogeochemical factors controlling arsenic mobility in three major inland basins of PR China. Applied Geochemistry, 77, 15-23.

Hansel, C. M., Benner, S. G., Neiss, J., Dohnalkova, A., Kukkadapu, R. K., & Fendorf, S. (2003). Secondary mineralization pathways induced by dissimilatory iron reduction of ferrihydrite under advective flow. Geochimica et Cosmochimica Acta, 67(16), 2977-2992.

Hartog, N. (2011). Anticipated temperature effects on biogeochemical reaction rates in seasonal aquifer thermal energy storage (ATES) systems: an evaluation using the Arrhenius equation. a a, 2, 2.

Hartog, N., Drijver, B., Dinkla, I., & Bonte, M. (2013, June). Field assessment of the impacts of Aquifer Thermal Energy Storage (ATES) systems on chemical and microbial groundwater composition. In Proceedings of the European Geothermal Conference, Pisa, Italy (pp. 3-7).

Holm, T. R., Eisenreich, S. J., Rosenberg, H. L., & Holm, N. P. (1987). Groundwater geochemistry of short-term aquifer thermal energy storage test cycles. Water Resources Research, 23(6), 1005-1019.

Harvey, C.F., Ashfaque, K.N., Yu, W., Badruzzaman, A.B.M., Ali, M.A., Oates, P.M., Michael, H.A., Neumann, R.B., Beckie, R., Islam, S., & Ahmed, M.F. (2006). Groundwater dynamics and arsenic contamination in Bangladesh. Chemical Geology, 228(1-3), 112-136.

Harvey, C.F., Swartz, C.H., Badruzzaman, A.B.M., Keon-Blute, N., Yu, W., Ali, M.A., Jay, J., Beckie, R., Niedan, V., Brabander, D., & Oates, P.M (2002). Arsenic mobility and groundwater extraction in Bangladesh. Science, 298(5598), 1602-1606.

Harvey, C. F., Swartz, C. H., Badruzzaman, A. B. M., Keon-Blute, N., Yu, W., Ali, M. A., & Oates, P. M. (2005). Groundwater arsenic contamination on the Ganges Delta: biogeochemistry, hydrology, human perturbations, and human suffering on a large scale. Comptes Rendus Geoscience, 337(1), 285-296.

Hashimoto, K., & Misawa, T. (1973). The solubility of γ-FeOOH in perchloric acid at 25 °C. Corrosion Science, 13(3), 229-231.

Henkel, S., Weidner, C., Roger, S., Schüttrumpf, H., Rüde, T. R., Klauder, W., & Vinzelberg, G. (2012). Untersuchung der Verockerungsneigung von Vertikalfilterbrunnen im Modellversuch. Grundwasser, 17(3), 157-169.

Henning, A., & Limberg, A. (1995). Das Grundwasser-Temperaturfeld von Berlin. Brandenburgische Geowiss. Beitr, 2(1), 97-104.

Hoque, M. A., McArthur, J. M., & Sikdar, P. K. (2012). The palaeosol model of arsenic pollution of groundwater tested along a 32 km traverse across West Bengal, India. Science of the Total Environment, 431, 157-165.

Hoque, M. A., McArthur, J. M., & Sikdar, P. K. (2014). Sources of low-arsenic groundwater in the Bengal Basin: investigating the influence of the last glacial maximum palaeosol using a 115-km traverse across Bangladesh. Hydrogeology Journal, 22(7), 1535-1547.

Horneman, A., van Geen, A., Kent, D.V., Mathe, P.E., Zheng, Y., Dhar, R.K., O'connell, S., Hoque, M.A., Aziz, Z., Shamsudduha, M., & Seddique, A.A. (2004). Decoupling of As and Fe release to Bangladesh groundwater under reducing conditions. Part I: Evidence from sediment profiles. Geochimica et Cosmochimica Acta, 68(17), 3459-3473.

Hossain, M. G., Reza, A. S., Lutfun-Nessa, M., & Ahmed, S. S. (2013). Factor and cluster analysis of water quality data of the groundwater wells of Kushtia, Bangladesh: implication for arsenic enrichment and mobilization. Journal of the Geological Society of India, 81(3), 377-384.

Houben, G. J. (2003). Iron oxide incrustations in wells. Part 1: genesis, mineralogy and geochemistry. Applied Geochemistry, 18(6), 927-939.

Houben, G. J. (2006). The influence of well hydraulics on the spatial distribution of well incrustations. Ground water, 44(5), 668-675.

Houben, G. J., & Weihe, U. (2010). Spatial distribution of incrustations around a water well after 38 years of use. Groundwater, 48(1), 53-58.

Houben, G., & Treskatis, C. (2003). Regenerierung und Sanierung von Brunnen. Oldenbourg-Industrieverlag.

Hudson-Edwards, K. A., Houghton, S. L., & Osborn, A. (2004). Extraction and analysis of arsenic in soils and sediments. TrAC Trends in Analytical Chemistry, 23(10-11), 745-752.

Islam, F. S., Gault, A. G., Boothman, C., Polya, D. A., Charnock, J. M., Chatterjee, D., & Lloyd, J. R. (2004). Role of metal-reducing bacteria in arsenic release from Bengal delta sediments. Nature, 430(6995), 68-71.

Jakobsen, R., & Cold, L. (2007). Geochemistry at the sulfate reduction–methanogenesis transition zone in an anoxic aquifer—A partial equilibrium interpretation using 2D reactive transport modeling. Geochimica et Cosmochimica Acta, 71(8), 1949-1966.

Jakobsen, R., Kazmierczak, J., Sø, H. U., & Postma, D. (2018). Spatial Variability of Groundwater Arsenic Concentration as Controlled by Hydrogeology: Conceptual Analysis Using 2-D Reactive Transport Modeling. Water resources research, 54(12), 10-254.

Jessen, S., Postma, D., Larsen, F., Nhan, P.Q., Trang, P.T.K., Long, T.V., Viet, P.H., & Jakobsen, R. (2012). Surface complexation modeling of groundwater arsenic mobility: Results of a forced gradient experiment in a Red River flood plain aquifer, Vietnam. Geochimica et Cosmochimica Acta, 98, 186-201.

Jesußek, A., Grandel, S., & Dahmke, A. (2013). Impacts of subsurface heat storage on aquifer hydrogeochemistry. Environmental earth sciences, 69(6), 1999-2012.

Jones, R. G., & Loeppert, R. H. (2013). Calcite Surface Adsorption of As (V), As (III), MMAs (V), and DMAs (V) and the Impact of Calcium and Phosphate. Soil Science Society of America Journal, 77(1), 83-93.

Kaiser, H. F. (1958). The Varimax criteria for analytical rotation in factor analysis: Psych., v. 23.

Keely, J. F., & Boulding, J. R. (1989). Performance evaluations of pump-and-treat remediations. Ground Water Issue Paper, EPA/540/4.

Kim, M. J., Nriagu, J., & Haack, S. (2002). Arsenic species and chemistry in groundwater of southeast Michigan. Environmental Pollution, 120(2), 379-390.

Kinniburgh, D.G., Smedley, P.L., Davies, J., Milne, C.J., Gaus, I., Trafford, J.M., Burden, S., Ihtishamul Huq, S.M., Ahmad, N., & Ahmed, K.M. (2003). The scale and causes of the groundwater arsenic problem in Bangladesh. In Arsenic in ground water (pp. 211-257). Springer, Boston, MA.

Kipp Jr, K. L. (1997). Guideto the Revised Heat and Solute Transport Simulator: HST3D Version 2. Water-resources investigations report, 97, 4157.

Kirk, G. J., Versteegen, A., Ritz, K., & Milodowski, A. E. (2015). A simple reactive-transport model of calcite precipitation in soils and other porous media. Geochimica et Cosmochimica Acta, 165, 108-122.

Kocar, B. D., & Fendorf, S. (2009). Thermodynamic constraints on reductive reactions influencing the biogeochemistry of arsenic in soils and sediments. Environmental science & technology, 43(13), 4871-4877.

Kramar, U., Norra, S., Berner, Z., Kiczka, M., & Chandrasekharam, D. (2017). On the distribution and speciation of arsenic in the soil-plant-system of a rice field in West-Bengal, India: a μ-synchrotron techniques based case study. Applied Geochemistry, 77, 4-14.

Lazareva, O., Druschel, G., & Pichler, T. (2015). Understanding arsenic behavior in carbonate aquifers: Implications for aquifer storage and recovery (ASR). Applied Geochemistry, 52, 57-66.

Ledesma-Ruiz, R., Pastén-Zapata, E., Parra, R., Harter, T., & Mahlknecht, J. (2015). Investigation of the geochemical evolution of groundwater under agricultural land: a case study in northeastern Mexico. Journal of Hydrology, 521, 410-423.

Lee, J. J., Jang, C. S., Wang, S. W., Liang, C. P., & Liu, C. W. (2008). Delineation of spatial redox zones using discriminant analysis and geochemical modelling in arsenic-affected alluvial aquifers. Hydrological Processes: An International Journal, 22(16), 3029-3041.

Liu, C. W., Lin, K. H., & Kuo, Y. M. (2003). Application of factor analysis in the assessment of groundwater quality in a blackfoot disease area in Taiwan. Science of the Total Environment, 313(1-3), 77-89.

Mai, N. T. H., Postma, D., Trang, P. T. K., Jessen, S., Viet, P. H., & Larsen, F. (2014). Adsorption and desorption of arsenic to aquifer sediment on the Red River floodplain at Nam Du, Vietnam. Geochimica et cosmochimica acta, 142, 587-600.

Majumder, S., Biswas, A., Neidhardt, H., Sarkar, S., Berner, Z., Bhowmick, S., Mukherjee, A., Chatterjee, D., Chakraborty, S., Nath, B., & Chatterjee, D. (2015). An insight into the spatio-vertical heterogeneity of dissolved arsenic in part of the Bengal delta plain aquifer in West Bengal (India). In Safe and Sustainable Use of Arsenic-Contaminated Aquifers in the Gangetic Plain (pp. 161-177). Springer, Cham.

McArthur, J.M., Banerjee, D.M., Hudson-Edwards, K.A., Mishra, R., Purohit, R., Ravenscroft, P., Cronin, A., Howarth, R.J., Chatterjee, A., Talukder, T., & Lowry, D. (2004). Natural organic matter in sedimentary basins and its relation to arsenic in anoxic ground water: the example of West Bengal and its worldwide implications. Applied Geochemistry, 19(8), 1255-1293.

McArthur, J.M., Banerjee, D.M., Sengupta, S., Ravenscroft, P., Klump, S., Sarkar, A., Disch, B., & Kipfer, R. (2010). Migration of As, and 3H/3He ages, in groundwater from West Bengal: Implications for monitoring. Water Research, 44(14), 4171-4185.

McArthur, J. M., Ravenscroft, P., Safiulla, S., & Thirlwall, M. F. (2001). Arsenic in groundwater: testing pollution mechanisms for sedimentary aquifers in Bangladesh. Water resources research, 37(1), 109-117.

McGuire, J. T., Long, D. T., & Hyndman, D. W. (2005). Analysis of Recharge-Induced Geochemical Change in a Contaminated Aquifer. Ground Water, 43(4), 518-530.

Medina, D. A. B., van den Berg, G. A., van Breukelen, B. M., Juhasz-Holterman, M., & Stuyfzand, P. J. (2013). Iron-hydroxide clogging of public supply wells receiving artificial recharge: near-well and in-well hydrological and hydrochemical observations. Hydrogeology journal, 21(7), 1393-1412.

Merkel, J., & Planer-Friedrich, B. (2008). Grundwasserchemie. Praxisorientierter Leitfaden zur numerischen Modellierung von Beschaffenheit, Kontamination und Sanierung aquatischer Systeme. Springer. Berlin. ISBN 978-3-540-87468-3.

Mishra, S. K. (1978). The electrokinetics of apatite and calcite in inorganic electrolyte environment. International Journal of Mineral Processing, 5(1), 69-83.

Muehe, E. M. & Fendorf, S. (2016). Impact of climate change on the dynamics of arsenic in paddy soils. Goldschmidt Conference 2016, Yokohama, Japan.

Mukherjee, A., Fryar, A. E., & Thomas, W. A. (2009). Geologic, geomorphic and hydrologic framework and evolution of the Bengal basin, India and Bangladesh. Journal of Asian Earth Sciences, 34(3), 227-244.

Neidhardt, H. (2012). Impact of groundwater abstraction and of the organic matter on release and distribution of arsenic in aquifers of the Bengal Delta Plain, India (Doctoral dissertation, Karlsruhe, Karlsruher Institut für Technologie (KIT), Diss., 2012). KIT Scientific Publishing.

Neidhardt, H., Norra, S., Tang, X., Guo, H., & Stüben, D. (2012). Impact of irrigation with high arsenic burdened groundwater on the soil–plant system: results from a case study in the Inner Mongolia, China. Environmental pollution, 163, 8-13.

Neidhardt, H., Schoeckle, D., Schleinitz, A., Eiche, E., Berner, Z., Tram, P.T., Lan, V.M., Viet, P.H., Biswas, A., Majumder, S., & Chatterjee, D. (2018). Biogeochemical phosphorus cycling in groundwater ecosystems–Insights from South and Southeast Asian floodplain and delta aquifers. Science of The Total Environment, 644, 1357-1370.

Nguyen, T. Q. (1995). Land subsidence due to groundwater withdrawal in Hanoi. Vietnam, 55-60.

Nickson, R., McArthur, J., Burgess, W., Ahmed, K. M., Ravenscroft, P., & Rahmanñ, M. (1998). Arsenic poisoning of Bangladesh groundwater. Nature, 395(6700), 338.

Nickson, R. T., McArthur, J. M., Ravenscroft, P., Burgess, W. G., & Ahmed, K. M. (2000). Mechanism of arsenic release to groundwater, Bangladesh and West Bengal. Applied Geochemistry, 15(4), 403-413.

Norra, S., Berner, Z. A., Agarwala, P., Wagner, F., Chandrasekharam, D., & Stüben, D. (2005). Impact of irrigation with As rich groundwater on soil and crops: a geochemical case study in West Bengal Delta Plain, India. Applied Geochemistry, 20(10), 1890-1906.

Norra, S., Berner, Z., Boie, I., Eiche, E., Kellermeier, E.C., Kizcka, M., Kramar, U., Neidhardt, H., Agarwala, P., Chandrasekharam, D., & Rout, R. (2012). Arsenic from groundwater into soils, plants and the food chain: Complementary case studies from West Bengal, Inner Mongolia and the Red River Delta, Vietnam. In Understanding the Geological and Medical Interface of Arsenic-As 2012: Proceedings of the 4th International Congress on Arsenic in the Environment, 22-27 July 2012, Cairns, Australia (p. 246). CRC Press.

Osborne, J. W., & Costello, A. B. (2009). Best practices in exploratory factor analysis: Four recommendations for getting the most from your analysis. Pan-Pacific Management Review, 12(2), 131-146.

Palmer, C. D., Blowes, D. W., Frind, E. O., & Molson, J. W. (1992). Thermal energy storage in an unconfined aquifer: 1. Field injection experiment. Water Resources Research, 28(10), 2845-2856.

Parkhurst, D. L., & Appelo, C. A. J. (2013). Description of input and examples for PHREEQC version 3: a computer program for speciation, batch-reaction, one-dimensional transport, and inverse geochemical calculations (No. 6-A43). US Geological Survey.

Parkhurst, D. L., Kipp, K. L., & Charlton, S. R. (2010). PHAST Version 2—A program for simulating groundwater flow, solute transport, and multicomponent geochemical reactions. US Geological Survey Techniques and Methods, 6, A35.

Perez, J. P. H., Freeman, H. M., Schuessler, J. A., & Benning, L. G. (2019). The interfacial reactivity of arsenic species with green rust sulfate (GRSO4). Science of The Total Environment, 648, 1161-1170.

Phi, T. H., & Strokova, L. A. (2015). Prediction maps of land subsidence caused by groundwater exploitation in Hanoi, Vietnam. Resource-Efficient Technologies, 1(2), 80-89.

Plant, J. A., Kinniburgh, D. G., Smedley, P. L., Fordyce, F. M., & Klinck, B. A. (2004). Arsenic and selenium.

Ponnamperuma, F. N., Tianco, E. M., & Loy, T. (1967). Redox equilibria in flooded soils: I. The iron hydroxide systems. Soil Science, 103(6), 374-382.

Possemiers, M. (2014). Aquifer Thermal Energy Storage under different hydrochemical hydrogeological conditions, Phd KU leuven, Science, Engineering & Technology.

Postma, D., Jessen, S., Hue, N.T.M., Duc, M.T., Koch, C.B., Viet, P.H., Nhan, P.Q., & Larsen, F. (2010). Mobilization of arsenic and iron from Red River floodplain sediments, Vietnam. Geochimica et Cosmochimica Acta, 74(12), 3367-3381.

Postma, D., Larsen, F., Hue, N. T. M., Duc, M. T., Viet, P. H., Nhan, P. Q., & Jessen, S. (2007). Arsenic in groundwater of the Red River floodplain, Vietnam: controlling geochemical processes and reactive transport modeling. Geochimica et Cosmochimica Acta, 71(21), 5054-5071.

Postma, D., Mai, N.T.H., Lan, V.M., Trang, P.T.K., Sø, H.U., Nhan, P.Q., Larsen, F., Viet, P.H., & Jakobsen, R. (2016). Fate of arsenic during Red River water infiltration into aquifers beneath Hanoi, Vietnam. Environmental science & technology, 51(2), 838-845.

Prommer, H., & Stuyfzand, P. J. (2005). Identification of temperature-dependent water quality changes during a deep well injection experiment in a pyritic aquifer. Environmental Science & Technology, 39(7), 2200-2209.

Prommer, H., & V.E.A. Post. (2010). A Reactive Multicomponent Model for Saturated Porous Media, Version 2.0, User's Manual, http://www.pht3d.org.

Prommer, H., Davis, G. B., & Barry, D. A. (1999). Geochemical changes during biodegradation of petroleum hydrocarbons: field investigations and biogeochemical modelling. Organic Geochemistry, 30(6), 423-435.

Prommer, H., Tuxen, N., & Bjerg, P. L. (2006). Fringe-controlled natural attenuation of phenoxy acids in a landfill plume: Integration of field-scale processes by reactive transport modeling. Environmental science & technology, 40(15), 4732-4738.

Rathi, B., Neidhardt, H., Berg, M., Siade, A., & Prommer, H. (2017). Processes governing arsenic retardation on Pleistocene sediments: Adsorption experiments and model-based analysis. Water Resources Research, 53(5), 4344-4360.

Rawson, J., Prommer, H., Siade, A., Carr, J., Berg, M., Davis, J. A., & Fendorf, S. (2016). Numerical modeling of arsenic mobility during reductive iron-mineral transformations. Environmental science & technology, 50(5), 2459-2467.

Rawson, J., Siade, A., Sun, J., Neidhardt, H., Berg, M., & Prommer, H. (2017). Quantifying reactive transport processes governing arsenic mobility after injection of reactive organic carbon into a Bengal Delta aquifer. Environmental science & technology, 51(15), 8471-8480.

Refait, P., Abdelmoula, M., & Génin, J. M. (1998). Mechanisms of formation and structure of green rust one in aqueous corrosion of iron in the presence of chloride ions. Corrosion Science, 40(9), 1547-1560.

Renard, F., Putnis, C. V., Montes-Hernandez, G., Ruiz-Agudo, E., Hovelmann, J., & Sarret, G. (2015). Interactions of arsenic with calcite surfaces revealed by in situ nanoscale imaging. Geochimica et Cosmochimica Acta, 159, 61-79.

Roman-Ross, G., Charlet, L., Cuello, G. J., & Tisserand, D. (2003). Arsenic removal by gypsum and calcite in lacustrine environments. In Journal de Physique IV (Proceedings) (Vol. 107, pp. 1153-156). EDP sciences.

Roman-Ross, G., Cuello, G. J., Turrillas, X., Fernandez-Martinez, A., & Charlet, L. (2006). Arsenite sorption and co-precipitation with calcite. Chemical Geology, 233(3), 328-336.

Romero, F. M., Armienta, M. A., & Carrillo-Chavez, A. (2004). Arsenic sorption by carbonate-rich aquifer material, a control on arsenic mobility at Zimapan, Mexico. Archives of Environmental Contamination and Toxicology, 47(1), 1-13.

Rotiroti, M., Sacchi, E., Fumagalli, L., & Bonomi, T. (2014). Origin of arsenic in groundwater from the multilayer aquifer in Cremona (northern Italy). Environmental science & technology, 48(10), 5395-5403.

Rowland, H.A., Omoregie, E.O., Millot, R., Jimenez, C., Mertens, J., Baciu, C., Hug, S.J., & Berg, M. (2011). Geochemistry and arsenic behaviour in groundwater resources of the Pannonian Basin (Hungary and Romania). Applied Geochemistry, 26(1), 1-17.

Roy, A. B., & Chatterjee, A. (2015). Tectonic framework and evolutionary history of the Bengal Basin in the Indian subcontinent. Current Science, 271-279.

Sadiq, M. (1997). Arsenic chemistry in soils: an overview of thermodynamic predictions and field observations. Water, air, and soil pollution, 93(1-4), 117-136.

Sharif, M. S. U., Davis, R. K., Steele, K. F., Kim, B., Hays, P. D., Kresse, T. M., & Fazio, J. A. (2011). Surface complexation modeling for predicting solid phase arsenic concentrations in the sediments of the Mississippi River Valley alluvial aquifer, Arkansas, USA. Applied Geochemistry, 26(4), 496-504.

Sheikhy Narany, T., Ramli, M. F., Aris, A. Z., Sulaiman, W. N. A., Juahir, H., & Fakharian, K. (2014). Identification of the hydrogeochemical processes in groundwater using classic integrated geochemical methods and geostatistical techniques, in Amol-Babol Plain, Iran. The Scientific World Journal, 2014.

Shtirkin, Y. (2013). A 3D multi-species reactive transport model to estimate geochemical reactions in groundwater at a former gasworks site in Germany. Master thesis, Karlsruhe Institute of Technology. (not published. The text will be sent on request).

Smedley, P. L., & Kinniburgh, D. G. (2002). A review of the source, behaviour and distribution of arsenic in natural waters. Applied Geochemistry, 17(5), 517-568.

Sø, H. (2007) Sorption and desorption of arsenate onto calcite. Master Thesis, Institute of EnvironmentandResources, DTU.

Sø, H. U., Postma, D., & Jakobsen, R. (2017). Do Fe-oxides control the adsorption of arsenic in aquifers of the Red River floodplain, Vietnam?. Procedia Earth and Planetary Science, 17, 300-303.

Sø, H. U., Postma, D., Jakobsen, R., & Larsen, F. (2011). Sorption of phosphate onto calcite; results from batch experiments and surface complexation modeling. Geochimica et Cosmochimica Acta, 75(10), 2911-2923.

Sowers, L., York, K. P., & Stiles, L. (2006). Impact of thermal buildup on groundwater chemistry and aquifer microbes. Proceedings of Ecostock, 1-7.

Stahl, M.O., Harvey, C.F., van Geen, A., Sun, J., Thi Kim Trang, P., Mai Lan, V., Mai Phuong, T., Hung Viet, P., & Bostick, B.C. (2016). River bank geomorphology controls groundwater arsenic concentrations in aquifers adjacent to the Red River, Hanoi Vietnam. Water Resources Research, 52(8), 6321-6334.

Steefel, C.I., Appelo, C.A.J., Arora, B., Jacques, D., Kalbacher, T., Kolditz, O., Lagneau, V., Lichtner, P.C., Mayer, K.U., Meeussen, J.C.L., & Molins, S. (2015). Reactive transport codes for subsurface environmental simulation. Computational Geosciences, 19(3), 445-478.

Stollenwerk, K.G., Breit, G.N., Welch, A.H., Yount, J.C., Whitney, J.W., Foster, A.L., Uddin, M.N., Majumder, R.K., & Ahmed, N. (2007). Arsenic attenuation by oxidized aquifer sediments in Bangladesh. Science of the Total Environment, 379(2-3), 133-150.

Stumm, W., & Morgan, J. J. (1981). Aquatic Chemistry. A Wiley-Interscience-Publication.

Suk, H., & Lee, K. K. (1999). Characterization of a ground water hydrochemical system through multivariate analysis: clustering into ground water zones. Ground water, 37(3), 358-366.

Swartz, C.H., Blute, N.K., Badruzzman, B., Ali, A., Brabander, D., Jay, J., Besancon, J., Islam, S., Hemond, H.F., & Harvey, C.F. (2004). Mobility of arsenic in a Bangladesh aquifer: Inferences from geochemical profiles, leaching data, and mineralogical characterization. Geochimica et Cosmochimica Acta, 68(22), 4539-4557.

Van Beek, C. K. (2011). Cause and prevention of clogging of wells abstracting groundwater from unconsolidated aquifers. IWA Publishing.

Van Geen, A., Bostick, B.C., Thi Kim Trang, P., Lan, V.M., Mai, N.N., Manh, P.D., Viet, P.H., Radloff, K., Aziz, Z., Mey, J.L., & Stahl, M.O. (2013). Retardation of arsenic transport through a Pleistocene aquifer. Nature, 501(7466), pp.204-207.

Van Geen, A., Zheng, Y., Cheng, Z., Aziz, Z., Horneman, A., Dhar, R.K., Mailloux, B., Stute, M., Weinman, B., Goodbred, S., & Seddique, A.A. (2006). A transect of groundwater and sediment properties in Araihazar, Bangladesh: Further evidence of decoupling between As and Fe mobilization. Chemical Geology, 228(1-3), 85-96.

Van Geen, A., Zheng, Y., Versteeg, R., Stute, M., Horneman, A., Dhar, R. & Graziano, J. H. (2003). Spatial variability of arsenic in 6000 tube wells in a 25 km2 area of Bangladesh. Water Resources Research, 39(5).

Van Halem, D., Moed, D. H., Verberk, J. Q. J. C., Amy, G. L., & Van Dijk, J. C. (2012). Cation exchange during subsurface iron removal. Water research, 46(2), 307-315.

Wagner, F. (2005). Prozessverständnis einer Naturkatastrophe: eine geo-und hydrochemische Untersuchung der regionalen Arsen-Anreicherung im Grundwasser West-Bengalens (Indien). Univ.-Verlag Karlsruhe.

Wallis, I., Prommer, H., Berg, M., Siade, A. J., Sun, J., & Kipfer, R. (2020). The river–groundwater interface as a hotspot for arsenic release. Nature Geoscience, 13(4), 288-295.

Wallis, I., Prommer, H., Pichler, T., Post, V., B. Norton, S., Annable, M. D., & Simmons, C. T. (2011). Process-based reactive transport model to quantify arsenic mobility during aquifer storage and recovery of potable water. Environmental science & technology, 45(16), 6924-6931.

Wallis, I., Prommer, H., Simmons, C. T., Post, V., & Stuyfzand, P. J. (2010). Evaluation of conceptual and numerical models for arsenic mobilization and attenuation during managed aquifer recharge. Environmental science & technology, 44(13), 5035-5041.

Wang, H. Y., Guo, H. M., Xiu, W., Bauer, J., Sun, G. X., Tang, X. H., & Norra, S. (2019). Indications that weathering of evaporite minerals affects groundwater salinity and As mobilization in aquifers of the northwestern Hetao Basin, China. Applied Geochemistry, 109, Article: 104416.

Wang, Y., Jiao, J. J., & Cherry, J. A. (2012). Occurrence and geochemical behavior of arsenic in a coastal aquifer–aquitard system of the Pearl River Delta, China. Science of the Total Environment, 427, 286-297.

Wang, Y., Morin, G., Ona-Nguema, G., Juillot, F., Guyot, F., Calas, G., & Brown Jr, G. E. (2010). Evidence for different surface speciation of arsenite and arsenate on green rust: an EXAFS and XANES study. Environmental science & technology, 44(1), 109-115.

Weidner, C., Henkel, S., Lorke, S., Rüde, T. R., Schüttrumpf, H., & Klauder, W. (2011). Investigation of clogging processes on vertical filter wells using an experimental model. Mine Water–Managing the Challenges, 79-83.

Weidner, C., Henkel, S., Lorke, S., Rüde, T. R., Schüttrumpf, H., & Klauder, W. (2012). Experimental modelling of chemical clogging processes in dewatering wells. Mine Water and the Environment, 31(4), 242-251.

Weiß, C. H. (2007). Statsoft, inc., tulsa, ok.: Statistica, version 8. AStA Advances in Statistical Analysis, 91(3), 339-341.

Wilkie, J. A., & Hering, J. G. (1996). Adsorption of arsenic onto hydrous ferric oxide: effects of adsorbate/adsorbent ratios and co-occurring solutes. Colloids and Surfaces A: Physicochemical and Engineering Aspects, 107, 97-110.

Winkel, L. H., Casentini, B., Bardelli, F., Voegelin, A., Nikolaidis, N. P., & Charlet, L. (2013). Speciation of arsenic in Greek travertines: Co-precipitation of arsenate with calcite. Geochimica et Cosmochimica Acta, 106, 99-110.

Winkel, L.H., Trang, P.T.K., Lan, V.M., Stengel, C., Amini, M., Ha, N.T., Viet, P.H., & Berg, M. (2011). Arsenic pollution of groundwater in Vietnam exacerbated by deep aquifer exploitation for more than a century. Proceedings of the National Academy of Sciences, 108(4), 1246-1251.

Xiao, T., Dai, Z., Viswanathan, H., Hakala, A., Cather, M., Jia, W., Zhang, Y., & McPherson, B. (2017). Arsenic mobilization in shallow aquifers due to CO 2 and brine intrusion from storage reservoirs. Scientific reports, 7(1), 2763.

Yokoyama, Y., Mitsunobu, S., Tanaka, K., Itai, T., & Takahashi, Y. (2009). A study on the coprecipitation of arsenite and arsenate into calcite coupled with the determination of oxidation states of arsenic both in calcite and water. Chemistry letters, 38(9), 910-911.

Yokoyama, Y., Tanaka, K., & Takahashi, Y. (2012). Differences in the immobilization of arsenite and arsenate by calcite. Geochimica et Cosmochimica Acta, 91, 202-219.

Yolcubal, I., & Akyol, N. H. (2008). Adsorption and transport of arsenate in carbonate-rich soils: Coupled effects of nonlinear and rate-limited sorption. Chemosphere, 73(8), 1300-1307.

Zachara, A., & Haenggi, M. (2013). Spatial stochastic models and metrics for the structure of base stations in cellular networks. IEEE Transactions on Wireless Communications, 12(11), 5800-5812.

Zachara, J. M., Kukkadapu, R. K., Fredrickson, J. K., Gorby, Y. A., & Smith, S. C. (2002). Biomineralization of poorly crystalline Fe (III) oxides by dissimilatory metal reducing bacteria (DMRB). Geomicrobiology Journal, 19(2), 179-207.

Zheng, Y., Stute, M., Van Geen, A., Gavrieli, I., Dhar, R., Simpson, H.J., Schlosser, P., & Ahmed, K.M. (2004). Redox control of arsenic mobilization in Bangladesh groundwater. Applied Geochemistry, 19(2), 201-214.

Zuurbier, K. G., Hartog, N., Valstar, J., Post, V. E., & van Breukelen, B. M. (2013). The impact of low-temperature seasonal aquifer thermal energy storage (SATES) systems on chlorinated solvent contaminated groundwater: Modeling of spreading and degradation. Journal of contaminant hydrology, 147, 1-13.

Appendix

Table A-1: Result of the hydrochemical analysis at the low-As site (L1 – LC) (the data from Eiche (2009)).

Parameter	L1	L2	L3	L4	L5	L6	L7	L8	LC
Depth [m]	24.0	27.0	30.0	33.0	36.5	39.0	41.0	45.0	54.0
T [°C]	26.0	26.1	26.8	27.0	26.1	27.2	27.6	26.9	27.0
pH [-]	6.2	6.5	6.4	6.5	6.5	6.4	6.6	6.7	7.2
diss O_2 [mg/L]	0.3	1.2	0.6	0.5	0.5	0.6	0.7	0.3	0.5
EC [µS/cm]	217	251	267	322	359	414	413	462	341
Eh [mV]	109	77	144	106	84	60	85	94	-148
As_{tot} [µg/L]	0.8	1.1	0.6	0.7	0.6	0.8	1.7	0.8	7.6
Fe^{2+} [mg/L]	0.08	0.05	0.02	0.04	0.03	<0.02	0.06	0.04	10.2
Mn^{2+} [mg/L]	2.6	0.6	0.6	0.4	0.3	0.5	0.5	2.8	0.6
Na^{+} [mg/L]	30.9	35.5	36.5	28.1	20.9	20.4	22.0	33.4	33.2
K^{+} [mg/L]	2.0	2.3	2.3	2.6	2.7	3.0	2.9	3.6	3.8
Ca^{2+} [mg/L]	8.0	10.0	11.0	21.0	25.0	33.0	32.0	38.0	22.0
Mg^{2+} [mg/L]	8.9	12.2	13.1	22.2	28.9	33.3	31.2	31.6	20.2
Sr [µg/L]	57.0	75.0	86.0	166.0	230.0	280.0	267.0	279.0	173.0
Ba [µg/L]	28.0	35.0	31.0	54.0	77.0	92.0	94.0	121.0	103.0
Al [µg/L]	5.9	8.3	4.8	4.9	10.2	6.1	7.6	5.7	5.9
Co [µg/L]	1.3	1.1	1.0	0.7	1.0	1.1	1.1	1.7	1.2
Ni [µg/L]	1.5	1.7	1.3	1.4	2.1	1.4	1.8	1.5	1.5
Cu [µg/L]	1.1	1.2	1.1	0.9	1.6	0.8	4.2	1.2	1.2
Zn [µg/L]	7.7	7.8	5.7	6.6	9.7	5.9	6.2	10.9	4.9
Se [µg/L]	0.7	0.4	0.4	0.2	0.5	0.1	0.2	<0.1	0.6
B [µg/L]	20.0	26.0	30.0	27.0	23.0	23.0	23.0	29.0	32.0
Sb [µg/L]	1.1	0.6	0.6	0.6	0.6	0.5	0.6	0.6	1.1
Hg [µg/L]	0.3	0.2	0.2	0.1	0.1	0.1	0.1	0.1	0.3
U [µg/L]	0.02	0.04	0.06	0.11	0.17	0.28	0.26	0.51	0.02
Cr [µg/L]	0.3	0.2	0.1	0.1	0.1	0.0	0.2	0.1	0.1
P_{tot} [µg/L]	30.0	28.0	25.0	30.0	27.0	6.0	26.0	20.0	387.0
Si_{tot} [mg/L]	18.1	18.2	18.5	18.3	18.0	18.7	19.0	19.3	17.8
HCO_3^{-} [mg/L]	140.0	171.0	183.0	232.0	264.0	311.0	305.0	352.0	241.0
Cl^{-} [mg/L]	4.6	3.8	3.9	3.6	3.3	3.5	4.0	3.5	5.3
Cl_{tot} [mg/L]	6.6	5.5	5.5	4.6	4.5	4.5	4.0	4.4	8.1
I_{tot} [µg/L]	240.0	237.0	251.0	192.0	180.0	174.0	165.0	154.0	168.0
S_{tot} [µg/L]	3125.0	2494.0	2696.0	1590.0	1399.0	756.0	854.0	635.0	1679.0
SO_4^{2-} [mg/L]	9.9	8.1	8.6	5.6	5.0	2.5	2.5	2.5	5.7
NO_3-N [mg/L]	<0.25	<0.25	<0.25	<0.25	<0.25	<0.25	<0.25	<0.25	0.6
NH_4-N [mg/L]	0.2	0.1	0.1	0.1	0.1	0.1	0.2	0.2	0.7
N_{tot} [mg/L]	<1.5	<1.5	<1.5	<1.5	<1.5	<1.5	<1.5	<1.5	<1.5
DOC [mg/L]	2.2	1.5	<1.5	<1.5	<1.5	<1.5	<1.5	<1.5	2.1

Table A-2: Result of the hydrochemical analysis at the high-As site (H1 – HC) (the data from Eiche (2009)).

Parameter	H1	H2	H3	H4	H5	H6	H7	H8	HC
Depth [m]	17.0	21.0	24.0	27.0	34.0	36.0	41.0	45.0	57.0
T [°C]	25.9	25.3	26.7	25.9	25.6	25.1	26.8	25.8	27.6
pH [-]	6.8	7.0	7.0	7.1	7.0	7.2	6.9	6.9	6.9
diss O_2 [mg/L]	0.4	0.6	1.0	0.8	0.7	0.5	1.5	1.3	1.1
EC [µS/cm]	825	481	721	357	686	708	605	622	646
Eh [mV]	-164	-130	-160	-117	-125	-114	-139	-135	-98
As_{tot} [µg/L]	330.0	441.0	311.0	218.0	340.0	615.0	207.0	306.0	8.0
Fe^{2+} [mg/L]	15.9	14.2	16.9	13.0	16.2	12.2	10.7	8.3	2.0
Mn^{2+} [mg/L]	0.3	0.4	0.2	0.4	0.1	0.4	1.9	1.5	1.0
Na^{+} [mg/L]	14.1	10.7	14.2	12.4	12.6	10.3	12.4	13.5	12.3
K^{+} [mg/L]	4.1	3.4	1.6	2.2	1.5	2.5	3.8	3.1	2.6
Ca^{2+} [mg/L]	128.0	109.0	127.0	127.0	121.0	130.0	86.0	98.0	119.0
Mg^{2+} [mg/L]	37.1	32.7	25.4	25.0	24.0	27.0	39.4	34.8	26.6
Sr [µg/L]	560.0	365.0	293.0	317.0	276.0	419.0	404.0	424.0	374.0
Ba [µg/L]	461.0	618.0	506.0	532.0	472.0	873.0	522.0	499.0	142.0
Al [µg/L]	4.1	2.5	3.6	3.6	3.1	4.8	4.2	5.6	4.1
Co [µg/L]	2.4	2.1	2.2	2.7	3.5	4.4	2.6	2.2	0.6
Ni [µg/L]	2.3	2.1	2.0	2.2	2.4	3.4	1.6	2.0	0.6
Cu [µg/L]	1.2	1.2	1.0	1.2	1.9	4.1	1.1	1.3	1.8
Zn [µg/L]	6.0	4.7	6.6	8.7	6.3	6.0	8.7	29.3	23.8
Se [µg/L]	0.6	0.3	0.2	0.1	0.2	0.3	0.3	0.0	0.4
B [µg/L]	20.0	19.0	17.0	17.0	16.0	16.0	17.0	16.0	17.0
Sb [µg/L]	0.4	0.7	0.5	1.0	0.7	1.4	0.9	0.5	0.5
Hg [µg/L]	<0.05	<0.05	<0.05	<0.05	<0.05	<0.05	<0.05	<0.05	<0.05
U [µg/L]	0.06	0.10	0.09	0.06	0.04	0.04	0.08	0.17	6.21
Cr [µg/L]	0.2	0.1	0.1	0.1	0.1	0.2	0.1	0.1	<LOD
P_{tot} [µg/L]	657.0	620.0	526.0	201.0	183.0	385.0	455.0	371.0	158.0
Si_{tot} [mg/L]	21.5	15.6	17.1	17.5	16.1	14.3	18.0	18.6	20.3
HCO_3^{-} [mg/L]	650.0	554.0	550.0	509.0	521.0	541.0	464.0	473.0	486.0
Cl^{-} [mg/L]	8.2	8.8	9.9	9.7	10.2	10.6	3.1	3.8	3.1
Cl_{tot} [mg/L]	9.3	10.4	10.9	12.2	11.4	11.9	4.1	4.7	4.0
I_{tot} [µg/L]	61.0	44.0	41.0	31.0	29.0	27.0	62.0	61.0	74.0
S_{tot} [µg/L]	33.0	21.0	16.0	22.0	94.0	<5	<5	33.0	7.0
SO_4^{2-} [mg/L]	<5	<5	<5	<5	<5	<5	<5	<5	<5
NO_3-N [mg/L]	<0.25	<0.25	<0.25	<0.25	<0.25	<0.25	<0.25	<0.25	2.5
NH_4-N [mg/L]	23.2	18.6	9.1	4.4	4.1	6.0	2.3	2.8	3.8
N_{tot} [mg/L]	15.1	11.9	6.4	2.5	2.8	4.2	<1.5	1.5	2.8
DOC [mg/L]	3.9	2.3	2.6	<1.5	1.7	1.6	1.6	1.6	1.7

Table A-3: Measured (Eiche, 2009) and initial concentrations of aqueous components (model input). Concentrations in mmol/L except As_{tot}, P in [µmol/L], temperature in [°C] and EC in [µS/cm]. EC values are calculated in PHREEQC based on ions concentrations.

Compound	Input	Measured range		Input	Measured range	
	Solution 1	min	max	Solution 2	min	max
EC	-	357	825	-	605	708
Temp	25.0	25.1	26.7	25.0	25.8	27.6
pH [-]	7.0	6.8	7.2	6.9	6.9	6.9
Fe^{2+}	0.25	0.22	0.31	0.17	0.04	0.19
NH_4^+	0.30	0.29	1.66	0.14	0.16	0.27
Ca^{2+}	3.00	2.73	3.25	2.30	2.15	2.98
HCO_3^-	9.00	8.48	10.83	8.00	7.73	8.10
As_{tot}	4.00	2.91	8.20	3.00	0.11	4.08
Mn^{2+}	0.02	<0.01	0.03	0.02	<0.01	0.03
Na^+	0.43	0.45	0.62	0.43	0.53	0.59
K^+	0.08	0.04	0.11	0.08	0.07	0.10
Mg^{2+}	1.00	1.00	1.55	1.00	1.11	1.64
P	10.0	5.90	21.19	10.0	5.10	14.68
Cl^-	0.28	0.23	0.30	0.28	0.09	0.11
SO_4^{2-}	<0.5	<0.5	<0.5	<0.5	<0.5	<0.5

Table A-4: Measured concentrations of aqueous components. Concentrations in mg/L except temperature in [°C], EC in [µS/cm] and all organic contaminants in [µg/L], Nov 2014 (ARCADIS, 2016).

Parameter	GK 17		B3-17			B4-5	
Depth [m]	7	15	10	17	25	9	15
Temp [°C]	14.7	14.9	16.8	17.4	17.4	16.5	17.3
pH	6.83	6.90	7.00	7.04	7.04	7.14	7.33
EC	1560	1500	1700	1750	1750	1760	1800
HCO_3^-	8.22	8.21	9.86	9.82	10.20	12.80	12.00
Cl^-	56	80	95	89	93	111	90
SO_4^{2-}	277	274	252	282	263	85	138
P as PO_4^{3-}	< 0.6	< 0.6	< 0.6	< 0.6	< 0.6	< 0.6	< 0.6
NO_3^-	70.5	18.3	< 1.0	< 1.0	< 1.0	< 1.0	< 1.0
Ca^{2+}	243	215	179	186	178	159	133
Fe^{2+}	0.07	0.06	2.55	3.96	3.01	0.29	1.07
K^+	2.75	2.54	7.79	5.02	6.39	4.54	5.24
Mg^{2+}	26.3	26.8	30.0	31.6	31.3	26.9	29.2
Mn^{2+}	0.12	0.27	0.59	0.46	0.50	0.13	0.09
Na^+	43.0	55.0	60.0	51.5	57.3	65.9	52.5
benzene	< 0.5	3.2	0.8	< 0.5	2.6	250.0	60.0
toluene	< 1	< 1	< 1	< 1	< 1	940	12
ethylbenzene	< 1	< 1	< 1	< 1	< 1	380	25
p-xylene	< 1	< 1	< 1	< 1	< 1	1900	39
o-xylene	< 1	< 1	< 1	< 1	< 1	710	23
naphthalene	0.68	0.76	0.73	0.16	0.36	3200	190
acenaphthene	0.19	0.13	99	100	250	230	360
fluorene	< 0.05	< 0.05	25	13	94	83	54
phenanthrene	< 0.05	< 0.05	3.50	1.30	6.90	22.0	4.80
anthracene	< 0.01	< 0.01	1.10	0.27	2.50	5.3	3.50
fluoranthene	< 0.01	< 0.01	1.00	0.06	0.95	4.8	1.60
pyrene	< 0.01	< 0.01	0.56	0.04	0.51	2.9	0.98

Parameter	B4-7			V2-10			V3-6	
Depth [m]	9	18	28	10	17	25	22	25
Temp [°C]	16.0	17.5	16.5	18.1	17.8	18.5	18.2	18.3
pH	6.91	6.92	7.11	6.77	6.77	6.77	6.88	6.85
EC	2210	2000	2000	1710	1680	1700	1700	1700
HCO_3^-	12.00	11.00	11.20	8.37	8.36	8.38	5.88	9.39
Cl^-	87	78	96	112	107	125	110	106
SO_4^{2-}	510	432	293	229	234	233	230	224
P as PO_4^{3-}	< 0.6	< 0.6	< 0.6	< 0.6	< 0.6	< 0.6	< 0.6	< 0.6
NO_3^-	< 1.0	< 1.0	< 1.0	76.3	66.2	68.6	58.3	67.4
Ca^{2+}	292	259	168	155	154	153	131	156
Fe^{2+}	5.45	3.80	1.61	0.31	0.42	2.15	0.31	0.35
K^+	5.35	3.71	6.36	5.67	5.49	5.63	5.91	6.08
Mg^{2+}	33.6	31.0	28.3	26.6	26.4	27.0	28.4	28.3
Mn^{2+}	0.87	0.82	0.26	0.43	0.41	0.42	0.38	0.42
Na^+	62.8	53.3	41.4	55.5	53.3	54.7	60.2	60.2
benzene	38.0	33.0	230.0	< 0.5	< 0.5	< 0.5	3.8	2.3
toluene	2	< 1	5	< 1	< 1	< 1	< 1	< 1
ethylbenzene	1	< 1	< 1	< 1	< 1	< 1	< 1	< 1
p-xylene	5	< 1	1	< 1	< 1	< 1	< 1	< 1
o-xylene	2	< 1	< 1	< 1	< 1	< 1	< 1	< 1
naphthalene	12.0	3.20	0.85	1.0	< 0.05	0.07	2.60	1.0
acenaphthene	300	99	3.80	0.08	< 0.05	< 0.05	2.90	0.09
fluorene	41	8	0.18	< 0.05	< 0.05	< 0.05	1.0	0.19
phenanthrene	0.17	0.12	< 0.05	< 0.05	< 0.05	< 0.05	0.30	0.17
anthracene	0.31	0.07	0.04	< 0.01	< 0.01	< 0.01	0.11	0.24
fluoranthene	0.08	0.03	0.02	< 0.01	< 0.01	< 0.01	0.26	0.51
pyrene	0.03	0.02	0.01	< 0.01	< 0.01	< 0.01	0.15	0.36

Table A-5: Measured (ARCADIS 2016) and modelled groundwater levels.

Observation Name	Observed Value [m]	Modelled Value [m]	Residual [m]
B3-16	87.50	87.51	0.01
B3-17	87.42	87.48	0.06
B3-18	87.60	87.56	-0.04
V3-9	87.72	87.75	0.03
V3-10	87.70	87.71	0.01
V3-11	87.70	87.70	0
V3-12	87.70	87.71	0.01
v2-5	87.75	87.77	0.02
V2-6	87.77	87.77	0
V2-7	87.81	87.83	0.02
V2-8	87.79	87.78	-0.01
V2-9	87.80	87.79	-0.01
V2-10	87.78	87.79	0.01

Table A-6: Result of the hydrochemical analysis (the data from Neidhardt, 2012).

Number	Depth [m]	Age [year]	pH [-]	HCO_3^- [mg/L]	As_{tot} [µg/L]	Fe^{2+} [µg/L]	DOC [mg/l]
1	17.3	3.6	7.1	261.8	159.3	12094.0	1.3
2	24.0	20.0	7.1	267.4	332.9	9724.0	0.6
3	37.3	7.0	7.2	201.6	217.2	7368.0	2.5
4	17.3	10.0	7.4	232.4	173.6	13402.0	2.0
5	24.0	14.0	8.0	142.8	78.4	9088.0	1.5
6	30.7	7.0	7.1	267.4	52.1	10380.0	0.6
7	24.0	6.0	7.1	294.0	194.5	34020.0	0.6
8	30.7	12.0	7.2	236.6	48.0	8140.0	1.5
9	20.7	4.0	7.4	221.8	8.1	49.1	1.5
10	24.0	3.0	7.4	246.4	3.2	80.1	1.7
11	24.0	0.2	7.5	147.0	40.0	2410.0	1.7
12	24.0	7.0	7.5	183.4	52.5	3138.0	1.3
13	30.7	3.0	7.8	183.4	29.8	2310.0	1.5
14	37.3	0.5	7.7	203.0	13.8	2402.0	1.4
15	16.7	15.0	7.6	183.4	34.0	2568.0	2.1
16	21.7	15.0	7.7	155.4	33.3	3248.0	1.3
17	24.0	1.0	7.2	194.6	46.2	2226.0	4.0
18	17.3	8.0	7.4	193.2	45.6	2312.0	2.7
19	37.3	20.0	7.3	225.4	30.0	971.4	1.4
20	37.3	20.0	6.0	186.2	19.6	15.0	1.4
21	24.0	8.0	7.4	215.6	38.2	7962.0	0.5
22	24.0	12.0	7.6	182.0	5.2	148.3	2.2
23	24.0	13.0	7.6	183.4	31.5	3978.0	1.5
24	31.7	4.0	7.6	124.6	8.6	1279.8	1.4
25	24.0	2.0	7.3	155.4	163.3	25120.0	3.0
26	0.0		7.3	183.4	47.6	148.6	2.3
27	24.0	10.0	6.5	233.8	158.6	15374.0	3.2
28	24.0	1.0	6.6	189.0	86.6	6294.0	2.3
29	24.0	1.0	6.8	165.2	54.8	2248.0	1.8
30	28.3	6.0	6.8	191.8	98.2	5196.0	1.5
31	0.0	3.0	6.8	161.0	55.3	4092.0	2.3
32	17.3	0.5	6.8	177.8	3.4	38.6	1.6
33	6.7	10.0	6.6	186.2	53.7	4400.0	1.9
34	40.0	15.0	6.9	173.6	36.4	5008.0	20.5
35	119.3	1.0	7.0	214.2	107.8	1681.8	1.9
36	26.0	15.0	6.8	214.2	19.4	2710.0	1.5
37	24.0	10.0	6.9	82.6	16.6	2582.0	1.9
38	24.0	2.0	7.4	95.2	14.9	2472.0	1.2
39	266.7	4.0	7.5	175.0	83.0	2450.0	1.8

Number	Depth [m]	Age [year]	pH [-]	HCO_3^- [mg/L]	As_{tot} [µg/L]	Fe^{2+} [µg/L]	DOC [mg/l]
40	17.3	10.0	6.9	212.8	40.8	176.4	2.5
41	30.7	8.0	6.8	257.6	60.4	8056.1	3.2
42	30.7	2.0	6.6	211.4	88.6	7527.7	2.4
43	24.0	2.0	6.7	305.2	37.9	5265.2	2.7
44	28.0	10.0	6.9	121.8	43.4	4767.4	2.6
45	22.7	10.0	6.8	257.6	22.7	2259.3	1.9
46	17.3	2.0	6.8	218.4	22.6	1956.2	1.6
47	22.7	7.0	6.7	196.0	33.7	2068.4	2.3
48	29.3		6.8	212.8	3.8	3328.0	2.5
49	36.7		6.6	207.2	64.1	4903.6	2.7
50	17.3		6.6	208.6	50.3	3864.4	1.5
51	150.7	2.0	7.0	249.2	6.8	839.7	2.4
52	50.7	3.0	6.7	183.4	49.3	3444.0	2.3
53	35.3	10.0	6.7	175.0	26.6	2680.1	1.8
54	28.7	12.0	6.7	387.8	131.5	6335.2	8.7
55	68.7		6.8	145.6	81.9	4512.6	1.7
56	110.7	3.0	6.8	183.4	1.5	5064.1	2.6
57	24.0	0.5	6.6	263.2	72.6	3200.6	3.6
58	27.3	15.0	6.7	235.2	19.7	4493.7	1.7
59	24.0	4.0	6.8	253.7	13.6	4826.1	1.6
60	50.7	4.0	6.8	244.6	9.3	2200.8	2.4
61	40.0	4.0	6.7	283.9	0.5	123.7	2.2
62	48.7	4.0	6.7	209.9	0.5	134.0	1.4
63	42.0	5.0	6.8	220.5	213.5	4507.1	1.8
64	42.0	5.0	6.9	215.9	16.2	115.8	2.8
65	22.0	12.0	6.8	232.5	6.7	3423.8	2.4
66	22.0				22.2	4275.4	2.4
67	270.7	3.0	6.9	250.7	91.0	2171.8	3.5
68	14.0	1.0	6.8	226.5	1.1	84.1	2.3
69	24.0	0.5	6.6	247.6	0.6	82.4	2.1
70	17.3	15.0	6.6	299.0	70.4	394.7	1.3
71	24.0	3.0	6.7	172.1	11.9	1628.6	1.4
72	17.3	5.0	6.6	270.3	1.0	65.1	1.8
73	124.0	6.0	6.7	252.2	117.4	3354.6	3.5
74	17.3	10.0	6.6	276.3	7.9	3545.7	1.5
75	17.3	1.0	6.8	297.5	28.3	4311.0	1.7
76	17.3	12.0	7.0	229.5	3.1	676.7	1.7
77	17.3	8.0	6.9	219.0	3.8	184.8	1.7
78	18.3	7.0	6.8	288.4	17.4	6594.0	1.7
79	24.0	5.0	6.7	274.8	22.4	8157.5	2.9

Number	Depth [m]	Age [year]	pH [-]	HCO_3^- [mg/L]	As_{tot} [µg/L]	Fe^{2+} [µg/L]	DOC [mg/l]
80	24.0	0.5	6.6	241.6	35.5	9364.6	4.9
81	0.0	16.0	6.6	226.5	60.8	19408.4	1.6
82	84.0	0.2	6.6	246.1	63.2	1411.8	2.1
83	27.3	8.0	6.7	270.3	89.2	7765.2	4.8
84	24.0	7.0	6.7	246.1	161.1	9679.4	3.9
85	30.7	12.0	6.7	258.2	230.0	45938.2	
86	27.3	15.0	6.7	382.0	292.7	5526.2	
87	30.7	2.0	6.8	338.2	124.3	2835.1	
88	50.7	0.7	6.9	201.0	13.6	53.3	
89	50.7	1.0	6.9	255.0	1.4	229.8	1.6
90	57.3	5.0	7.0	250.5	1.5	94.7	1.9
91	17.3	16.0	6.7	234.0	33.2	8664.6	5.2
92	24.0	0.2	6.7	255.1	49.7	11173.9	3.7
93	33.3	10.0	6.9	303.5	53.9	1071.8	1.0
94	110.7	1.5	7.0	283.9	13.7	1471.3	1.2
95	20.0	5.0	6.9	232.5	0.8	205.3	3.2
96	17.3	7.0	7.3	214.4	6.1	2498.1	2.2
97	18.3	4.0	7.1	166.1	60.6	3390.6	2.2
98	133.3	4.0	7.0	306.5	86.4	692.3	1.5
99	133.3	4.0	7.1	305.0	36.3	8.5	0.1
100	17.3	8.0	7.2	199.0	16.9	3910.5	1.5
101	17.3	5.0	7.1	232.5	3.1	2682.3	3.0
102	24.0	0.5	7.0	193.2	21.4	2467.5	3.2
103	24.0	2.0	7.1	172.1	7.2	1070.4	1.7
104	18.0	12.0	7.5	178.2	9.4	1707.7	1.4
105	21.3	12.0	7.5	190.2	21.1	3811.3	1.4
106	24.0	1.0	7.6	172.1	22.1	4533.2	2.4
107	24.0	2.0	7.7	279.4	19.9	7726.6	3.2
108	20.7	5.0	7.9	234.1	70.4	11406.8	5.0
109	24.0	5.0	7.8	299.0	166.9	4922.6	1.6
110	24.0	7.0	7.8	206.9	171.5	3569.4	3.1
111	0.0	8.0	7.9	238.6	15.8	3954.7	1.3
112	0.0	8.0	8.0	267.3	6.7	108.4	0.8
113	24.0	10.0	8.0	182.7	71.5	6236.2	2.4
114	24.0	3.0	7.6	170.6	30.0	1243.8	1.2
115	17.3	7.0	7.7	208.4	52.2	4192.3	1.4
116	24.0	0.5	7.7	143.5	0.6	472.7	1.8
117	30.0	16.0	7.1	231.0	37.9	6543.2	1.2
118	0.0	15.0	7.0	237.0	4.6	13906.1	6.2
119	18.3	5.0	7.3	216.0	3.2	1379.4	2.8

Number	Depth [m]	Age [year]	pH [-]	HCO_3^- [mg/L]	As_{tot} [µg/L]	Fe^{2+} [µg/L]	DOC [mg/l]
120	183.3	4.0	7.2	264.0	34.8	1297.8	2.0
121	25.0	1.0	7.2	193.5	50.4	4052.0	0.9
122	166.7	4.0	7.5	241.5	77.4	1072.9	1.3
123	166.7	4.0	7.3	231.0	101.1	1283.1	1.9
124	24.0	1.0	7.3	202.5	159.6	4853.1	2.3
125	24.0	7.0	7.2	219.0	2.3	47.8	1.1
126	24.0	5.0	7.2	177.0	61.0	1040.4	0.7
127	24.0	15.0	7.2	184.5	57.0	3955.5	1.1
128	19.3	5.0	7.1	237.0	38.6	54.9	2.4
129	100.0	2.0	7.4	217.5	39.1	10.1	0.7
130	100.0	2.0	7.3	225.0	84.7	1042.1	0.6
131	24.0		7.3	232.5	84.9	5460.9	1.0
132	24.0	20.0	7.1	234.0	285.0	3303.8	1.5
133	133.3	1.0	7.2	264.0	31.9	367.8	1.9
134	24.0	3.0	7.1	235.5	9.7	1171.1	2.8
135	26.7	3.0	7.1	238.5	50.2	7769.6	1.2
136	17.3	5.0	7.1	330.0	2.1	10.7	2.6
137	17.3	7.0	7.3	205.5	19.5	299.8	2.2
138	18.0	15.0	7.6	165.0	1.1	35.0	1.8
139	17.3	3.0	7.2	231.0	0.9	125.6	2.4
140	17.3	12.0	7.3	255.0	2.1	1486.2	2.6
141	24.0	5.0	7.3	214.5	21.5	2306.9	1.7
142	17.3	3.0	7.2	223.5	17.0	464.3	1.8
143	17.3	2.0	7.2	232.5	1.3	2201.1	2.4
144	24.0	5.0	7.1	99.0	12.1	1427.9	3.1
145	17.3	15.0	7.2	292.5	29.0	4400.1	1.1
146	24.0	7.0	7.1	244.5	86.2	5258.8	3.6
147	24.0	4.0	7.1	246.0	89.8	3464.4	2.5
148	30.0	7.0	7.2	220.5	55.7	3313.9	0.6
149	24.0	4.0	7.1	202.5	0.9	72.3	3.4
150	14.0	5.0	7.4	216.0	10.5	933.2	1.2
151	16.7	8.0	7.1	249.0	18.3	6075.2	0.6
152	24.0	7.0	7.0	217.5	290.4	4548.2	3.0
153	24.0	2.0	7.1	174.0	131.0	4189.1	2.3
154	24.0	3.0	7.1	220.5	66.1	276.7	1.0
155	140.0	4.0	7.1	322.5	39.3	632.6	3.4
156	140.0	4.0	7.5	324.0	63.5	14.5	3.7
157	17.3	3.0	7.5	264.0	38.4	238.1	3.4
158	23.3	17.0	7.3	207.0	50.1	3327.0	1.5

Number	Depth [m]	Age [year]	pH [-]	HCO_3^- [mg/L]	As_{tot} [µg/L]	Fe^{2+} [µg/L]	DOC [mg/l]
159	20.0	3.0	7.2	222.0	128.5	4819.3	3.4
160	26.7	7.0	7.2	214.5	122.1	5535.4	1.1
161	133.3	1.0	7.5	243.1	2.3	548.4	1.2
162	33.3	3.0	7.5	143.0	54.9	1421.4	4.4
163	73.3	2.0	7.4	273.0	3.1	327.1	3.1
164	26.7	2.0	7.5	150.8	31.9	1789.0	4.5
165	46.7	12.0	7.5	196.3	0.4	21.4	1.3
166	46.7	18.0	7.4	254.8	0.3	39.3	1.5
167	46.7	8.0	7.5	239.2	0.4	40.6	0.9
168	16.7	8.0	7.4	255.5	1.4	18.4	1.6
169	83.3	4.0	7.5	162.5	0.4	29.1	0.8
170	56.7	3.0	7.5	156.0	0.8	87.9	1.0
171	46.7	6.0	7.6	220.5	0.3	30.7	1.3
172	146.7	1.0	7.7	276.0	0.8	18.0	0.4
173	56.7	7.0	7.7	202.5	0.8	23.3	1.4
174	16.7	2.0	7.6	246.0	35.2	3389.8	1.6
175	16.7	12.0	6.7	94.5	31.4	2346.5	0.7
176	26.7	3.0	7.3	202.5	34.7	4302.5	1.6
177	76.7	0.9	7.4	232.5	3.2	174.7	1.6
178	16.7	24.0	7.6	279.0	18.3	1709.3	0.8
179	54.7	2.0	7.1	201.0	120.4	31.2	1.5
180	24.0	2.0	7.2	222.0	116.1	3884.7	1.6
181	20.0	6.0	7.4	187.5	123.8	3645.0	1.2

Table A-7: Result of the hydrochemical analysis (the data from Neidhardt, 2012).

Number	Na^+ [mg/L]	Mg^{2+} [mg/L]	K^+ [mg/L]	Ca^{2+} [mg/L]	P_{tot} [µg/L]	Mn^{2+} [µg/L]	Cl^- [mg/l]
1	34.5	41.9	3.3	122.1	1858.1	257.9	43.5
2	36.2	30.1	3.4	103.1	1211.4	542.6	16.0
3	20.5	25.6	3.7	101.7	1085.5	477.4	14.4
4	28.6	29.5	2.2	127.2	1550.9	705.9	74.8
5	19.6	26.4	3.2	119.1	1714.2	306.5	8.0
6	16.1	34.1	3.3	108.4	1713.3	231.6	15.5
7	57.3	29.5	3.2	117.3	3196.2	392.6	16.6
8	11.9	25.1	2.6	109.3	1880.2	214.6	28.0
9	28.9	29.5	5.1	117.6	109.6	334.0	27.0
10	98.8	43.7	6.2	155.1	55.3	218.2	120.2
11	9.0	13.4	2.8	69.2	1598.4	309.3	9.8
12	11.7	16.7	3.3	84.1	1286.7	635.8	6.2
13	11.9	17.7	3.3	110.7	310.1	402.6	5.1
14	20.6	22.0	4.3	135.9	187.0	304.0	24.8
15	13.6	17.8	3.0	89.2	356.4	367.2	4.3
16	23.7	16.6	3.0	78.1	427.1	343.8	15.8
17	17.4	25.9	4.1	116.8	195.8	604.0	18.3
18	14.7	30.2	3.4	97.5	136.1	589.8	21.4
19	10.1	26.4	3.3	115.0	281.0	328.6	37.3
20	23.7	24.7	3.3	100.3	20.5	8.5	6.0
21	27.8	32.7	4.8	125.1	1226.6	326.5	36.1
22	27.8	34.6	1.7	121.3	30.3	229.3	96.0
23	11.5	18.8	0.9	73.0	646.5	87.6	6.3
24	8.6	8.9	0.8	55.7	335.3	130.6	7.9
25	10.3	18.4	2.2	80.4	1850.3	500.1	3.6
26	12.8	18.8	2.7	70.9	32.1	168.2	8.0
27	18.7	26.6	2.8	114.3	1553.5	517.6	17.8
28	16.6	21.5	3.9	90.1	1542.0	339.9	22.1
29	8.2	14.3	2.5	70.9	1318.2	547.0	12.2
30	19.1	18.0	2.8	82.1	1585.9	351.2	15.9
31	43.4	25.6	4.3	125.6	575.8	478.6	64.5
32	30.0	26.3	4.3	108.8	11.0	604.9	41.7
33	13.4	18.6	2.4	149.9	933.1	540.2	18.2
34	24.5	23.3	3.7	110.6	954.1	477.1	61.0
35	13.1	20.2	3.4	110.4	430.4	259.9	4.0
36	19.4	17.4	2.2	77.9	1435.7	103.5	9.8
37	5.9	17.3	5.1	138.5	223.0	405.3	4.6
38	23.2	21.4	4.0	171.9	383.6	344.3	19.4
39	10.0	20.4	2.7	140.4	142.6	117.1	2.6

Number	Na^+ [mg/L]	Mg^{2+} [mg/L]	K^+ [mg/L]	Ca^{2+} [mg/L]	P_{tot} [µg/L]	Mn^{2+} [µg/L]	Cl^- [mg/l]
40	21.4	23.9	2.7	122.4	66.8	194.6	26.1
41	25.7	33.4	2.6	170.6	1717.4	225.7	44.3
42	21.0	23.1	3.0	132.9	1383.9	193.3	16.2
43	51.3	35.7	2.2	133.8	1320.2	207.7	100.6
44	37.9	33.0	2.5	113.2	1470.2	174.1	76.9
45	13.3	22.5	3.2	108.3	247.7	384.6	17.7
46	11.2	20.3	3.3	90.8	227.1	483.2	7.4
47	11.8	16.0	2.2	82.3	687.2	332.3	16.0
48	14.7	15.7	2.6	87.3	209.1	375.3	9.7
49	10.4	20.5	2.0	89.9	1238.7	215.2	9.1
50	11.9	18.0	2.7	94.6	704.9	296.6	10.9
51	46.8	20.2	3.0	74.2	45.3	58.8	4.4
52	12.5	19.6	2.6	78.0	1188.6	133.7	10.5
53	9.6	17.9	2.8	81.2	784.3	235.6	13.5
54	37.4	40.9	1.8	168.0	967.2	198.5	15.6
55	11.2	14.8	1.8	57.9	558.0	102.2	2.4
56	9.9	20.0	2.8	74.3	22.9	397.5	4.7
57	33.2	32.1	1.2	120.3	965.8	324.7	52.9
58	15.8	21.2	4.8	100.4	1152.7	186.1	14.4
59	15.5	21.7	4.7	113.6	1066.2	209.1	15.4
60	12.8	22.3	1.9	100.3	217.6	1092.4	12.5
61	14.4	24.4	2.2	106.8	57.2	1695.6	6.5
62	10.5	20.0	1.9	83.6	58.0	1596.7	1.7
63	16.2	21.8	2.3	83.6	196.7	842.8	11.5
64	16.3	21.5	2.4	84.8	7.6	5.3	9.3
65	12.8	18.0	3.0	100.2	233.8	348.9	13.1
66	15.5	24.6	4.0	113.7	669.9	326.1	13.0
67	14.0	20.9	3.3	91.7	53.6	123.5	2.2
68	12.0	22.8	3.8	107.9	42.8	19.0	20.4
69	66.8	36.0	15.8	140.5	62.8	86.7	146.8
70	18.9	26.0	3.8	147.3	128.0	560.7	36.8
71	11.3	12.3	3.2	69.0	367.0	254.4	7.1
72	24.0	32.2	10.3	133.6	33.2	309.9	49.3
73	16.1	23.3	3.0	99.2	245.2	75.0	3.5
74	20.7	25.3	3.9	122.4	302.6	179.9	29.4
75	20.6	25.5	3.8	137.2	854.8	235.4	29.5
76	15.5	21.0	3.6	94.9	108.3	217.1	13.4
77	16.2	21.0	4.8	92.4	511.6	88.7	10.5
78	14.3	32.8	8.6	126.7	640.7	235.2	40.1
79	33.8	35.9	13.9	128.8	1044.8	346.0	80.8

Number	Na^+ [mg/L]	Mg^{2+} [mg/L]	K^+ [mg/L]	Ca^{2+} [mg/L]	P_{tot} [µg/L]	Mn^{2+} [µg/L]	Cl^- [mg/l]
80	34.0	22.3	2.9	119.1	1088.2	327.4	57.1
81	20.0	21.5	2.2	89.2	2134.4	392.3	5.8
82	16.8	23.8	4.7	94.4	127.9	81.2	12.0
83	21.3	25.5	5.5	118.6	1472.7	232.7	40.9
84	18.1	26.0	3.6	99.9	1268.6	520.3	15.7
85	17.8	27.1	7.0	115.0	2479.8	809.8	16.6
86	60.3	35.2	2.8	128.3	1511.6	77.7	7.7
87	25.7	17.0	1.5	61.9	681.4	45.0	33.7
88	4.4	5.4	0.8	20.3	20.6	202.6	27.6
89	27.7	22.7	1.8	90.7	19.1	502.8	3.0
90	30.0	21.7	1.6	91.7	20.3	522.8	3.8
91	48.4	20.9	6.2	103.2	1386.0	116.1	64.6
92	50.9	26.5	5.2	124.0	1846.3	97.1	75.9
93	44.6	25.4	2.0	124.9	447.6	2524.4	32.3
94	34.1	28.3	3.6	95.0	44.9	86.2	4.6
95	111.8	33.4	12.1	178.2	20.7	175.5	83.9
96	20.2	17.5	3.4	95.6	1081.8	499.7	42.8
97	10.4	13.9	3.0	81.7	1003.9	260.5	7.0
98	29.1	32.7	4.7	104.6	75.8	75.9	7.8
99	29.9	32.4	5.1	117.6	13.2	33.4	9.0
100	20.6	15.4	3.8	98.2	223.5	231.2	33.7
101	17.1	19.1	3.7	127.0	167.6	458.4	25.6
102	7.0	13.1	5.3	96.8	410.8	643.3	6.6
103	6.7	14.7	2.6	88.9	200.0	290.1	9.3
104	14.1	18.7	3.8	104.0	496.2	367.7	8.0
105	46.3	25.4	4.0	150.8	588.8	530.1	98.3
106	13.4	20.5	2.9	120.5	1007.9	694.3	87.1
107	28.4	27.4	2.5	139.0	1666.2	266.6	33.4
108	15.7	24.0	9.3	117.8	2954.1	257.1	19.4
109	59.7	21.2	3.5	114.9	1132.7	151.6	7.8
110	43.5	22.8	3.5	113.9	258.7	50.9	9.4
111	46.5	26.0	3.3	115.9	1251.5	181.4	20.6
112	43.5	24.9	3.2	107.1	145.0	168.2	21.2
113	14.7	21.1	2.5	97.2	1312.9	231.1	7.5
114	10.7	12.1	3.7	89.6	546.4	372.0	7.8
115	8.3	11.5	2.3	116.7	875.5	580.1	8.6
116	11.0	25.9	17.9	89.3	29.3	488.4	21.8
117	15.6	20.9	2.2	81.9	1316.6	374.3	21.9
118	9.7	20.2	3.7	106.7	179.8	568.9	14.3
119	9.3	16.4	2.6	113.4	43.2	397.7	10.7

Number	Na^+ [mg/L]	Mg^{2+} [mg/L]	K^+ [mg/L]	Ca^{2+} [mg/L]	P_{tot} [µg/L]	Mn^{2+} [µg/L]	Cl^- [mg/l]
120	14.3	21.2	3.4	107.4	21.9	62.8	5.0
121	10.8	20.9	2.7	80.4	1200.6	184.2	10.9
122	9.5	14.0	2.4	70.3	131.1	60.9	2.2
123	13.2	19.4	3.3	98.6	159.7	84.7	2.3
124	13.8	16.4	3.7	84.7	816.7	471.2	3.6
125	15.1	24.1	4.0	110.6	9.6	512.2	46.7
126	10.8	14.3	3.0	69.8	1212.4	274.8	3.6
127	14.5	17.6	2.5	78.7	1191.4	340.6	11.1
128	18.8	23.5	2.7	105.6	15.0	649.8	32.7
129	13.1	20.8	2.6	89.2	43.7	5.7	2.6
130	12.7	22.2	2.2	85.5	164.0	119.8	2.7
131	18.5	17.5	1.8	78.7	1182.0	514.8	10.9
132	26.8	22.5	3.3	91.9	1339.6	489.5	18.5
133	15.1	21.9	2.8	108.4	52.1	220.2	4.8
134	21.5	25.0	2.2	98.3	46.2	188.0	35.5
135	20.2	21.5	4.9	104.0	1211.0	279.6	25.5
136	24.4	36.8	8.2	138.2	4.2	333.5	37.2
137	18.7	20.0	12.9	82.4	292.1	486.4	18.4
138	8.6	17.1	2.9	75.1	11.2	32.3	16.7
139	20.2	24.0	2.4	92.6	19.6	321.9	19.3
140	13.3	27.3	2.5	100.8	27.8	396.7	13.4
141	13.0	17.4	2.9	81.5	408.5	263.1	4.4
142	28.3	26.6	4.1	117.9	3.4	361.7	84.1
143	18.0	22.4	3.3	91.0	51.3	199.3	11.1
144	5.6	7.2	2.2	38.2	652.8	97.6	7.0
145	31.1	40.6	3.7	159.9	617.7	255.5	25.5
146	18.0	26.4	3.2	107.8	730.7	374.4	41.2
147	25.9	20.7	2.7	90.1	591.1	277.5	6.9
148	21.7	16.8	2.0	79.6	1060.5	316.5	1.1
149	16.5	24.8	2.4	101.8	7.6	197.0	79.8
150	14.5	15.8	2.8	81.8	66.3	211.9	6.6
151	23.5	22.0	4.1	98.8	551.0	585.1	2.9
152	17.7	20.5	3.5	76.3	1932.2	340.4	8.0
153	14.3	15.6	3.8	62.1	1408.6	254.6	8.7
154	17.9	23.5	3.7	82.5	86.1	233.2	7.2
155	30.1	29.6	3.9	109.0	2.2	113.1	10.7
156	30.3	30.0	3.9	112.2	53.3	125.0	11.0
157	20.7	25.0	2.7	96.5	9.6	166.0	6.3
158	10.7	20.4	3.0	76.9	884.4	145.2	4.5
159	13.1	21.7	3.6	80.1	1056.3	145.0	3.5

Number	Na^+ [mg/L]	Mg^{2+} [mg/L]	K^+ [mg/L]	Ca^{2+} [mg/L]	P_{tot} [µg/L]	Mn^{2+} [µg/L]	Cl^- [mg/l]
160	15.4	22.4	2.9	81.9	783.2	152.8	4.5
161	22.3	24.1	2.4	82.3	3.0	83.8	3.0
162	27.8	15.7	1.6	51.1	523.6	110.8	31.0
163	27.3	27.5	3.2	94.6	7.1	76.6	3.8
164	27.6	15.0	1.4	52.8	405.7	82.0	19.4
165	16.7	22.7	1.7	72.6	9.1	156.5	4.7
166	28.3	27.9	2.4	84.8	16.9	277.4	4.6
167	28.8	25.5	2.1	82.0	3.9	150.6	2.9
168	39.3	34.1	44.5	98.5	31.4	402.3	38.0
169	10.0	17.6	1.8	55.2	17.7	286.5	1.3
170	13.0	17.9	1.6	55.8	28.3	203.7	1.5
171	32.7	23.0	2.2	70.4	33.1	145.0	1.7
172	23.2	29.7	2.7	93.3	3.6	77.6	0.7
173	25.5	21.5	2.1	62.5	38.5	296.0	1.8
174	15.4	24.9	2.0	102.0	631.3	122.8	28.5
175	15.9	21.7	3.3	86.4	112.0	418.6	2.1
176	15.7	18.3	3.4	89.7	460.8	412.2	21.3
177	17.6	21.7	3.0	82.6	18.6	577.9	3.4
178	38.8	24.8	4.1	124.5	122.7	398.3	15.8
179	17.0	19.0	2.3	69.5	221.4	162.8	6.7
180	25.8	19.8	1.6	74.5	1550.5	109.0	7.0
181	14.0	17.3	3.0	68.8	1510.2	210.4	4.2

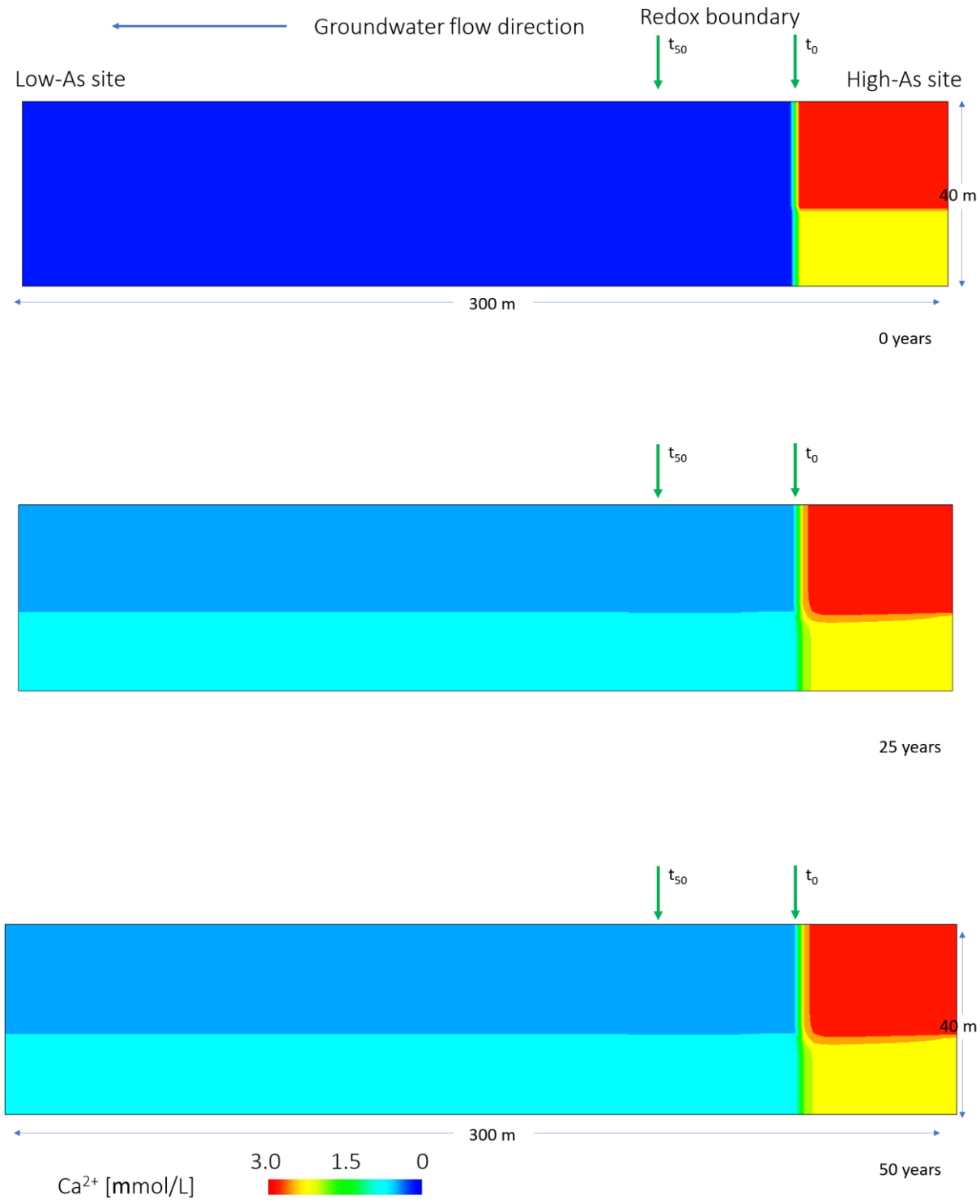

Figure A-1. Calcium distribution in a cross-section in the Van Phuc aquifer. The simulation results after 0, 25 and 50 years. The redox boundary position after 0 and 50 years is indicated by arrows t_0 and t_{50}, respectively.

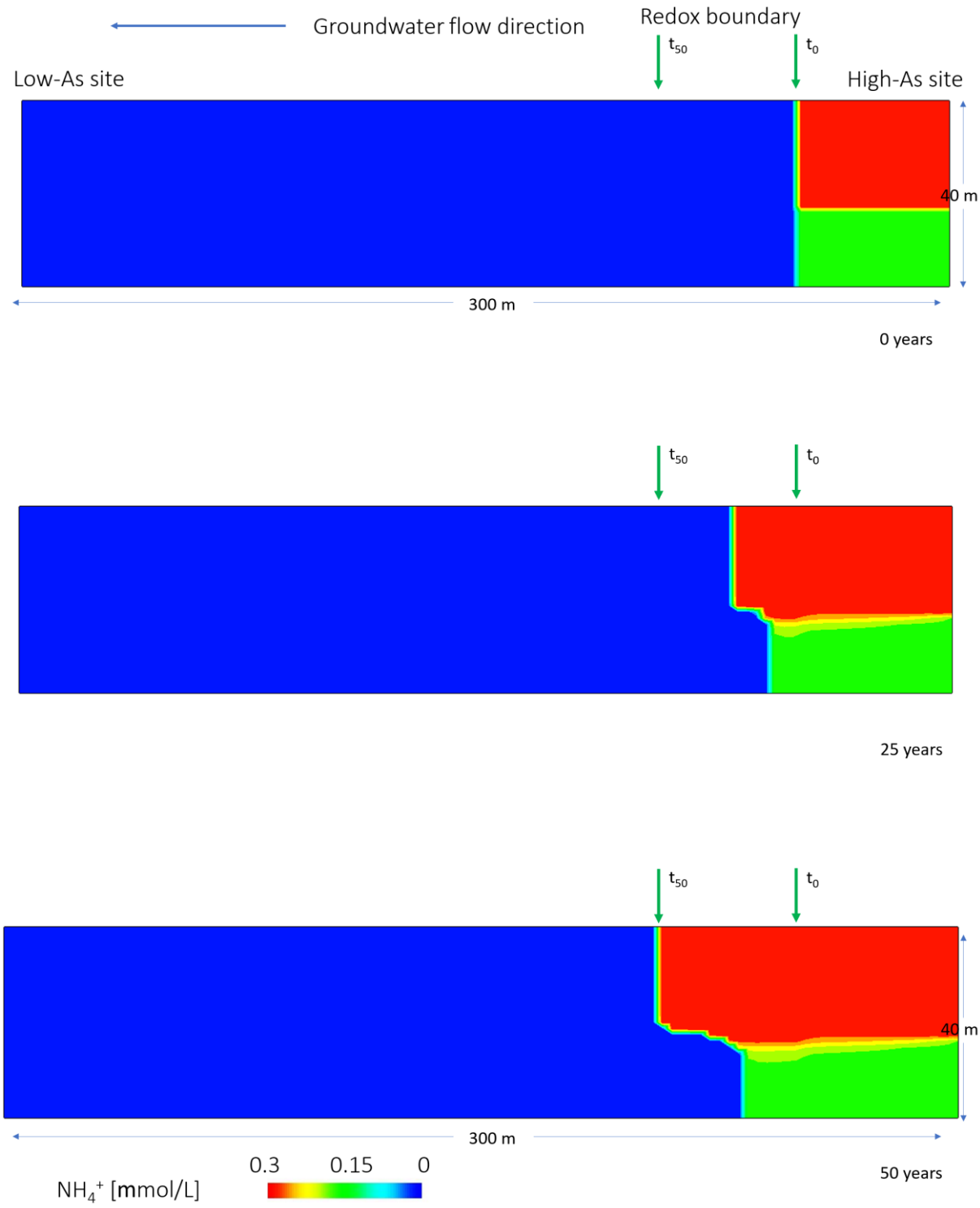

Figure A-2. Ammonium distribution in a cross-section in the Van Phuc aquifer. The simulation results after 0, 25 and 50 years. The redox boundary position after 0 and 50 years is indicated by arrows t_0 and t_{50}, respectively.

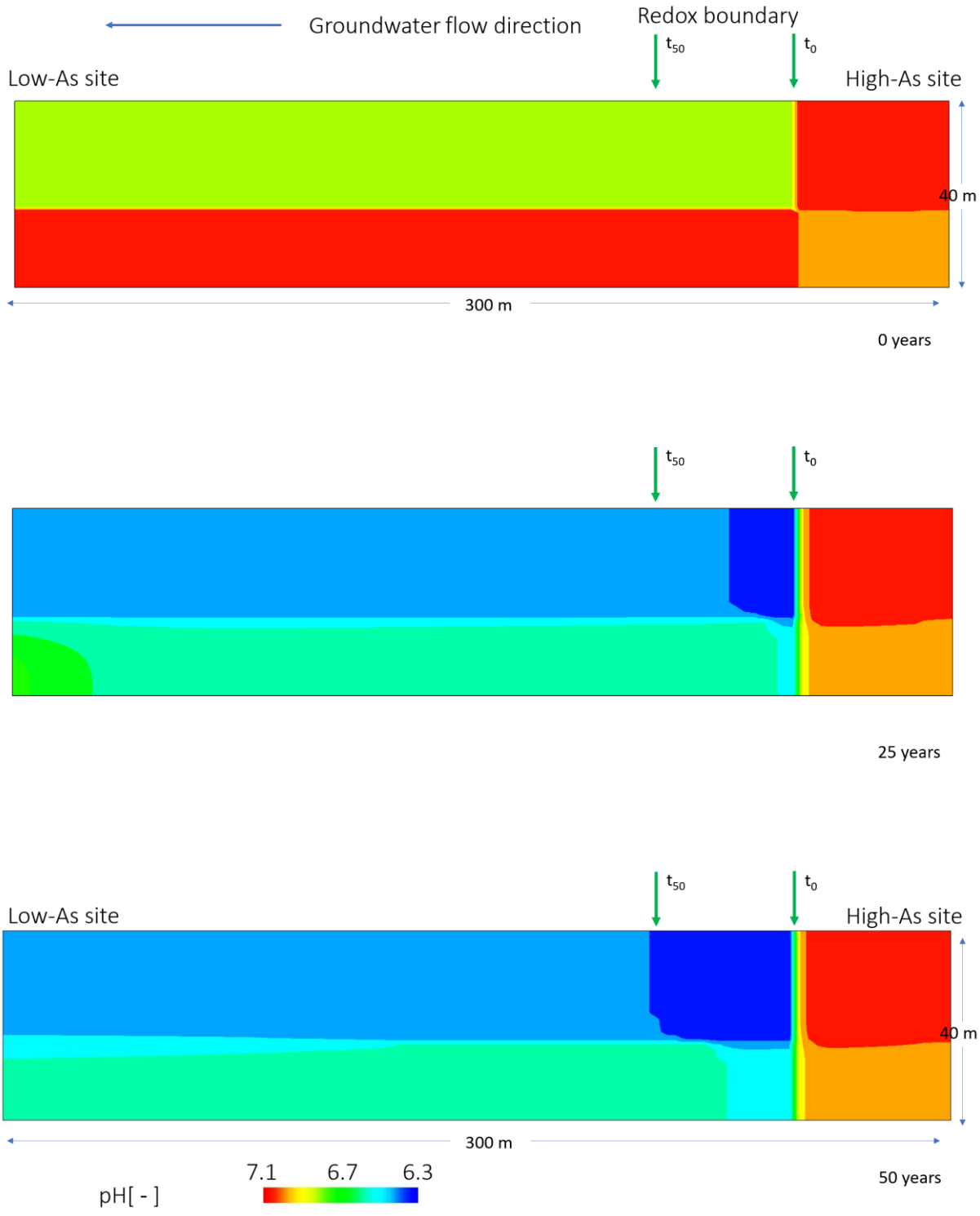

Figure A-3. pH distribution in a cross-section in the Van Phuc aquifer. The simulation results after 0, 25 and 50 years. The redox boundary position after 0 and 50 years is indicated by arrows t_0 and t_{50}, respectively.

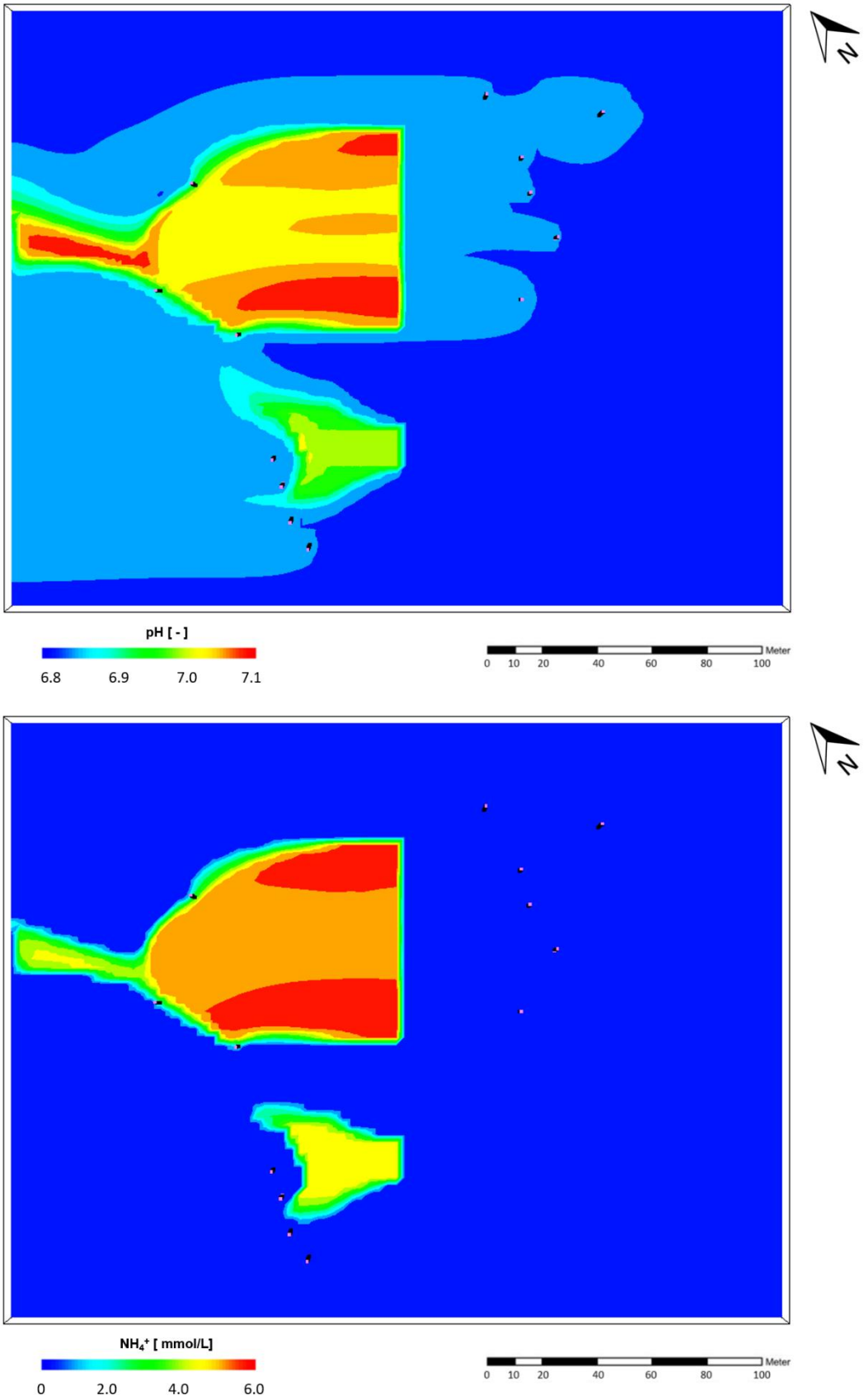

Figure A-4. Calculated distribution of pH and NH_4^+ in the aquifer.

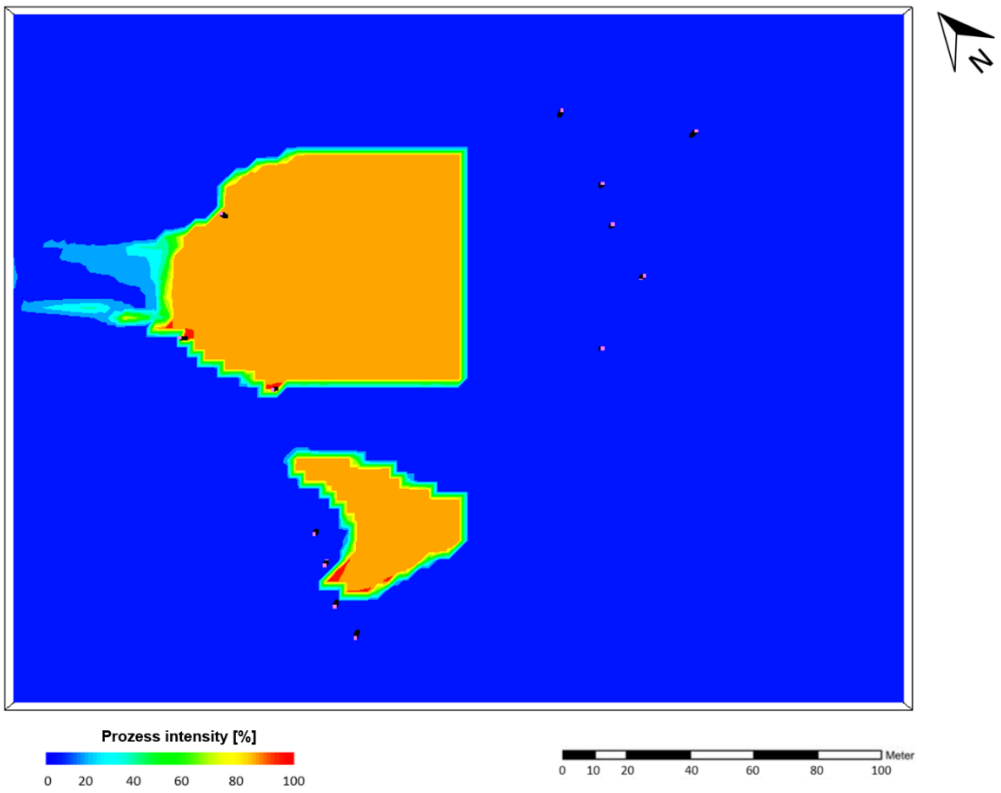

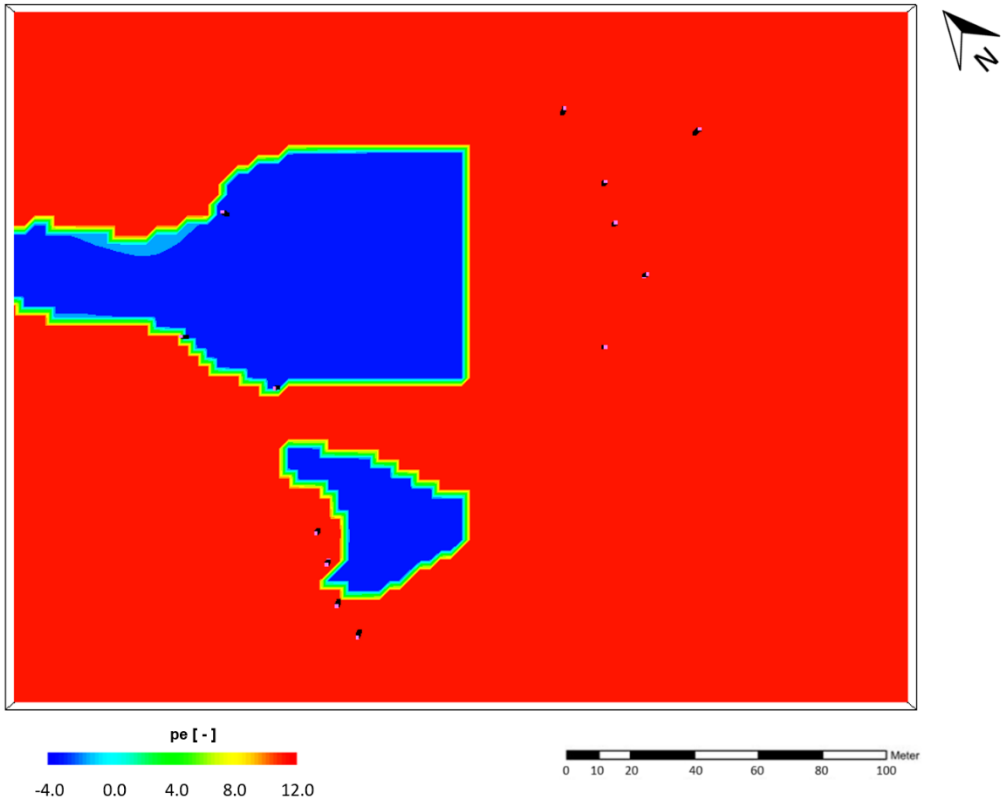

Figure A-5. Calculated distribution of pyrite and pe in the aquifer.

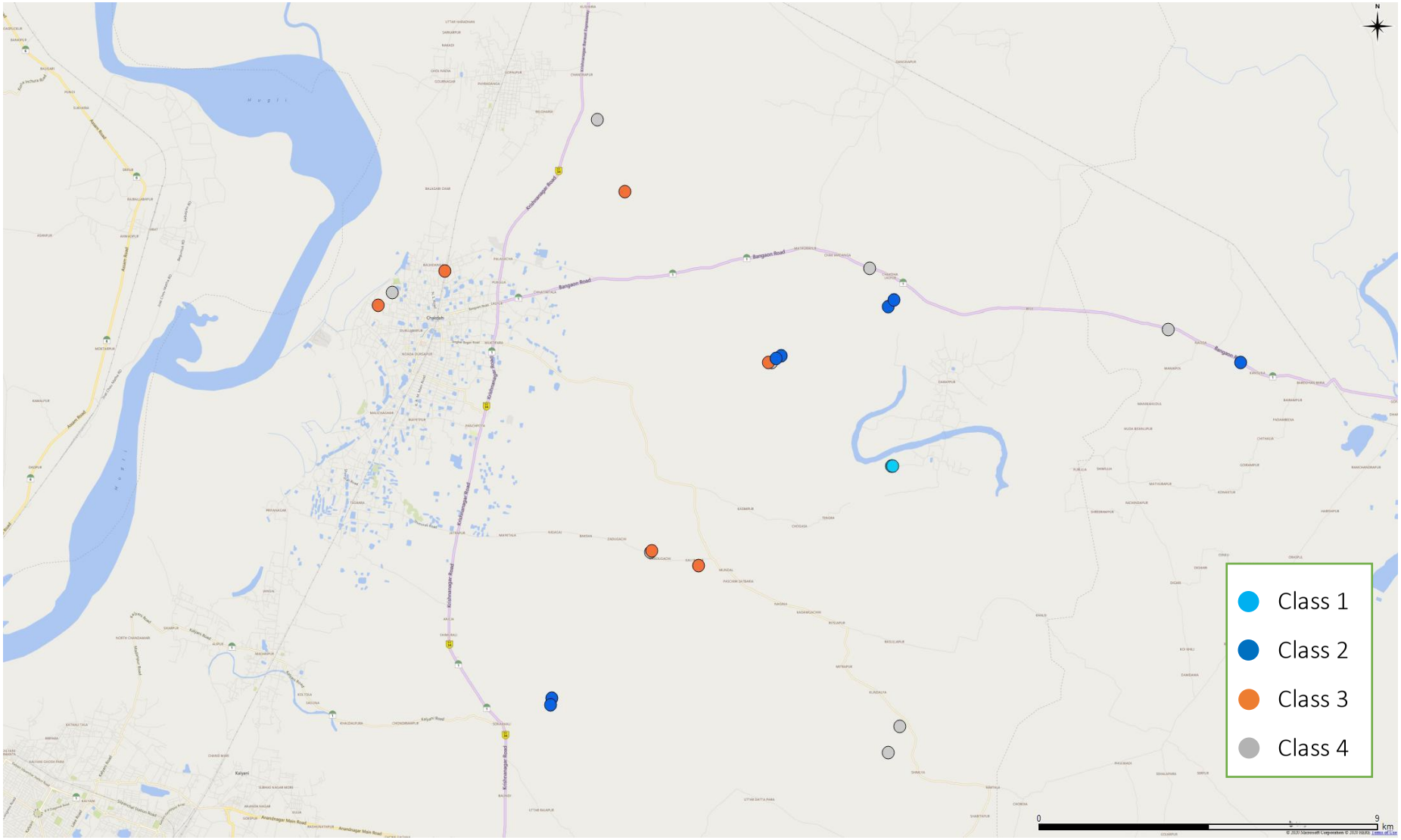

Figure A-6: Results of cluster analysis. Samples are grouped into four classes (background image from: bing.com).

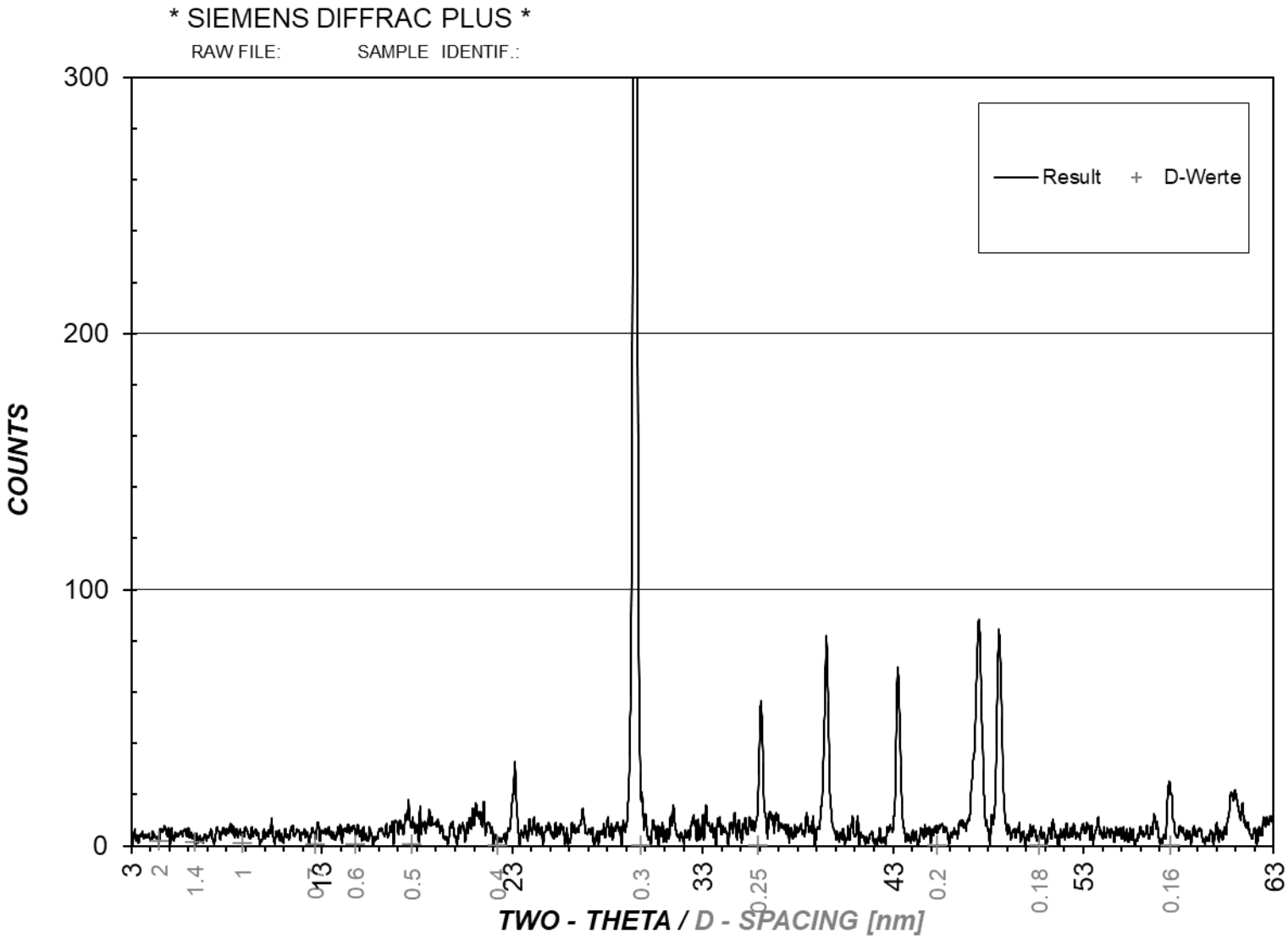

Figure A-7: Results of X-ray diffraction.